Atomic Energy Control Board
P.O. Box 1046
Ottawa, Canada
K1P 5S9

Commission de contrôle de l'énergie atomique
C.P. 1046
Ottawa, Canada
K1P 5S9

INFO-0312

NUMERICAL COMPUTATION OF UNDERWATER EXPLOSIONS DUE TO FUEL-COOLANT INTERACTIONS

by

J.H.S. Lee (principal investigator),
D.L. Frost, R. Knystautas,
A. Teodorczyk, G. Ciccarelli
SWACER, Inc.

and

P. Thibault and J. Penrose
Combustion Dynamics

A research report prepared for the Atomic Energy Control Board, Ottawa, Canada

March 1989

Canada

Research report

90-01367/

NUMERICAL COMPUTATION OF UNDERWATER EXPLOSION DUE TO MOLTEN FUEL-COOLANT INTERACTION

ABSTRACT

If coarse molten material is released into a coolant the possibility exists for a violent steam explosion. A detailed quantitative description of the processes involved in steam explosions is currently beyond the capabilities of the scientific community. However, a conservative estimate of the pressure transients resulting from a steam explosion can be obtained by studying the dynamics of the shock associated with the expansion of a high-pressure vapour bubble.

In this study, the hydrodynamic equations governing the shock propagation of an expanding bubble were integrated numerically using the Flux Corrected Transport (FTC) code. Simpler acoustic models based on experience with underwater explosions were also developed and used to estimate pressure transients and to calculate the peak pressures for benchmark cases. The results were found to be an order of magnitude higher than the corresponding pressures obtained using a complex model developed by Henry. A simplified version of the Henry model was developed by neglecting the complex description of the two-phase flow inside the ruptured tube and the arbitrarily assumed heat transfer and condensation rates. Results from the simplified model were found to be generally similar to, but had higher peak pressures than those obtained using the Henry model.

It is concluded that the results produced by simple acoustic models, or by a simplified Henry model, are more conservative than the corresponding results obtained with the original Henry model.

RÉSUMÉ

Si de grosses parcelles de matière en fusion sont déversées dans un réfrigérant, il est possible qu'une violente explosion de vapeur survienne. Malheureusement les scientifiques n'ont pas les moyens, pour le moment, d'établir une description quantitative détaillée des processus en cause. Toutefois, on peut obtenir une estimation prudente des transitoires de pression dues à une explosion de vapeur en étudiant la dynamique du choc lié à l'expansion de la bulle de vapeur à haute pression.

Dans la présente étude, les équations hydrodynamiques régissant la propagation du choc d'une bulle qui grossit ont été intégrées numériquement en utilisant le "Flux Corrected Transport Code". Des modèles acoustiques plus simples conçus à partir de l'expérience acquise en matière d'explosions sous-marines ont été mis au point et utilisés pour estimer les transitoires de pression et pour calculer les pointes de pression des cas de référence. Les résultats se sont avérés d'un ordre de grandeur plus élevé que les pressions correspondantes qui avaient été obtenues à partir du modèle complexe mis au point par Henry. On a mis au point une version simplifiée du modèle Henry en négligeant la description complexe de l'écoulement diphasique à l'intérieur du tube rompu, ainsi que les taux de transfert de chaleur et de condensation choisis arbitrairement. Les résultats obtenus à partir du modèle simplifié se sont avérés généralement semblables à ceux obtenus à partir du modèle Henry, sauf que les pointes de pression étaient supérieures.

Le rapport conclut que les résultats obtenus à partir des modèles acoustiques simples ou du modèle Henry simplifié sont plus prudents que les résultats correspondants qui ont été obtenus à partir du modèle Henry original.

DISCLAIMER

The Atomic Energy Control Board is not responsible for the accuracy of the statements made or opinions expressed in this publication and neither the Board nor the authors assume liability with respect to any damage or loss incurred as a result of the use made of the information contained in this publication.

TABLE OF CONTENTS

1 INTRODUCTION....2
2 SUMMARY OF RESULTS OF VARIOUS INVESTIGATIONS....3
2.1 Review of Underwater Explosions....3
2.2 Numerical Simulation of Underwater Explosions....5
2.3 Approximate Models....6
2.3.1 Incompressible Model....7
2.3.2 Compressible Models....8
2.3.3 Comparison of Models....10
2.4 Simplified Henry Model....11
2.5 Parametric Study....13
2.5.1 Initial Conditions....14
2.5.2 Computational Results....15
3 CONCLUSIONS....18
4 RECOMMENDATIONS....19
REFERENCES....20
FIGURES
APPENDICES
A. A REVIEW OF UNDERWATER EXPLOSIONS
B. SIMPLIFIED HENRY MODEL
C. NUMERICAL SIMULATION OF UNDERWATER EXPLOSIONS
D. DERIVATION OF INITIAL BUBBLE CONDITIONS

1 INTRODUCTION

In a previous study (Lee & Knystautas, 1987) on the potential for steam explosion from a molten fuel-moderator interaction, it was concluded that an energetic steam explosion capable of inflicting severe structural damages cannot be ruled out as an improbable event. A critical review of the so-called "Henry Model" in a licensing submission indicated that the model is neither the most conservative nor represents the most probable or prototypical situation. Furthermore, the analysis carried out using the "Hicks and Menzies" thermodynamic model did not provide a realistic estimate of the dynamic pressure transients even though it may have provided the maximum work potential of a steam explosion. Therefore it was proposed that a hydrodynamic shock wave model be developed to describe the dynamic pressure transients associated with a violent steam explosion.

The mechanisms of steam explosion are understood only on a qualitative basis. It is generally acknowledged that the sequence of events are as follows: i) break-up of the molten fuel and dispersion of the coarse fragments to form a coarse mixture with the moderator, ii) triggering of the steam explosion by causing the vapor film on the molten fuel fragments to collapse locally, iii) propagation of the explosion throughout the mixture, and iv) production of shock and hydrodynamic flow generated by the expanding steam bubble. The state-of-the-art in the field does not permit the above mentioned processes to be modelled quantitatively. In the present study, we shall by-pass the first three processes and study in detail only the shock and hydrodynamic flow generated by the steam bubble since the interest is on the pressure transients developed to estimate the structural loadings. As a conservative estimate, the initial conditions will be the same as that in the Hicks and Menzies model analyzed previously. However, instead of assuming an infinitely slow isentropic expansion to calculate the work potential as in the Hicks and Menzies thermodynamic model, the Navier Stokes equations are integrated numerically to obtain the shock flow structure. The model is thus similar to that of an underwater explosion. The only difference is that in the case of an underwater explosion of a TNT high explosive charge the gas bubble is noncondensible combustion products while a condensible steam bubble is considered in the present case. For pedagogical reasons, it appears logical to review briefly the state-of-the-art in the theoretical description of underwater explosions prior to the development of the present model.

As is well known in underwater explosions, compressibility effects are negligibly small even for very high pressure transients. Thus the incompressible model of Rayleigh (1917) or the slightly compressible acoustic models of Trilling (1952) or Kirkwood and Bethe (1942) quite often yield results extremely accurate as compared to the exact numerical solution of the Navier-Stokes equations. Thus it seems logical to develop such approximate models and evaluate their accuracy with the exact solution and use these models henceforth for parametric studies where numerous test cases have to be run.

Finally, it was recommended in the previous study (Lee & Knystautas, 1987) that the analyses and computational procedures of the "Henry Model" be clarified to permit the results as stated in the licensing submission to be duplicated independently. It was further pointed out that certain features of the "Henry Model" are unnecessarily complicated and their omission would not significantly influence the final results. Thus a simplified Henry model is developed wherein the essential features of the original model are retained and the unnecessary complications are eliminated. This simplified Henry model can then be used should further results based on the original model be desired.

The present report summarizes the results of the above mentioned studies. To permit better access to the results, details of each of the various investigations are given in a separate appendix. In the next section, a summary of the essential results of each of the various studies are presented. General conclusions and recommendations are then given.

2 SUMMARY OF RESULTS OF VARIOUS INVESTIGATIONS

2.1 Review of Underwater Explosions

Underwater explosions have been studied by numerous investigators since World War II for a wide variety of explosives ranging from condensed explosives, and electric discharges, to collapsing vapor bubbles and fuel-oxygen detonations. The initial stage of an underwater explosion involves the sudden release of energy that results in the formation of a high-pressure bubble. The underwater explosion of a conventional solid explosive creates a bubble of hot product gases at high temperature (2000—4500K) and pressure (15,000—40,000 MPa), whereas in the case of a fuel-coolant interaction, the pressures generated within the steam bubble are lower (10's—100's MPa). The sudden energy release generates a primary shock wave in the surrounding water and acoustic oscillations in the gas bubble. Initially, the shock wave propagates at a supersonic velocity, however it

quickly decays to the speed of sound in water (approximately 1500 m/s). This process is followed by rapid expansion of the steam bubble. The expanding bubble creates a convective radial flow ahead of it due to the displacement of the water. The bubble overshoots its equilibrium radius as a result of the inertia of the surrounding water and eventually collapses and oscillates. The dynamics of the oscillations of the gas bubble are controlled by the size, pressure and compressibility of the bubble, and the density of the surrounding liquid. Following the initial shock wave, a series of smaller pressure waves are generated at the minimum radius of each bubble oscillation cycle. A schematic of an underwater explosion is shown in Fig. 1 (from Swisdak, 1976).

The most comprehensive compilation of information on underwater explosions is that of Cole (1948), although it does not include the developments in the field over the last 40 years, particularly the use of numerical computation for studying underwater explosions. A more recent review is that of Holt (1977). The importance of interface effects in underwater explosion phenomena has been pointed out by Shepherd (1988). State-of-the-art calculations of underwater explosions involve numerical solution of the governing equations (continuity, momentum and energy conservation) together with appropriate equations of state for the gas bubble and the surrounding water. An example of such calculations can be found in Sternberg and Hurwitz (1976) (more details are given in Sternberg and Walker, 1971). They carried out spherical shock wave computations using a conventional Lagrangian artificial viscosity scheme, augmented by a sharp shock routine in which the main shock is fitted by the method of characteristics, with exact tracking of the shock inside the Lagrangian cells. The pressure profiles versus reduced distance at various times for a spherical Pentolite explosion are shown in Fig. 2. The decay of the peak shock pressure with reduced distance is shown in Fig. 3. At first, the shock pressure drops very rapidly, then beyond about 10 charge radii, the pressure drops off roughly inversely proportional to distance. Also included in Fig. 3 are experimental results for 36 and 23 kg spherical pentolite charges obtained at Woods Hole (Cole, 1948). The numerical results agree well with the experimental results.

During the propagation of a strong shock in water, a portion of the initial energy is dissipated due to shock heating of the water. Energy is deposited in successive spherical shells of water as they are traversed by the initial shock. The heating is confined to a layer surrounding the bubble because the shock wave decays rapidly after leaving the bubble interface. The amount of dissipation increases with the strength of the shock. The fraction of the initial energy that is dissipated as well as the energy distribution between the gas and

the surrounding water was computed by Sternberg and Hurwitz (1976) as a function of shock position for four different explosives and is shown in Fig. 4.

The extremely high pressures associated with underwater explosions using condensed explosives require the use of empirical equations of state for water which are valid under such extreme conditions. Improved equations of state for water make it possible to calculate the temperature distribution in the water and consider the possibility of vaporization at the interface as the pressure in the water near the interface returns to ambient pressure after the passage of the shock. Due to the lower pressure levels associated with underwater explosions generated by fuel-coolant interactions, the simple Tait equation of state for water can be used:

$$p = B[(\rho/\rho_o)^n - 1]; \quad B = 304\ MPa,\ n = 7.15, \tag{1}$$

where p is the pressure in MPa, and ρ and ρ_0 are the density and ambient density, respectively, which is found to be typically valid for pressures as high as 2500 MPa (Glass and Heuckroth, 1963). A more detailed description of underwater explosions can be found in Appendix A.

2.2 Numerical Simulation of Underwater Explosions

The decay of the shock wave generated during an underwater explosion can be determined by simultaneously solving the mass and momentum equations for a spherical coordinate system:

$$\frac{\partial \rho}{\partial t} + \frac{1}{r^2}\frac{\partial \rho u r^2}{\partial r} = 0 \tag{2}$$

$$\frac{\partial \rho u}{\partial t} + \frac{1}{r^2}\frac{\partial \rho u^2 r^2}{\partial r} + \frac{\partial p}{\partial r} = 0\ , \tag{3}$$

(ρ, u, p, are the density, velocity, and pressure, respectively, at a given radial position r and time t), in conjunction with the Tait equation of state. Due to the nonlinear form of these equations, a numerical solution requires the use of a finite-difference code capable of handling sharp pressure gradients occurring at the shock front without excessive instabilities or artificial diffusion. One algorithm which has a very good track record in the

simulation of transient compressible flows is the Flux Corrected Transport (FCT) method of Boris (1976) which is particularly noted for its relatively low level of artificial diffusion.

Calculations were carried out using a fully nonlinear, one-dimensional finite-difference numerical code based on the FCT algorithm. To calculate an initial bubble pressure for the code calculation, a procedure based on the "Hicks and Menzies" approach similar to that used in an earlier contract (Lee and Knystautas, 1987) was used. In particular, during fuel-coolant interaction, it was assumed that the fuel and coolant transfer heat at constant volume until an equilibrium temperature is reached. With the assumption of constant volume heat transfer and using steam tables, the initial high temperature and pressure inside the bubble can be calculated. An initial pressure of 28.0 MPa was used in the calculations (see Appendix D for the details of the calculation method). The motion of the bubble interface was derived independently by solving Trilling's acoustic bubble oscillation equation (described in section 2.3) with an initial bubble velocity of 19.1 m/sec which was obtained from the linear acoustic relation for the fluid velocity behind the transmitted shock.

The pressure profiles derived from the FCT code calculations are shown in Fig. 5. The flow inside the bubble was also calculated by the code in order to estimate the magnitude of the gas-dynamic oscillations occurring due to the sudden pressure release from the bubble. Inside the bubble, the FCT calculation shows relatively small gas-dynamic oscillations which are amplified near the centre of the bubble due to focussing effects. Near the interface, the pressure remains very close to that obtained assuming uniform isentropic expansion in the bubble. The FCT calculations also show a sharp spike in pressure at the interface which is due to a very slight error in the density at this point which is greatly amplified by the 7.15 power in the Tait equation of state. The solid lines in Fig. 5 are the results using an approximate acoustic model that agree remarkably well with results from the more complete finite-difference FCT analysis. A description of various approximate methods for simulating underwater explosions will now be given.

2.3 Approximate Models

A variety of models have been proposed to describe the oscillation of an underwater bubble. In the simplest models, the liquid surrounding the bubble is assumed to be incompressible. More accurate models include the effect of the compressibility of the liquid. For the purpose of modelling the growth of a steam bubble following a fuel-coolant interaction, calculations were carried out with the following three different analytical

models (in increasing order of complexity): an incompressible model (Rayleigh, 1917), a "quasi-acoustic" model which assumes constant sound speed in the liquid (Lyuboshits and Pervushin, 1972; Trilling, 1952; Keller and Kolodner, 1956), and the fully compressible model of Kirkwood and Bethe (1942). In each of the models, the gas inside the bubble is assumed to be ideal which is further assumed to expand and compress isentropically such that

$$p(R) = p_o \left(\frac{R_o}{R}\right)^{3\gamma} \tag{4}$$

where p_o = initial pressure in bubble
R_o = initial bubble radius
γ = ratio of the specific heats of the gas

When the models take the liquid compressibility into account, the Tait equation of state for water is used.

2.3.1 Incompressible Model

The dynamics of the oscillation of a gas bubble in a fluid was first analyzed by Rayleigh (1917). Assuming *incompressible* flow and neglecting surface tension and liquid viscosity, Rayleigh used the momentum equation to derive a differential equation for the motion of the bubble boundary. The equation is easily extended to include the effects of surface tension and liquid viscosity (e.g., see Plesset and Prosperetti 1977). If the radial growth of the bubble is known as a function of time, then the pressure history in the liquid can be determined using the Bernoulli equation.

Assuming incompressible flow, the velocity in the liquid surrounding a spherical expanding bubble, from the continuity equation, is

$$u(r,t) = \frac{R^2}{r^2}\dot{R} \tag{5}$$

where r = distance from the bubble center
R = bubble radius
$\dot{R}$ = bubble radial velocity

Using the momentum equation together with the above continuity equation, the Rayleigh-Plesset equation for the growth of the bubble radius is

$$R\ddot{R} + \frac{3}{2}(\dot{R})^2 = \frac{1}{\rho}\left\{ p_b - p_\infty - \frac{2\sigma}{R} - \frac{4\mu\dot{R}}{R} \right\} \tag{6}$$

where $\ddot{R}$ = bubble radial acceleration
ρ = liquid density
p_b = pressure in the bubble
p_∞ = pressure at infinity
σ = surface tension
μ = liquid viscosity

The above equation neglects the effect of heat flow into or out of the bubble, so the bubble motion is controlled by the inertia of the liquid. The pressure distribution in the liquid is found from the general nonsteady Bernoulli equation to be

$$p(r,t) = p_\infty + \frac{R}{r}\left\{ p_b - p_\infty - \frac{2\sigma}{R} - \frac{4\mu\dot{R}}{R} \right\} + \frac{1}{2}\rho\dot{R}^2\frac{R}{r}\left\{ 1 - \left(\frac{R}{r}\right)^3 \right\} \tag{7}$$

The Rayleigh equation provides a good description of the bubble growth and oscillation provided that the initial pressure is sufficiently small that the bubble velocity remains much smaller than the sound speed in the liquid. This equation is also limited by the fact that the assumption of incompressible flow prevents any acoustic wave energy transfer from the gas to the surrounding water. Consequently, in spite of its nonlinear form, the oscillations obtained from this equation are always undamped.

2.3.2 Compressible Models

The inclusion of compressibility effects into the analysis essentially prevents a direct integration of the momentum equation since the velocity field can only be obtained by a simultaneous solution of both the mass and momentum equations. For the case of weakly compressible flow, the velocity field may be derived from the velocity potential which, in turn, may be assumed to obey the spherical acoustic wave equation:

$$\left[\frac{\partial}{\partial t} + c_o\frac{\partial}{\partial r}\right] r\phi = 0 \; ; \; u = -\frac{\partial\phi}{\partial r} \tag{8}$$

Trilling (1952) has shown that the inclusion of this additional equation and the exclusion of all terms of the order of $(u/c_o)^2$ or higher, where c_o is the ambient liquid sound speed, results in the following acoustic bubble oscillation equation:

$$R\ddot{R}\left(1 - \frac{2\dot{R}}{c_o}\right) = 1.5\dot{R}^2\left(1 - \frac{4\dot{R}}{3c_o}\right) = \frac{p(R) - p_o}{\rho_o} + \frac{R\dot{p}}{\rho_o c_o} \tag{9}$$

which reduces to the Rayleigh equation when $\dot{R} \ll c_o$. For small oscillations, this equation may be linearized. The intrinsic assumption in the acoustic equations is that the pressure waves, radiated from the bubble, travel at the sound speed in the liquid which is assumed to be constant. Naturally, as the initial bubble pressure is increased, the wave trajectory is determined by the velocity $u + c$ where both the fluid velocity, u, and the local sound speed, c, become time dependent variables which must also be determined as part of the overall solution. A relatively complex bubble oscillation equation taking these effects into account was in fact derived by Kirkwood and Bethe (1942).

In the acoustic approximation, the time dependent pressure and velocity fields outside the bubble may be derived from the time history of the bubble oscillation. Appropriate methods for calculating the external flow field have been presented by Trilling (1952), Keller and Kolodner (1956) and Lyuboshits and Pervushin (1972). Following the analysis of the latter, the calculation may be performed by assuming $G(r,t) = r\partial\phi/\partial t$ obeys the acoustic wave equation

$$\frac{\partial G}{\partial t} + c_o\frac{\partial G}{\partial r} = 0 \tag{10}$$

where G may be expressed through the momentum equation as

$$G(r,t) = r\left[h(r,t) + \tfrac{1}{2}u(r,t)^2\right] \tag{11}$$

where $h = \int(dp/\rho)$ and u denote the enthalpy and fluid velocity, respectively. Since in the linear acoustic limit, the enthalpy $h = (p - p_o)/\rho_o$, the characteristic equation approximately states that the total pressure (i.e., static + stagnation) in the liquid decays at a rate proportional to $1/r$ along the straight characteristic emanating from the bubble surface and

corresponding to the wave velocity in the ambient fluid. Furthermore, in this acoustic approximation, the velocity of the fluid may be estimated as

$$u(r,t) = \dot{R}\left(\frac{R}{r}\right)^2 + \frac{G(r,t)}{r\,c_o}\left(1 - \frac{R}{r}\right) \tag{12}$$

which consists of an incompressible flow term near the bubble surface and an acoustic decay term in the far-field. On the basis of the above equations, and the acoustic bubble oscillation equation, the pressure and velocity for any radius r and time t may thus be obtained (details are given in Appendix C).

2.3.3 Comparison of Models

To investigate the relative merits of the various models, a series of calculations were performed using the Rayleigh (incompressible), Trilling (acoustic), Kirkwood and Bethe (nonlinear acoustic) as well as a linearized acoustic equation over a bubble pressure range of 10 - 1000 MPa. The results, showing the radial bubble growth and oscillation as a function of time, as shown in Figs. 6 and 7. As expected, the models show very good agreement at low initial pressure with the exception that the Rayleigh equation fails to describe properly the acoustic oscillation decay. The acoustic effects also result in a reduction in the maximum bubble radius during the first oscillation and decrease in the overall oscillation period. It is also interesting to note that the acoustic model of Trilling, which assumes constant wave propagation velocity, leads to bubble oscillation trajectories which are very close to the more complex Kirkwood and Bethe model. In fact, from Fig. 7, the initial bubble growth phase, calculated using the acoustic model, is very close to the corresponding Kirkwood and Bethe results, even up to a pressure of 1000 MPa.

To compare the approximate acoustic model of Trilling with the finite-difference FCT model, the calculations described earlier using the FCT code were repeated with the acoustic model. Fig. 5 shows a comparison of the results (recall that the initial bubble radius and pressure are 1 m and 28.0 MPa, respectively). The acoustic calculation assumes uniform conditions inside the bubble, and therefore the pressure profiles are flat for radial positions less than the bubble radius. It is clear from the pressure profiles that the solutions obtained outside the bubble are *virtually identical* for both methods. Overall, the performance of the acoustic model is excellent and results in profiles which are, in fact, better resolved near the shock than the FCT calculation which was performed using 100

computations cells inside the bubble and nearly 4000 cells outside. Considering that computational times for these FCT and acoustic calculations were *10 hrs* and *1.5 min*, respectively, on a machine with a computational power similar to the VAX780, it would appear that the acoustic model represents the most economically appropriate model for the calculation of bubble growth due to a fuel-coolant interaction. Since the Trilling oscillation equation is also based on the acoustic approximation, and is in very close agreement with the more general Kirkwood and Bethe equation, it would seem that the use of this equation is preferable to using a complete finite difference analysis to solve for the motion of the bubble interface. Indeed, due to the very large gradients which are observed near the interface, and the constant compromises made in finite difference codes to resolve both stability and artificial diffusion problems, we have found that the use of such codes to predict the gas-water interface motion is probably considerably less accurate than bubble oscillation equations which are derived from integral methods and not susceptible to computational errors near the interface.

2.4 Simplified Henry Model

Henry and Fauske (1983) proposed a model for the analysis of the thermal interactions following a hypothetical severe blockage of a fuel channel. The sequence of major events assumed in Henry model is: (i) a severe flow blockage leading to, (ii) melting of the fuel bundles, (iii) thermal attack on the pressure/calandria tube walls, (iv) resulting in rupture of the tubes, (v) discharging hot molten fuel and hydrogen mixture from the ruptured tube to the coolant-moderator, (vi) the rapid heat transfer from the molten fuel fragments to the coolant-moderator, (vii) which gives rise to rapid steam generation, and (viii) the expansion of the vapor bubble, resulting in strong hydrodynamic transients in the calandria vessel. In view of the unknown quantities and the numerous arbitrary assumptions inherent in the Henry model, it is felt that it can be greatly simplified and yet retain its essence to facilitate the use of the model itself. The details of the simplified model can be found in Appendix B. A summary of the results is given in the following.

In the detailed Henry model, two discharge scenarios, based on the stratified or dispersed flow models, are analyzed. The stratified flow model assumes that hydrogen and molten fuel are separated, with the hydrogen occupying the upper half of the then ballooned pressure tube. The dispersed flow model assumes that hydrogen and molten fuel mix homogeneously throughout the cross section of the pressure tube and flow toward the break at the same speed. We feel that the main heat source is the molten fuel in view of its

high temperature and heat capacity and we therefore neglect the contribution from the hydrogen. This dispenses with the need to analyze a two phase heat source. The simplified core melt efflux scenario and growth of the steam bubble are illustrated schematically in Fig. B-1.

The core melt efflux velocity is taken to be given by the Bernoulli relation and the acoustic considerations used by Henry are disregarded. The pressure tube rupture area follows that used by Henry, namely that it is of fish-scale diamond shape and that it grows to a maximum size in time t_o. The expression for the rate of heat release by the molten fuel is the same as in the Henry model except that it neglects the time of flight across the bubble and the relaxation factor, which is totally arbitrary. The simplified model disregards the steam recondensation at the bubble surface. We feel that, at this stage, this is a non-essential second-order effect especially since reliable quantitative data are not available. The heat flux from the core melt goes into vaporization of steam in the bubble and the rate of steam generation is identical to the Henry formalism except that we neglect the efflux of hydrogen into the bubble. The bubble pressure is determined from the moles of steam in the bubble. The bubble growth and pressure field outside the bubble are determined from Rayleigh's model, identical to that used by Henry.

The simplified Henry formalism was used to carry out calculations of steam bubble growth and pressure field in the moderator coolant. Two core melt temperatures were chosen to represent the heat source term, namely $T_F = 2473K$ and $T_F = 3273K$. The rupture time t_o was taken arbitrarily as by Henry to be $t_o = 1$ ms. The pressure field was calculated for the unbounded coolant environment (the so-called infinite sea model). The results from the simplified analysis are compared to those available in the report of the detailed Henry model calculations at different radial positions. Figs. B-2 and B-3 show the pressure field as a function of time at $r = 0.292$ m and $r = 0.635$ m. The qualitative trend of the results for the simplified and detailed Henry model is similar. The simplified Henry calculations give peak pressures about twice that of the detailed Henry calculation. However, it must be pointed out that the curves extracted from the Henry report do not specify what T_F was used in the calculations nor any other pertinent details. In spite of this, since the simplified model neglects mitigative effects such as steam recondensation, relaxation factors and core melt transit time considerations, then the higher values are not too surprising. These effects as used in the detailed Henry model are accounted for on an entirely arbitrary basis. The more important reassuring conclusion is that the simplified model is qualitatively correct

and thereby provides a convenient means to carry out a range of calculations using a variety of input parameters.

Figs. B-4 and B-5 show pressure-time profiles at three different radial positions; namely, r = 0.2 m, r = 0.5 m and r = 4.23 m. Fig. B-4 corresponds to a core melt temperature T_F = 2473K, while Fig. B-5 is for T_F = 3273K. It is to be pointed out that the peak pressure is equivalent to the steam bubble pressure. The decay of the steam bubble pressure with time, as the bubble grows, is shown in Fig. B-6 which again corresponds to T_F = 2473K and T_F = 3273K, respectively. The peak bubble pressure is 10 MPa which corresponds to the pressure tube pressure P_o = 10 MPa. Obviously, if the bubble pressure exceeded that level then this would choke off the core melt efflux. Finally, the spatial pressure distribution and bubble interface position are shown in Figs. B-7 and B-8 at different times. The bubble pressure is constant corresponding to the flat initial portion of each curve. Thereafter, the pressure field decays asymptotically to P_∞ as $r \rightarrow \infty$.

2.5 Parametric Study

The acoustic model of Trilling described above has been used to calculate the pressure field generated due to the rapid expansion of a steam bubble during a molten fuel-coolant interaction. Four different cases have been considered to investigate the effects of varying the fuel mass discharged and the ratio of coolant mass to fuel mass. The conditions for the 4 cases calculated are shown below in Table 1. The parameters that are listed are as follows:

m_f = *mass of fuel*
m_c/m_f = *ratio of coolant to fuel mass*
R_o = *initial bubble radius*
p_o = *initial pressure (for instantaneous heat transfer)*
t_{pres} = *pressurization time*

Case	mf (kg)	mc/mf	Ro (m)	po (MPa)	tpres (ms)
1 (reference)	300	0.2	0.244	1500	2.00
4	75	0.2	0.1528	1500	1.26
7	300	2.0	0.526	300	4.30
8	75	2.0	0.330	300	2.65

Table 1 Summary of Test Cases

In the reference case it is assumed, following a fuel channel blockage, that the entire contents of one fuel channel melts and interacts with a given amount of coolant. To determine more realistic values for the initial conditions for the bubble growth, it is assumed that heat is transferred from the molten fuel to the coolant over a finite time period. The details of the calculation of the initial bubble conditions are given below.

2.5.1 Initial Conditions

The *reference case*, for example, assumes that $m_c/m_f = 0.2$, so that if the initial fuel mass is 300 kg, then the initial coolant mass is 60 kg. The initial conditions for the fuel and coolant are taken to be the following:

$$T_f = 3073K$$
$$T_c = 330K$$
$$\rho_i = 984\ kg/m^3$$
$$R_i = 0.244\ m$$

To obtain an accurate value for the coolant heat capacity over the temperature range of interest, values for c_v were taken from steam tables (Haar et al., 1984). Taking the average gives a value of $c_v = 3.8$ kJ/kgK. Equation (2) (from Appendix C) can be used to find that the equilibrium temperature following constant volume heat transfer is 1233K. From the T-s diagram for water/steam (from Haar et al., 1984), following a constant volume line, from an initial temperature of 330K to a final temperature of 1233K gives a corresponding equilibrium pressure of 1500 MPa.

This initial pressure is conservatively high due to the assumption in the calculation that the heat is transferred *instantaneously* to the coolant. In reality, of course, there is a characteristic time over which the thermal energy is transferred from the molten fuel to the coolant. An estimate for this thermal equilibration time may be determined using the diameter of the coolant volume together with a typical propagation speed for a steam explosion wave to travel through the fuel-coolant mixture. Propagation speeds are on the order of 100's m/s (for example, see Mitchell and Corradini, 1981), so that equilibration times are on the order of milliseconds. For a propagation speed of 250 m/s, the corresponding equilibration time (for an initial bubble diameter of 0.49 m) is about 2 ms. For an isentropic expansion of the bubble, the bubble pressure is related to the radius as follows:

$$p(R) = p_o (R_o/R)^{3\gamma} \qquad (13)$$

To simulate the finite heat transfer time, it is assumed that, during the heat transfer stage, the pressure p_o increases in a linear fashion for a time equal to the equilibration time (denoted t_{pres} for pressurization time in the figures). As a result of the finite pressurization time, the maximum pressure attained in the bubble is lower than the corresponding value assuming instantaneous heat transfer.

2.5.2 Computational Results

Case #1: Reference Case

In this case the total mass of fuel in one fuel channel (300 kg) is assumed to interact with 60 kg of moderator ($m_c/m_f = 0.2$). In Fig. 8 the bubble pressure and radius are shown as function of time for the first 10 ms of bubble growth. A maximum pressure of about 140 MPa is attained inside the bubble. Note that the small kink that is evident on the pressure profiles (at t = 2 ms) is due to the disturbance that is created when the energy input is "turned off" at the end of the pressurization time. The pressure transients at three other locations inside the calandria are shown in Figs. 9-11. In Fig. 11 the pressure transient at the calandria wall is given (i.e., r = 4.23 m). A peak pressure of about 11.5 MPa is attained at the calandria wall. This value is *larger* than the corresponding value predicted using the simplified Henry model by a factor of about 6 (see Appendix B for the results of the simplified Henry model). Therefore the results of the numerical simulation represent a more conservative prediction than the corresponding results from the Henry model. Overpressure profiles in the moderator are shown at 4 different times (0.5, 2.0, 2.7, and 10.0 ms) in Figs. 12-15. The time of 2.7 ms corresponds to the time at which the initial shock wave reaches the calandria wall.

Case #4: Effect of fuel mass discharged

In this case, the same value of the ratio of coolant to fuel is used as in the reference case ($m_c/m_f = 0.2$), but the fuel mass is assumed to be 25% of the total fuel in one channel (i.e., $m_f = 75$ kg). With the smaller amount of fuel participating in the explosion, the resulting steam bubble has a smaller diameter. The bubble pressure and radius are shown as functions of time in Fig. 16. Figs. 17-19 show the pressure transients at three different

locations within the calandria. A peak overpressure of about 7.0 MPa is attained at the calandria wall.

Case #7: Effect of ratio of coolant mass to fuel mass

In this case it is assumed that the total mass of fuel in one fuel channel (m_f = 300 kg) interacts with a large mass of moderator (m_c/m_f = 2.0). Due to the larger amount of water participating in the interaction, the peak bubble pressure is lower although the resulting steam bubble is larger. In Fig. 20, the peak bubble pressure attained is shown to be about 55.0 MPa. Figs. 21-23 show the pressure transients in the moderator at three different locations. From Fig. 23, the peak pressure attained at the calandria wall is about 9.0 MPa.

Case #8:

In this case 75 kg of fuel are assumed to interact with 150 kg of moderator (m_c/m_f = 2.0). The bubble pressure and radius are shown as a function of time in Fig. 24, and the pressure transients at two different locations are shown in Figs. 25, 26. From Fig. 26, the peak overpressure attained is less than 6.0 MPa, the smallest of all the cases considered.

The impulse ($\int p dt$) for each pressure transient over the time shown in the figures (10 ms) was calculated and the results are shown below in Table 2:

Case	Radial Position (m)	Impulse ($\int p dt$) (× 0.1MPa-s)
1	Inside bubble	1.86
1	0.35	1.69
1	2.12	0.63
1	4.23	0.31
4	Inside bubble	1.20
4	0.26	1.03
4	2.12	0.30
4	4.23	0.14
7	Inside bubble	1.99
7	0.63	1.92
7	2.12	0.95
7	4.23	0.46
8	Inside bubble	1.32
8	2.12	0.47
8	4.23	0.22

Table 2 Summary of Pressure Impulses

3 CONCLUSIONS

In this report numerical computations have been carried out to simulate the underwater explosion due to molten fuel-coolant interaction. The overpressure transients that are generated in the calandria following an energetic steam explosion have been calculated using a numerical code based on the fully nonlinear one-dimensional governing equations. This exact model predicts peak pressures within the calandria that are over an order of magnitude higher than the corresponding pressures predicted using from Henry model. In addition, calculations were carried out using a variety of approximate models for underwater explosion. The acoustic model of Trilling was found to produce pressure and velocity profiles outside of the bubble that are virtually identical to the corresponding profiles generated using the finite-difference code. In addition, compromises in the finite-difference code are necessary to resolve interface stability and artificial diffusion problems. The approximate models also have run-times that are several orders of magnitude less than those for the numerical code.

By eliminating the complex two phase transient flow inside the ruptured pressure tube, uncertainties in the heat transfer rates of the ejected molten fragments into the steam bubble, as well as the arbitrary assumption for the steam condensation rate, the simplified version of the Henry model appears to give the same qualitative results as the original model. However, the simplified model gives higher peak pressures, a fact that could be due to the neglected steam condensation. However, in view of the numerous arbitrary assumptions made in the original Henry model, it is difficult to assess if the simplified model is less accurate. However, it is more consistent and requires less arbitrary input. Also, its simplicity permits the model to be more accessible for others to carry out parametric studies.

A parametric study was carried out to calculate the pressure transients (and impulses) and pressure profiles within the calandria for a postulated fuel-coolant interaction scenario. Four different cases were considered in which the mass of fuel and the ratio of coolant mass to fuel mass were varied. The largest peak pressure at the calandria wall was attained for the reference case (in which the total fuel mass of one fuel channel, 300 kg, interacts with 60 kg of moderator). The peak pressures generated decrease with decreasing fuel mass and increasing ratio of coolant mass to fuel mass. The peak pressure values computed at the calandria wall were nearly an order of magnitude larger than the

corresponding values computed using the simplified Henry model. The largest impulse at the calandria wall was attained for the third case considered, in which a large quantity of moderator is assumed to interact coherently with the entire contents of the fuel channel. In this case the steam bubble generated is larger than that for the reference case, and the longer duration of the pressure transient counterbalances the lower peak pressure, generating a larger impulse.

4 RECOMMENDATIONS

The present contract was undertaken to provide a more representative *upper bound* for the peak pressures and impulses generated during a coherent explosive event. In this report, a numerical code based on a hydrodynamic shock wave model was used to describe the blast waves generated during the underwater explosion of a pressurized volume of steam following a postulated loss of coolant scenario. In the shock wave model, the initial conditions used by the code assume that a given amount of molten fuel is mixed with an optimum amount of moderator to produce the initial supercompressed liquid state prior to the explosion. Therefore, the model assumes *a priori* that a coarse mixture is formed plus a coherent wave propagation occurs. The probability of the shock wave model, i.e., the possibility of a coherent wave propagation and explosion are not considered in the present contract. A detailed experimental program is required to determine the necessary conditions for a large-scale coherent explosion of a coarse mixture. To address this question in the short-term, experiments are being initiated at McGill University to measure the explosion pressure (which is a measure of the coherence of a steam explosion) as the mass of the melt is scaled up, hence the volume of the coarse mixture. The effect of triggering and confinement on the coherence of the explosion will also be investigated.

To address the question of what are the necessary conditions for a large-scale coherent explosion of a coarse mixture to occur, a longer-term (5 years) research program is required. This program will address the fundamental processes involved in an energetic fuel-coolant interaction, e.g., triggering, film instability, fine fragmentation processes, hydrodynamic effects from an exploding fragment, and how these effects lead to propagation of the interaction. This program will require large-scale work which we anticipate to be funded jointly by the nuclear industry and McGill through an NSERC University-Industry Cooperative Grant. Implementation of such a program will establish a

strong base of expertise in fuel-coolant interactions in Canada which will provide valuable information for the reactor safety problem.

REFERENCES

M. I. Balashkand et al., Exploratory Geophysics, No. 15, Nedra, Moscow (1966).

M. I. Balashkand et al., Current State and Problems of Exploratory Geophysics, Nedra, Moscow (1970).

L. Bjorno and P. Levin, "Underwater Explosion Research Using Small Amounts of Chemical Explosives", *Ultrasonics* (1976).

J. P. Boris, "Flux Corrected Transport Modules for Solving Generalized Continuity Equations", Naval Research Laboratory Memorandum 3237 (1976).

D. W. Boyer, "An Experimental Study of the Explosion Generated by a Pressurized Sphere", *J. Fluid Mech.*, Vol. 9, p. 401 (1960).

R. H. Cole, Underwater Explosions, Princeton University Press, Princeton, N.J. (1948).

N. L. Coleburn, *Bull. Am. Phys. Soc.*, Vol. 6, p. 20 (1962).

S. Fujikawa and T. Akamatsu, "Effects of the Non-Equilibrium Condensation of Vapor on the Pressure Wave Produced by the Collapse of a bubble in a Liquid", *J. of Fluid Mech.*, Vol. 97, Part 3, pp. 481-512 (1980).

I. I. Glass and L. E. Heuckroth, "Hydrodynamic Shock Tube", *Phys. of Fluids*, Vol. 6, No. 4, pp. 543-547 (1963).

L. Haar, J. S. Gallagher, and G. S. Kell, NBS/NRC Steam Tables, Hemisphere Publishing, Montreal, (1984).

A. N. Hicks, "Optimization of Explosives for Use Underwater", Naval Construction Research Establishment, Scotland, United Kingdom (1968).

M. Holt, "Underwater Explosions", *Ann. Rev. of Fluid Mech.*, Vol. 9, pp. 187-214, (1977).

J. Keller and I. I. Kolodner, "Damping of Underwater Explosion Bubble Oscillations", *J. Appl. Phys.*, Vol. 27, pp. 1152-1161 (1956).

J. G. Kirkwood and H. Bethe, OSRD Report No. 588 (1942).

S. M. Kogarko and A. V. Lyubimov, "Examples of the Generation of Shock Waves in a Liquid", *Soviet Physics - Acoustics*, Vol. 15, No. 1, pp. 60- 63 (1969).

S. M. Kogarko, O. E. Popov, and A. S. Novikov, "Underwater Explosion of a Gas Mixture as a Source of Pressure Waves", Translated from *Fizida Goreniya i Vzryva*, Vol. 11, No. 5, pp. 795-767 (1975).

J. H. S. Lee, and R. Knystautas, "Molten Fuel-Moderator Interaction: An Investigation of the Potential for Steam Explosion", AECB Report INFO- 0227 (1987).

V. M. Lyuboshits and V. YE. Pervushin, "Numerical Analysis of the Fluctuation of a Gas Cavity in a Compressible Fluid", *Fluid Mechanics- Soviet Research*, Vol. 1, No. 1, pp. 61-70 (1972).

D. E. Mitchell and M. L. Corradini, "Intermediate Scale Steam Explosion Phenomena: Experiments and Analysis", SAND81-0124, NUREG/CR-2145, (1981)

S. Patterson and A. H. Begg, "Underwater Explosion", *Propellants and Explosives*, Vol. 3, pp. 63-69 (1978).

W. G. Penney, "The Pressure-Time Curve for Sub-Marine Explosion", *Underwater Explosion Research*, Vol. 1, The Shock Wave, Office of Naval Research (1950).

M. S. Plesset and A. Prosperetti, "Bubble Dynamics and Cavitation", *Ann. Rev. Fluid Mech.*, Vol. 9, pp. 145-185, (1977).

L. Rayleigh, *Phil. Mag.*, Vol. 34, pp. 94-98 (1917).

M. H. Rice and J. M. Walsh, J. Chem. Phys., Vol. 26, p. 284 (1957).

J. M. Richardson, A. B. Arons, and R. R. Halverston, *J. Chem. Phys.*, Vol. 15, p. 1785 (1947).

J. E. Shepherd, "Interface Effects in Underwater Explosions", ONR/GIT Workshop on Underwater Explosions, Atlanta, Georgia, Aug.2-3, (1988).

H. M. Sternberg and W. A. Walker, "Calculated Flow and Energy Distribution Following Underwater Detonation of a Pentolite Sphere", *Phys. Fluids*, Vol. 14, No. 9, pp. 1869-1878 (1971).

H. M. Sternberg and H. Hurwitz, "Calculated Spherical Shock Waves Produced by Condensed Explosives in Air and Water", 6th Symp. (Intl.) Detonation, Office of Naval Research - Department of the Navy ACR-221, pp. 528-539, (1976)

E. Swift et al., "Photography of Underwater Explosions II", NavOrd report by U.S. Navy Bureau of Ordnance.

M. M. Swisdak (Ed.) *Explosion Effects and Properties. Part II - Explosion Effects in Water*, NSWC/WOL TR 76-116, (1976).

L. Trilling, "The Collapse of a Gas Bubble", *Journal of Applied Physics*, Vol. 23, No. 1, pp. 14-17 (1952).

W. A. Walker and H. M. Sternberg, "The Chapman-Jouget Isentrope and the Underwater Shock Wave Performance of Pentolite", *Proceedings of the 4th Symposium (International) on Detonation* ACR-126, U.S. Gov't. Printing Office, Wash., D.C. pp. 27-38 (1965).

H. F. Willis, "Underwater Explosions: Time Interval Between Successive Explosions", British Report WA-47-21 (1941).

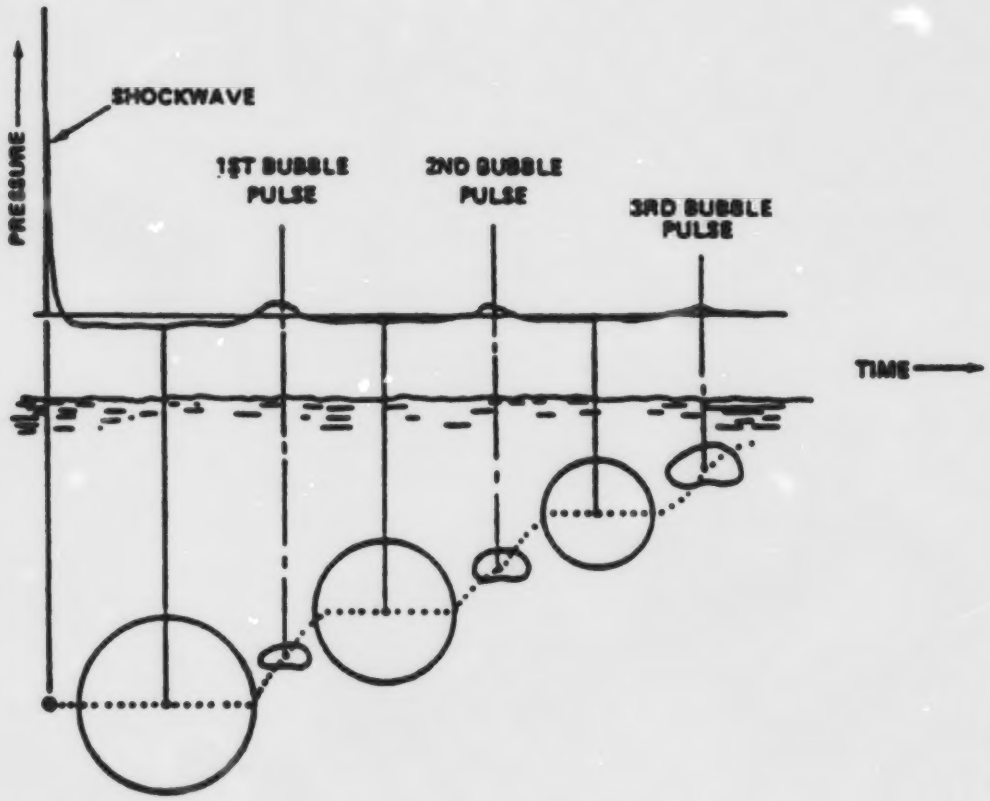

Fig. 1 **Schematic of an underwater explosion (from Swisdak, 1976)**

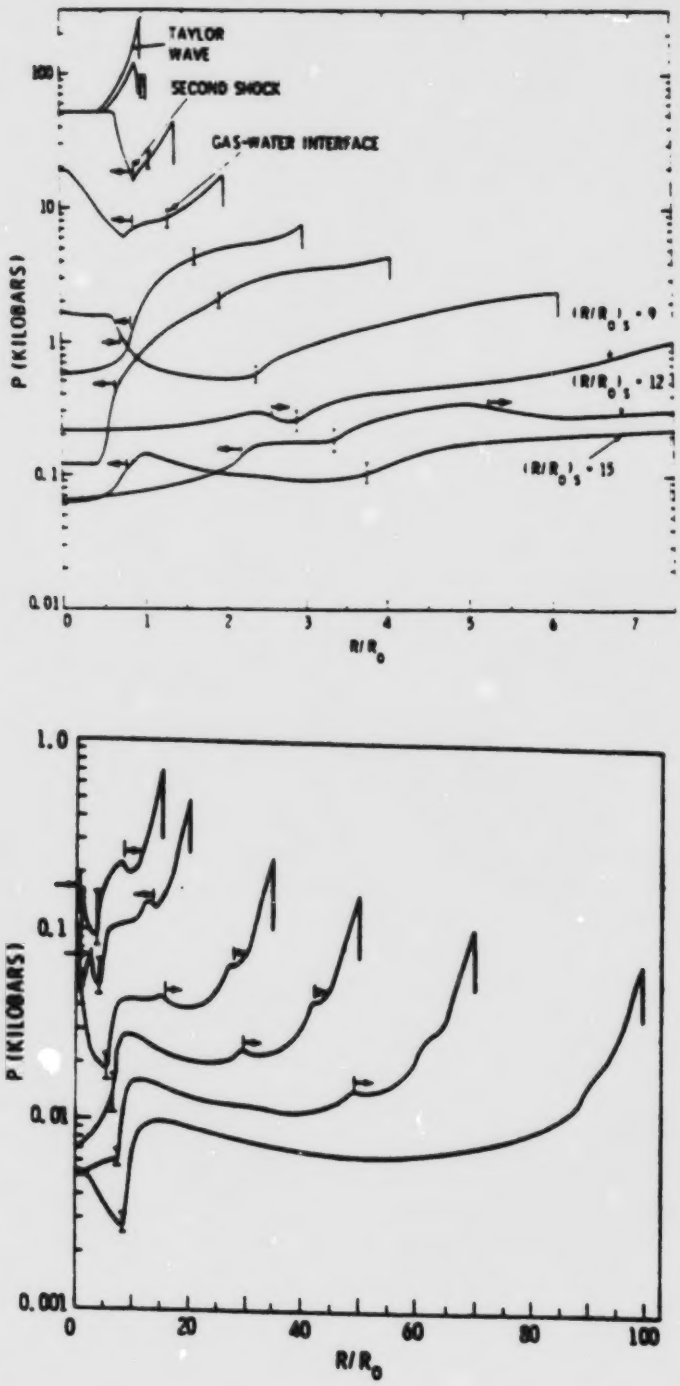

Fig. 2 **Pressure vs. reduced distance for a spherical Pentolite detonation at early times (top) and later times (bottom) (from Sternberg and Walker, 1971)**

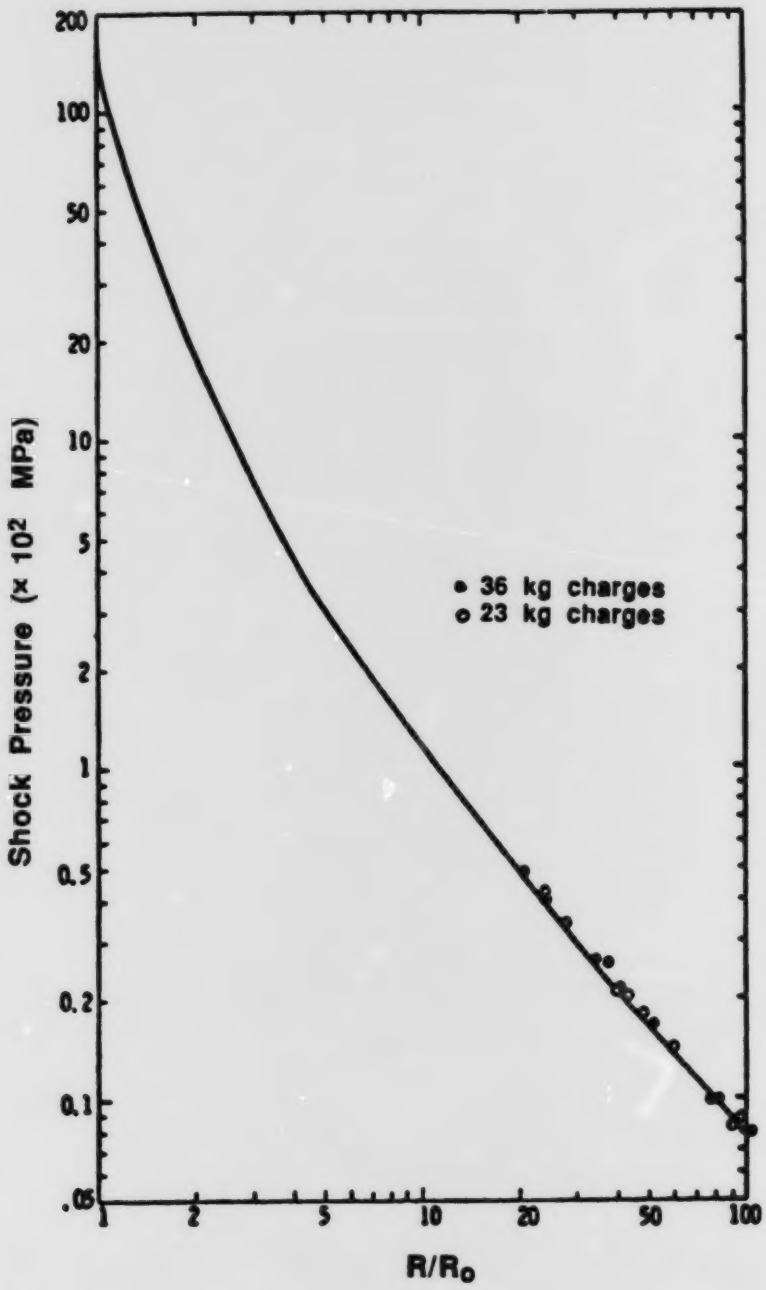

Fig. 3 **Calculated and experimental peak-pressures versus reduced distance (Sternberg et al., 1971)**

(a). Pentolite, centrally detonated

(b). PBX 9404, centrally detonated

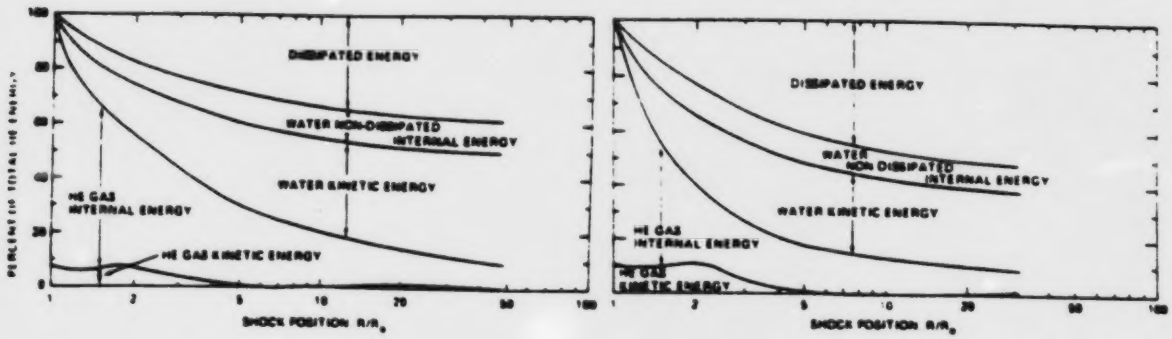

(c). Pentolite constant volume explosion. $\rho_0 = 1.65$.

(d). Pentolite constant volume explosion. $\rho_0 = 0.4125$.

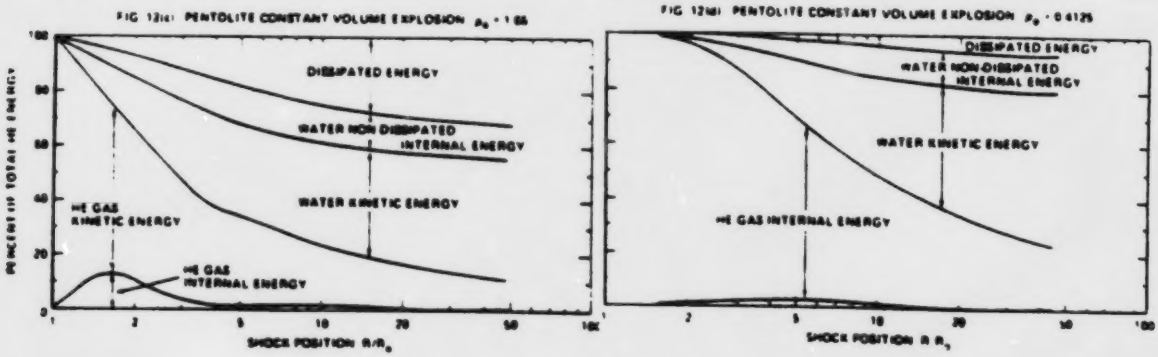

Fig. 4 Energy distribution as a function of shock position for four explosives (from Sternberg and Hurwitz, 1976)

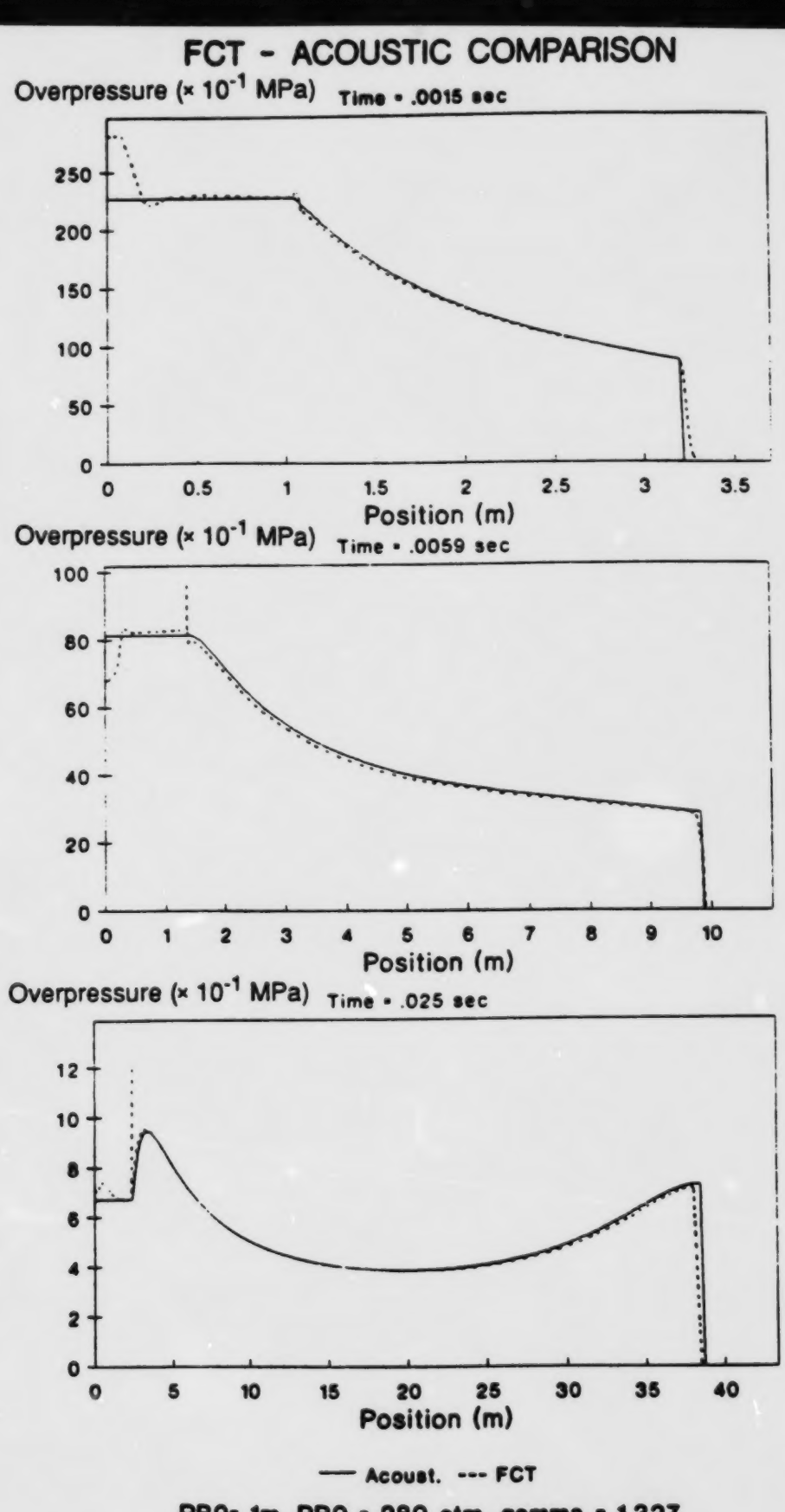

Fig. 5 **Pressure profiles computed using the acoustic model and the FCT numerical code at various times**

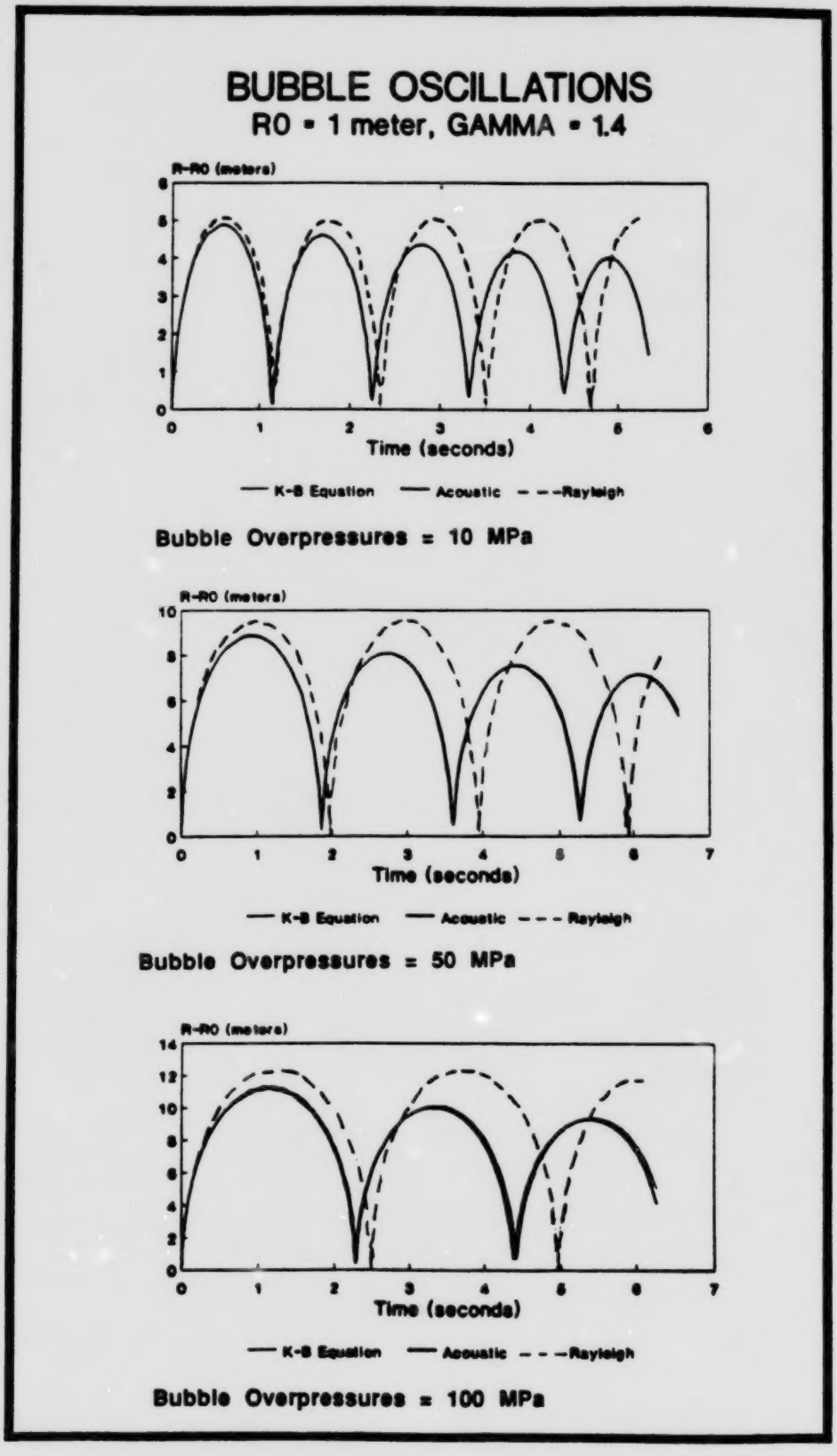

Fig. 6 **Bubble oscillations computed using various numerical models with initial bubble overpressures ranging from 10 to 100 MPa**

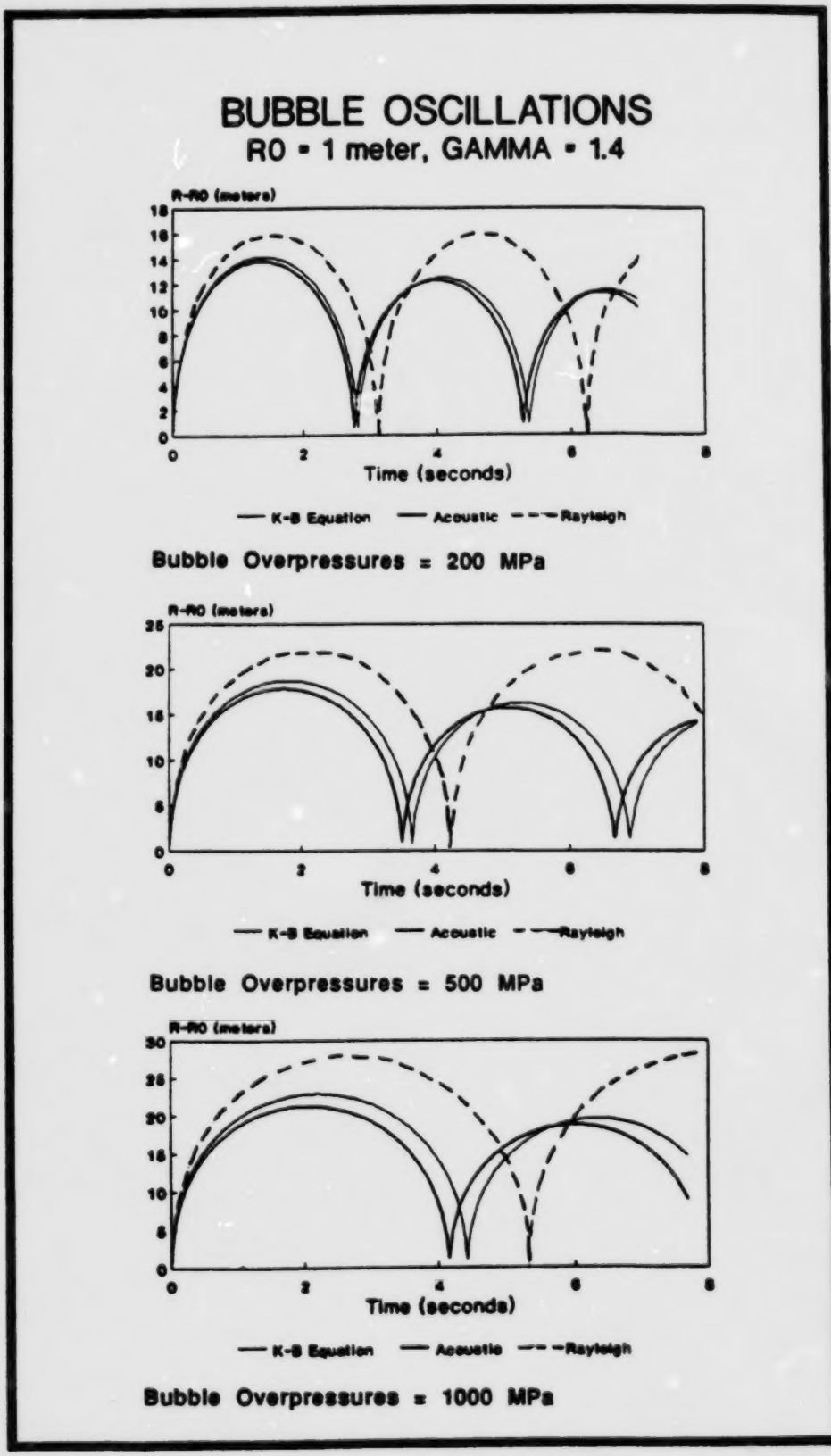

Fig. 7 **Bubble oscillations computed using various numerical models with initial bubble overpressures ranging from 200 to 1000 MPa**

Case #1
Bubble Pressure and Radius

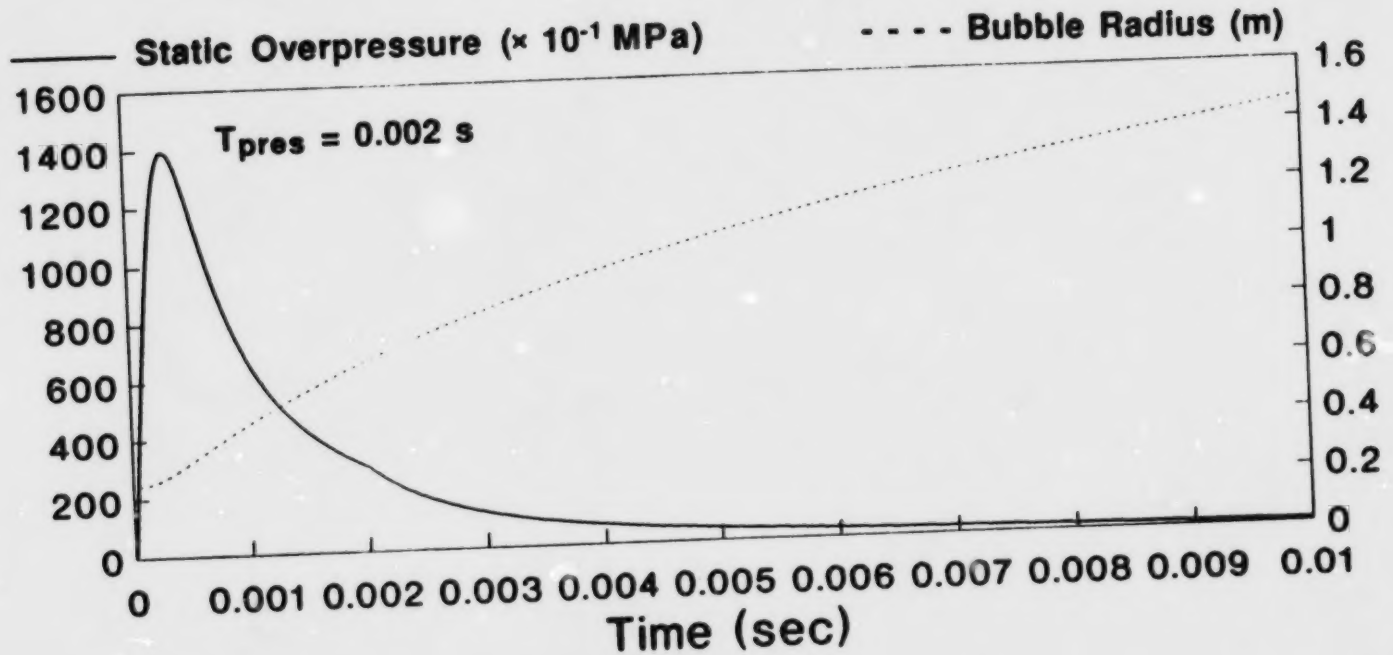

Fig. 8 **Bubble pressure and bubble radius as a function of time**

Case #1
Pressure at R = .35 m

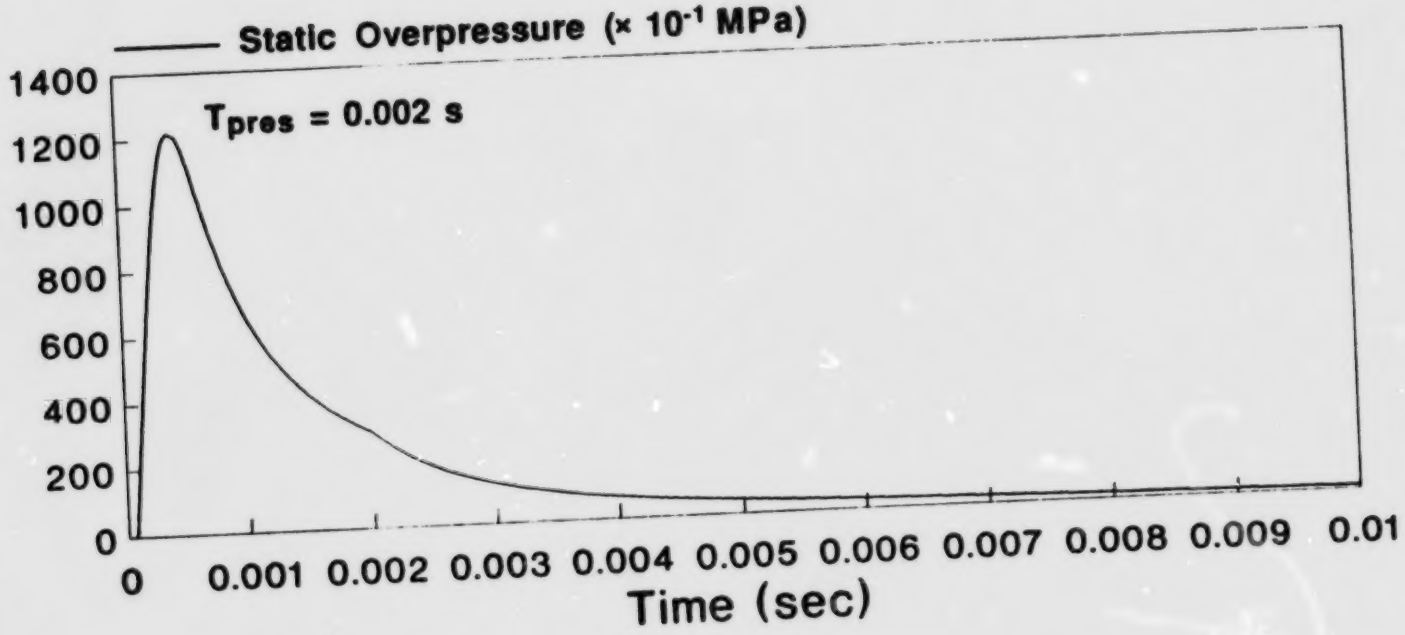

Fig. 9 Static overpressure transient in the moderator at r = 0.35 m from bubble center

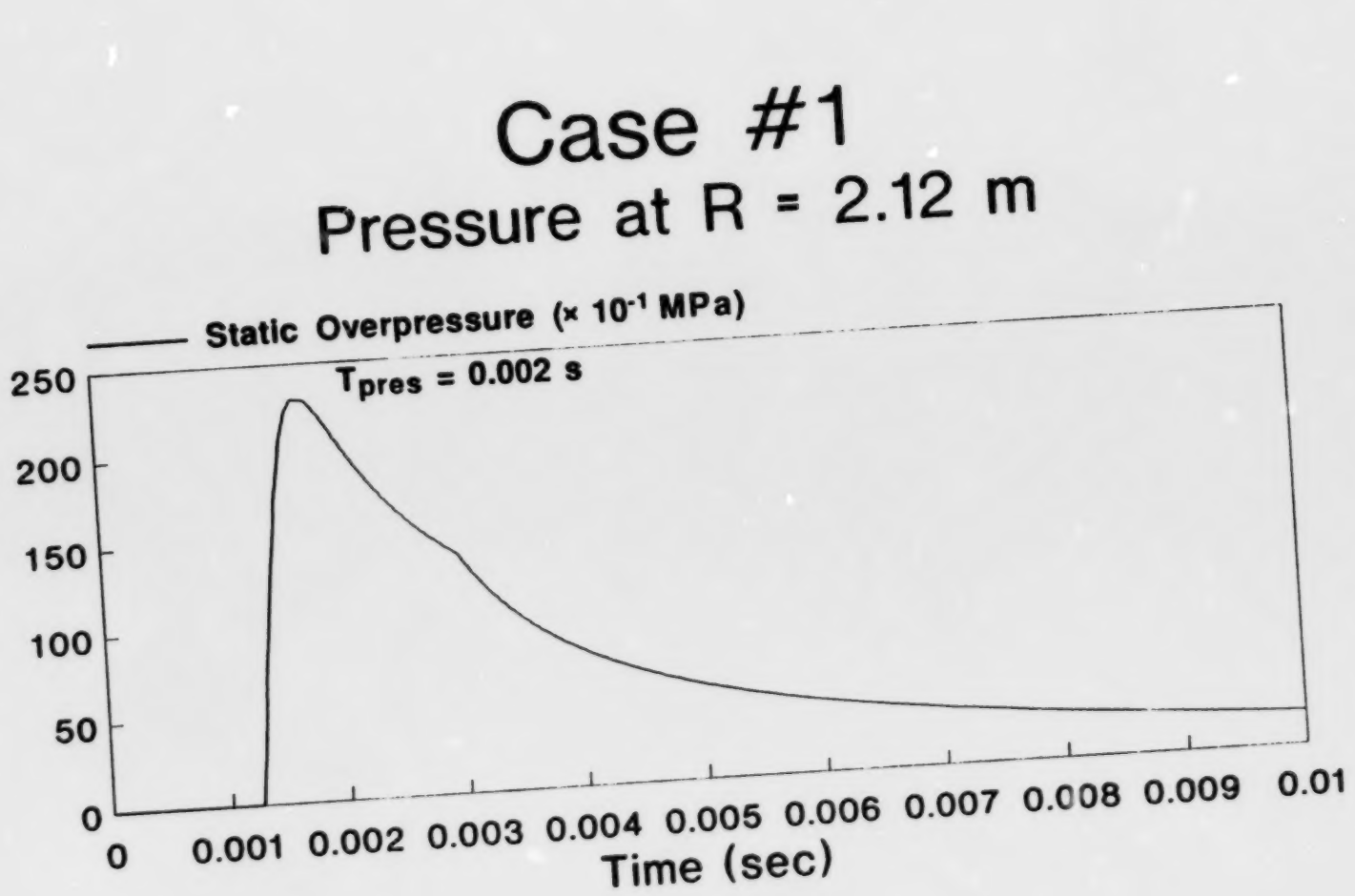

Fig. 10 Static overpressure transient in the moderator at r = 2.12 m from bubble center

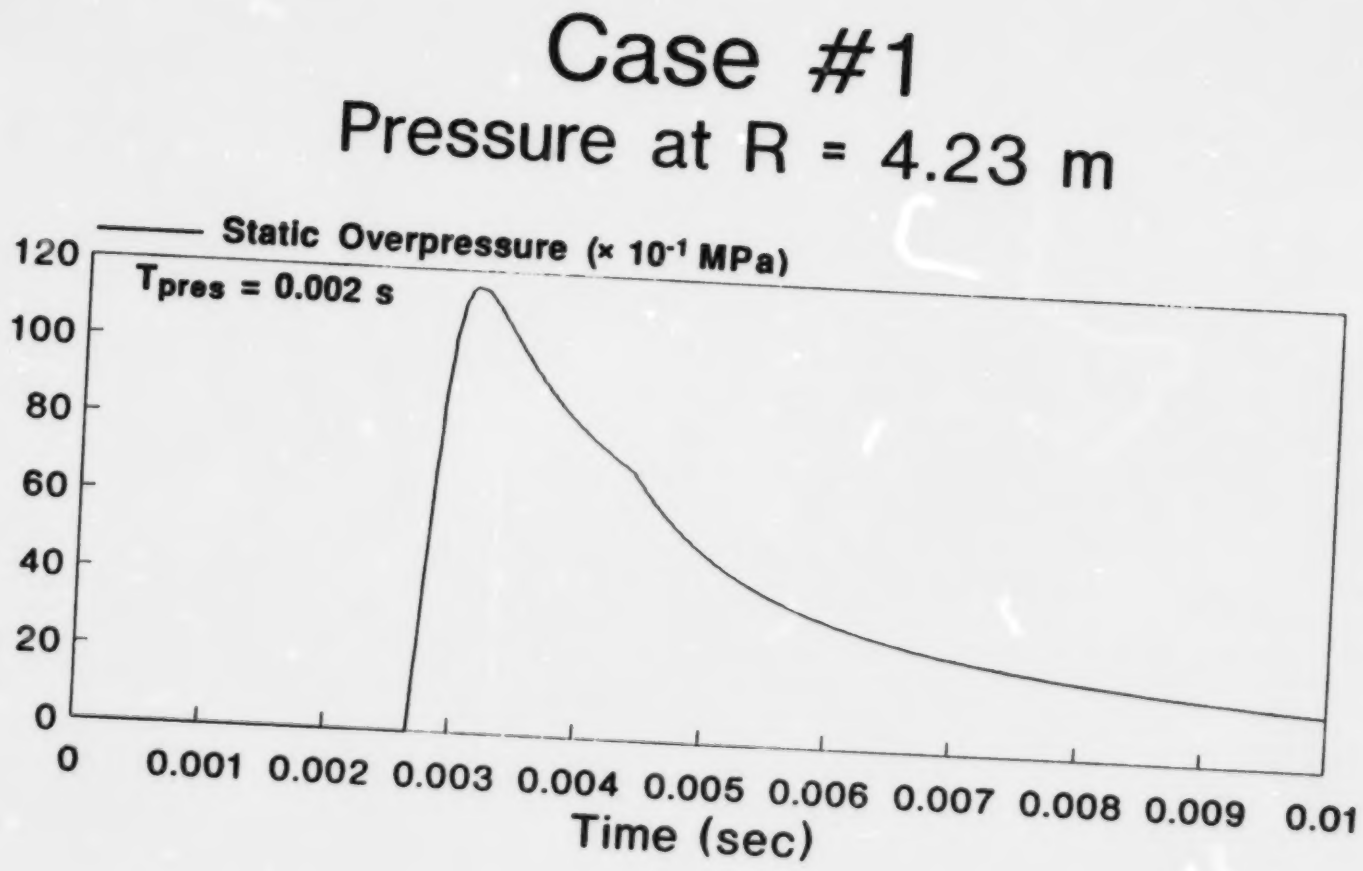

Fig. 11 Static overpressure attained at the calandria wall (r = 4.23 m) as a function of time

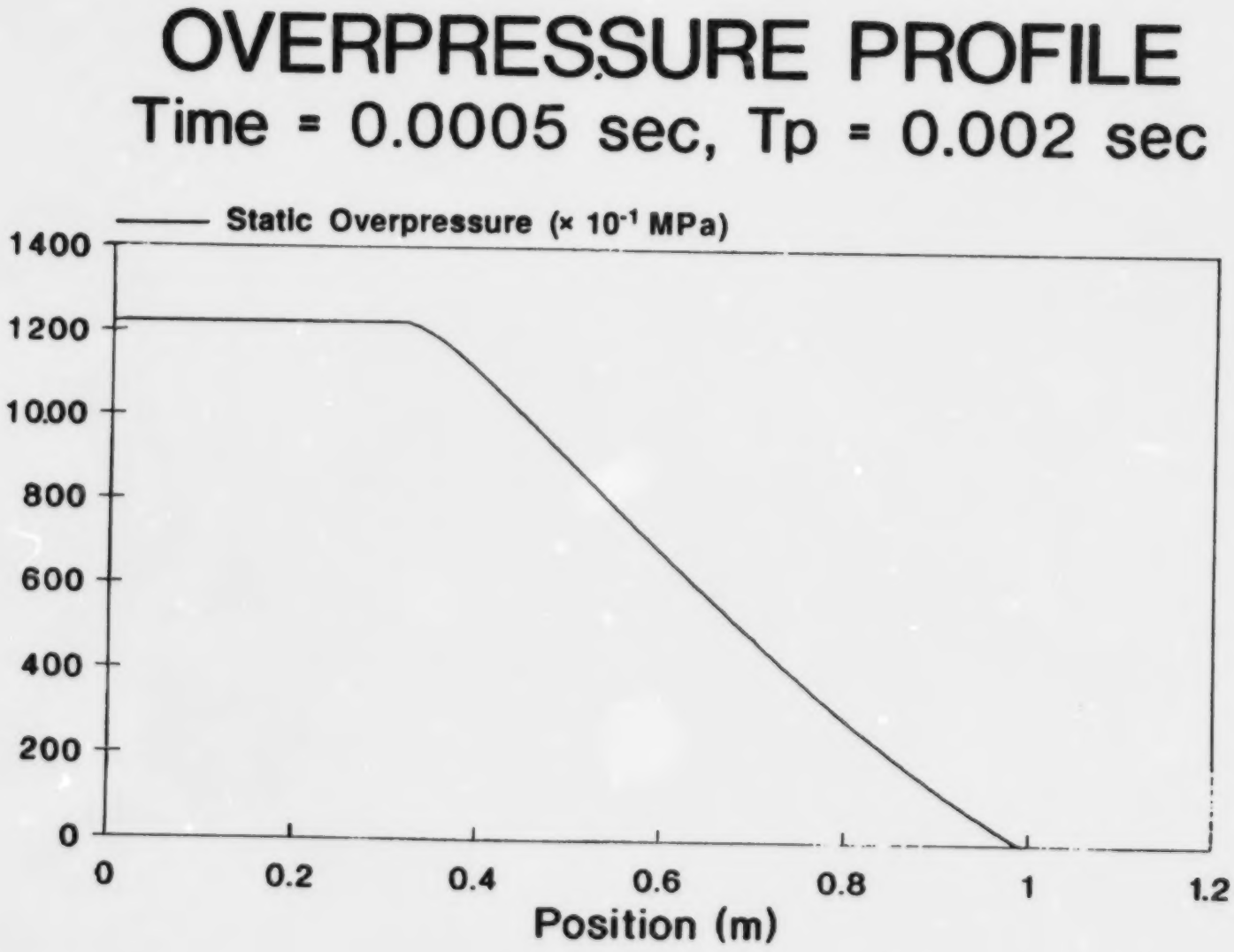

Fig. 12 Overpressure profile as a function of distance from the bubble center at t = 0.5 ms

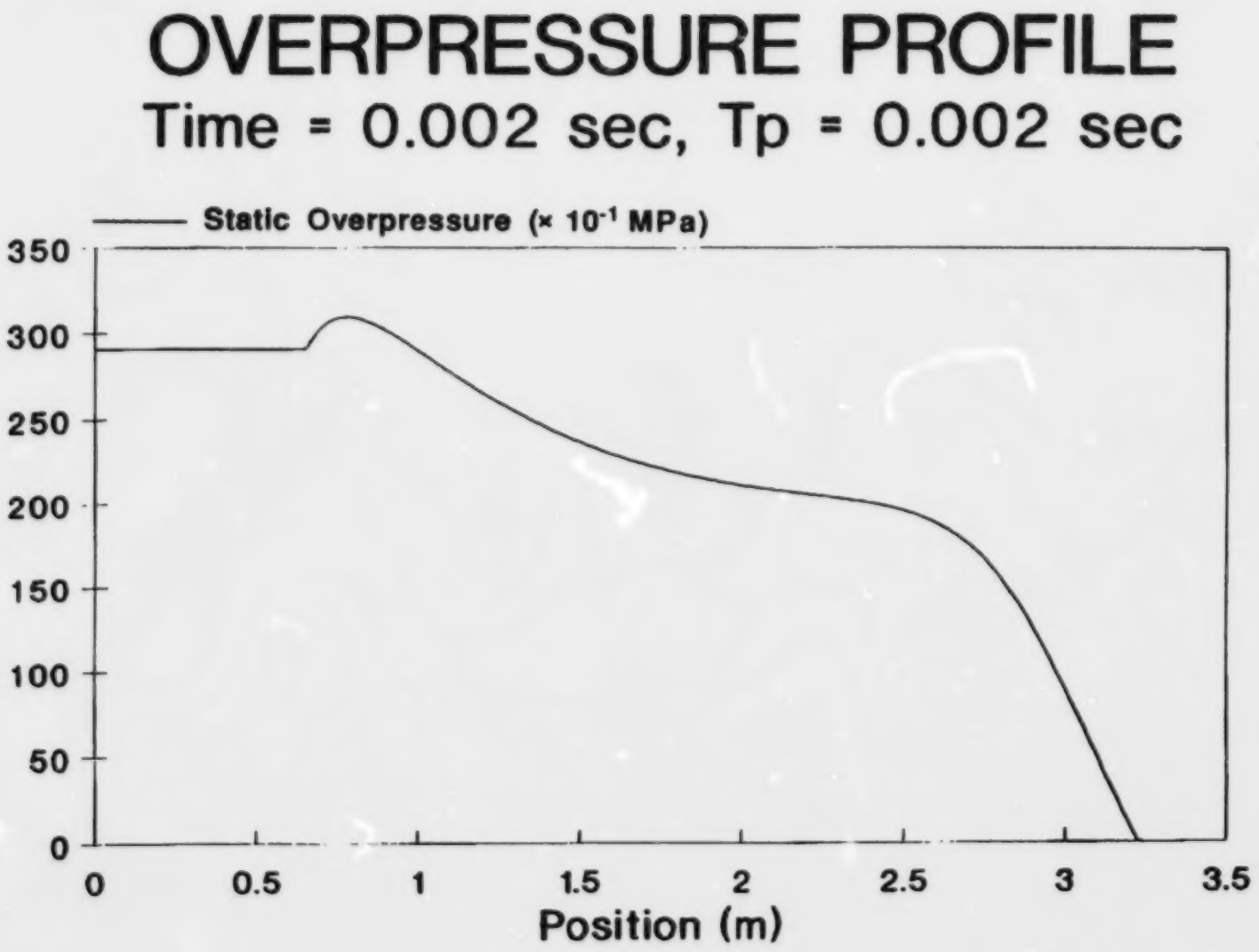

Fig. 13 Overpressure profile as a function of distance from the bubble center at t = 2.0 ms

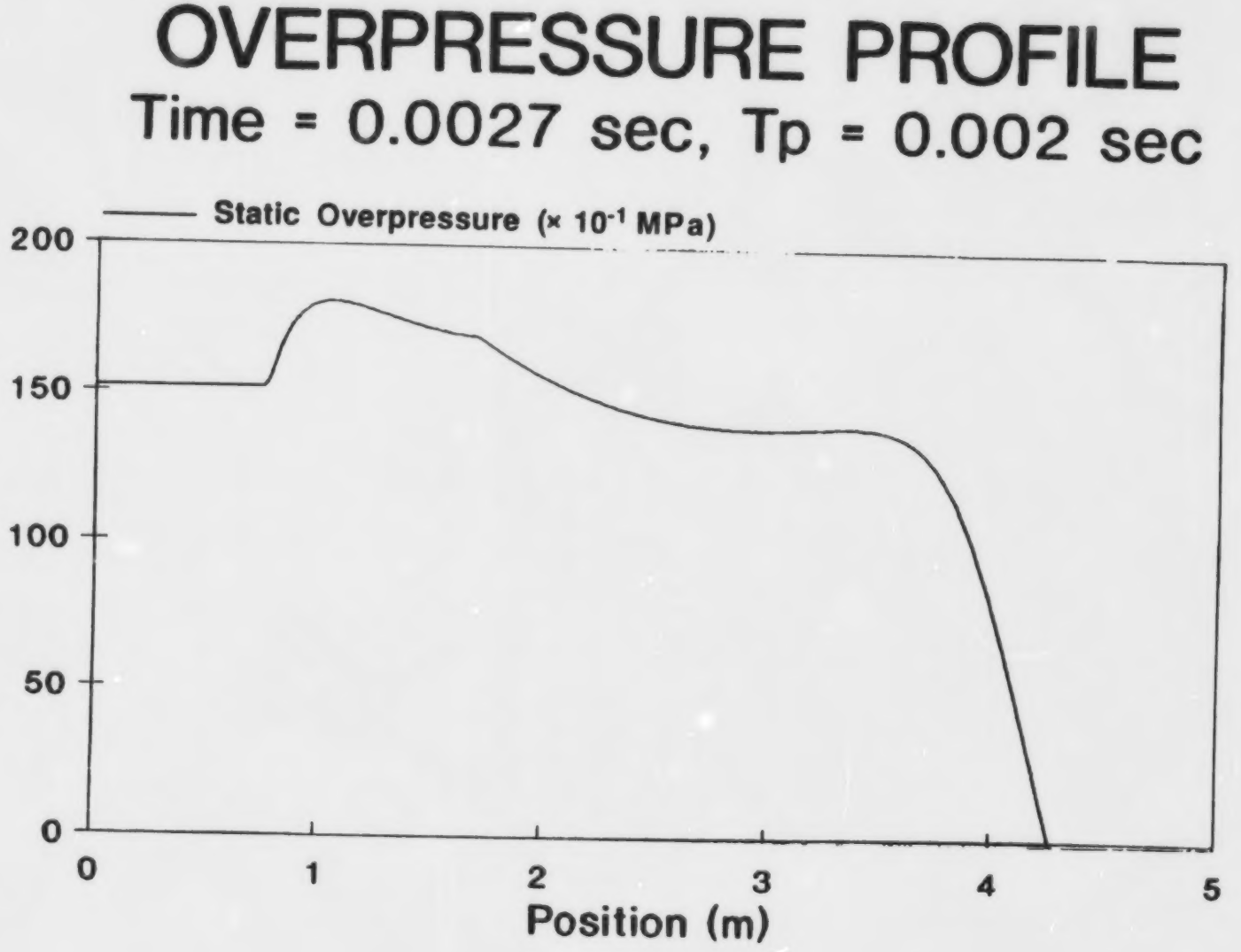

Fig. 14 Overpressure profile as a function of distance from the bubble center at t = 2.7 ms, (corresponds to the time at which the initial shock wave reaches the calandria wall)

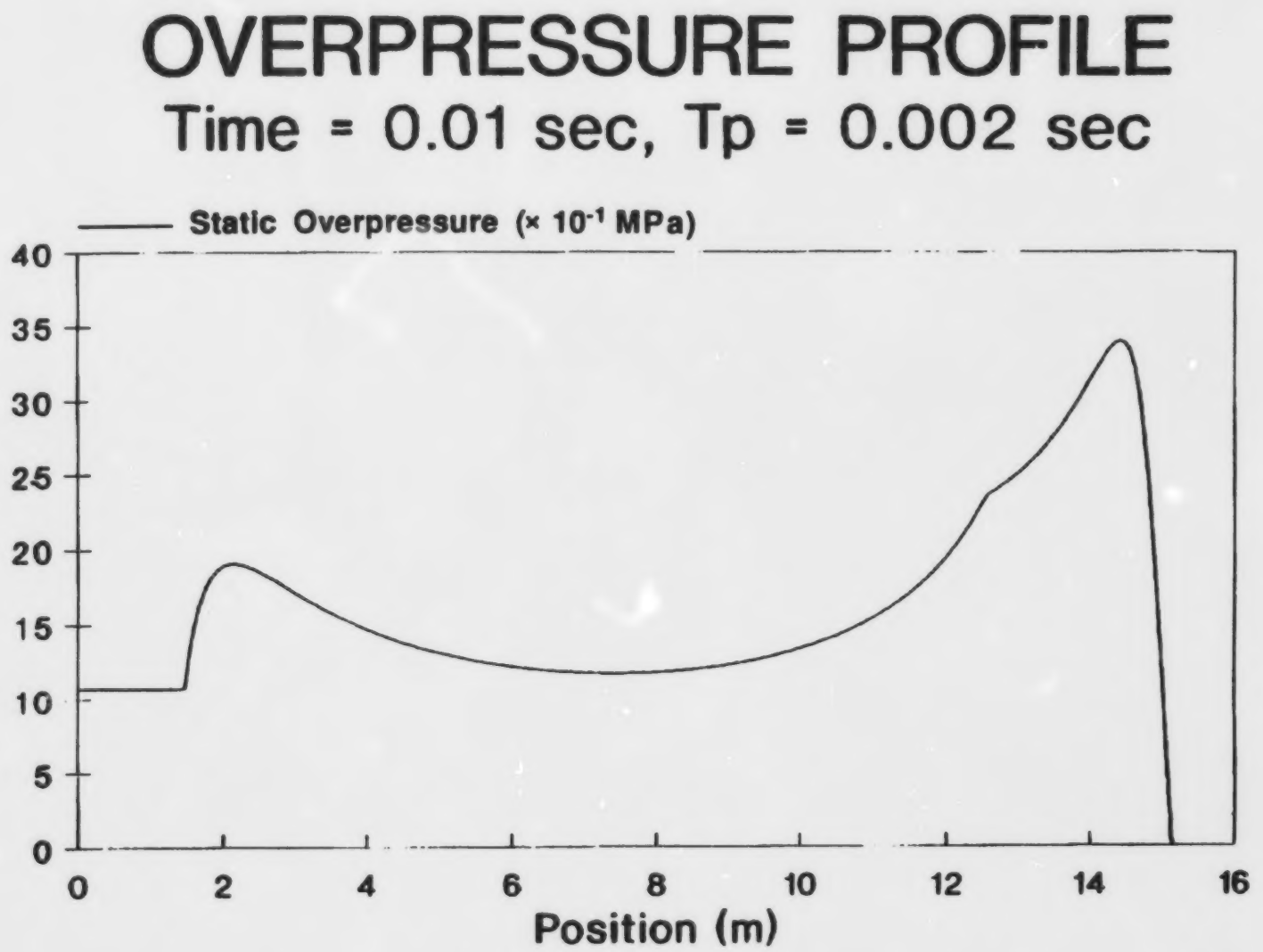

Fig. 15 **Overpressure profile as a function of distance from the bubble center at t = 10.0 ms**

Case #4

Bubble Pressure and Radius

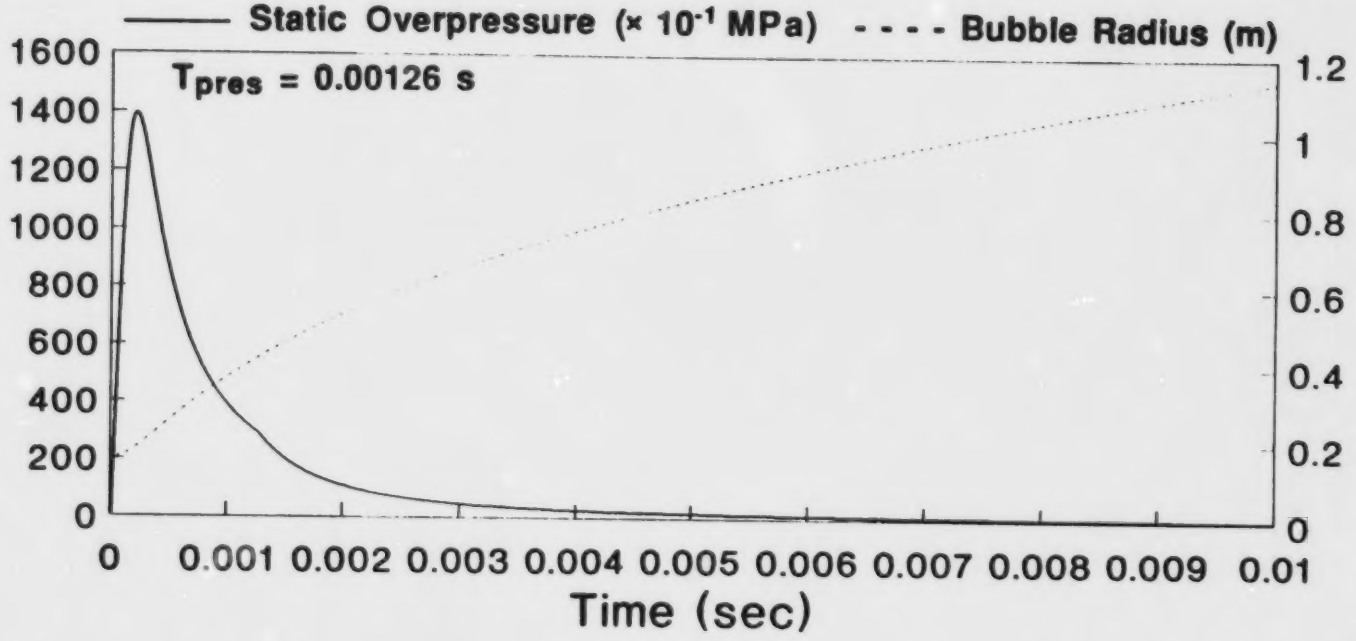

Fig. 16 **Bubble pressure and bubble radius as a function of time**

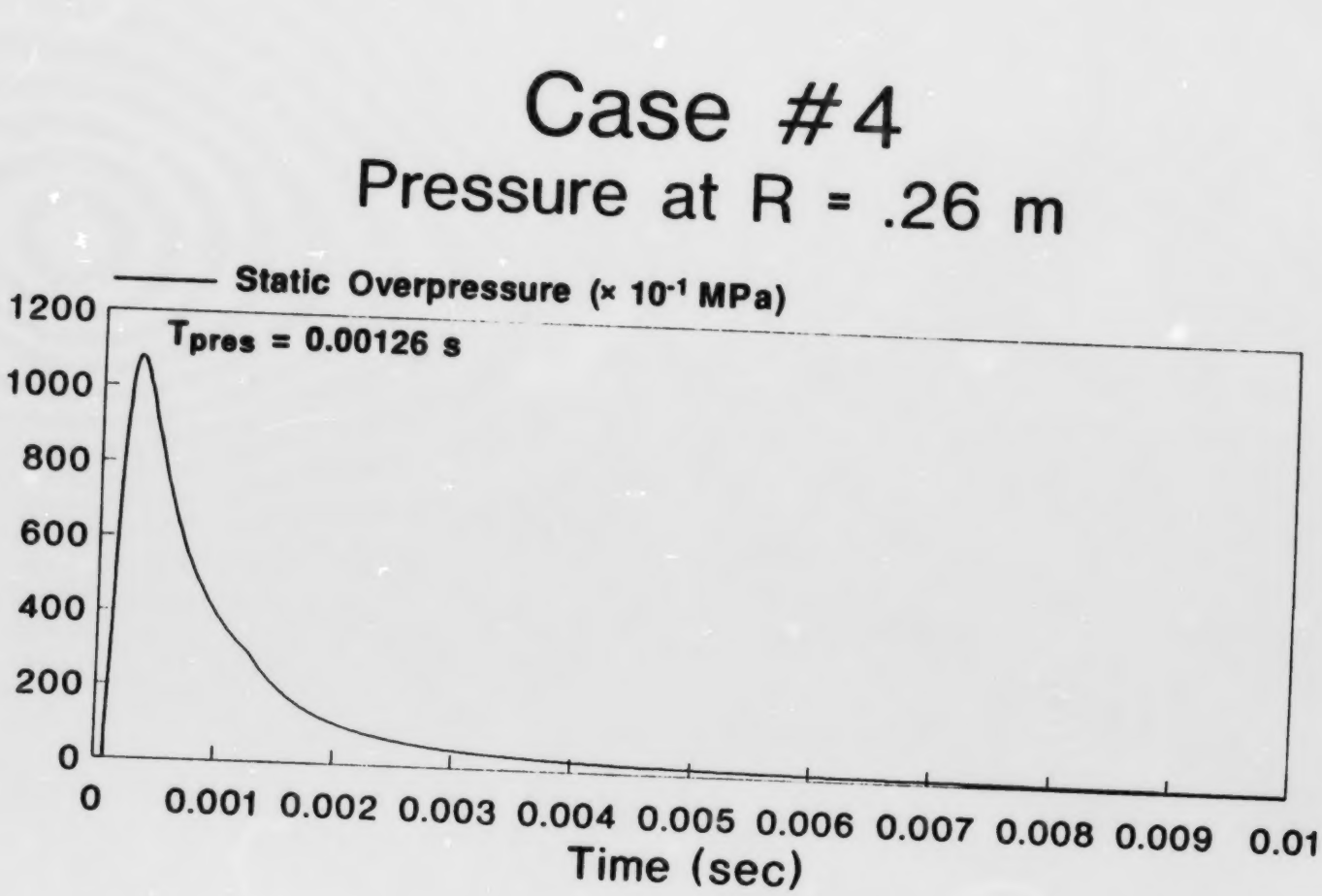

Fig. 17 Static overpressure transient in the moderator at r = 0.26 m from bubble center

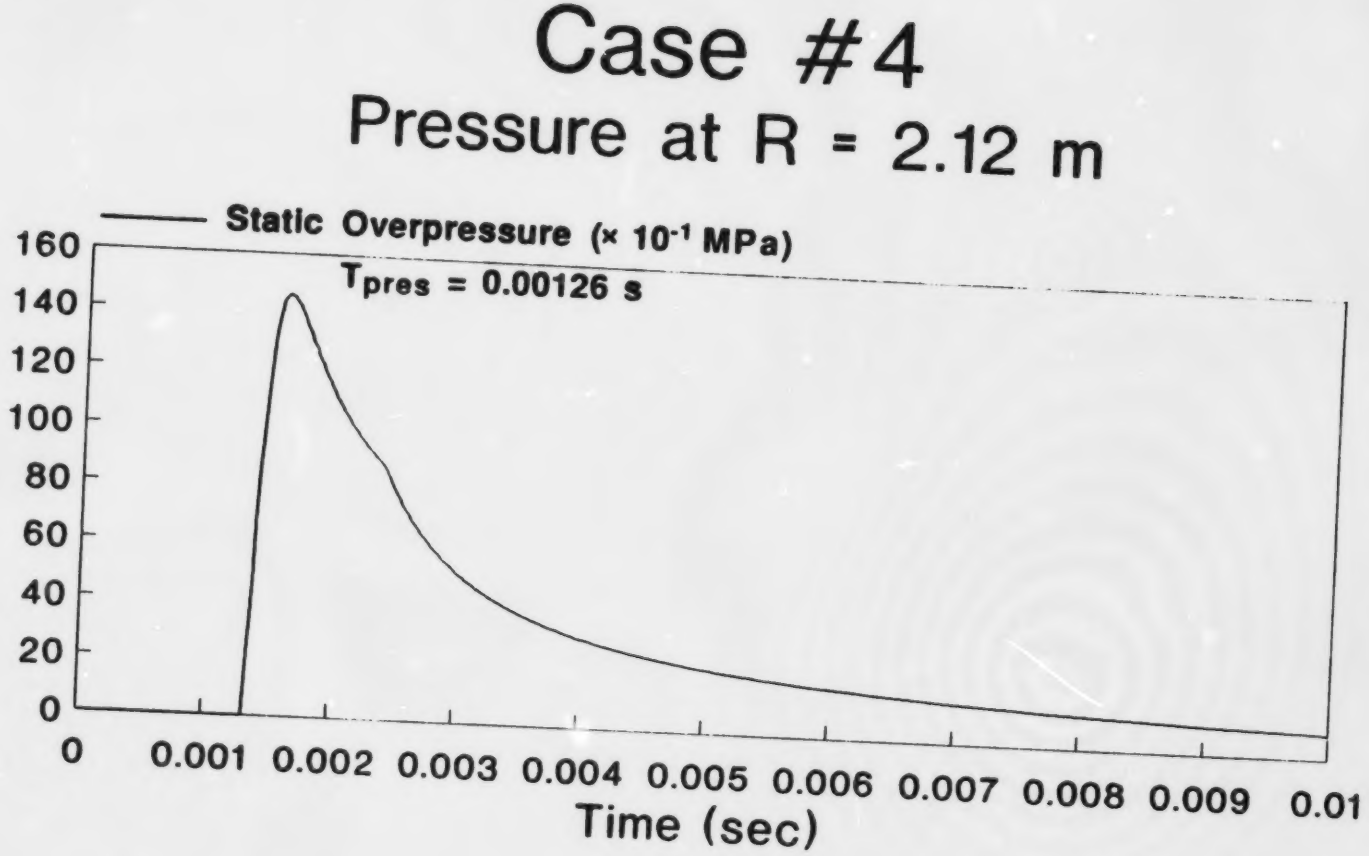

Fig. 18 Static overpressure transient in the moderator at r = 2.12 m from bubble center

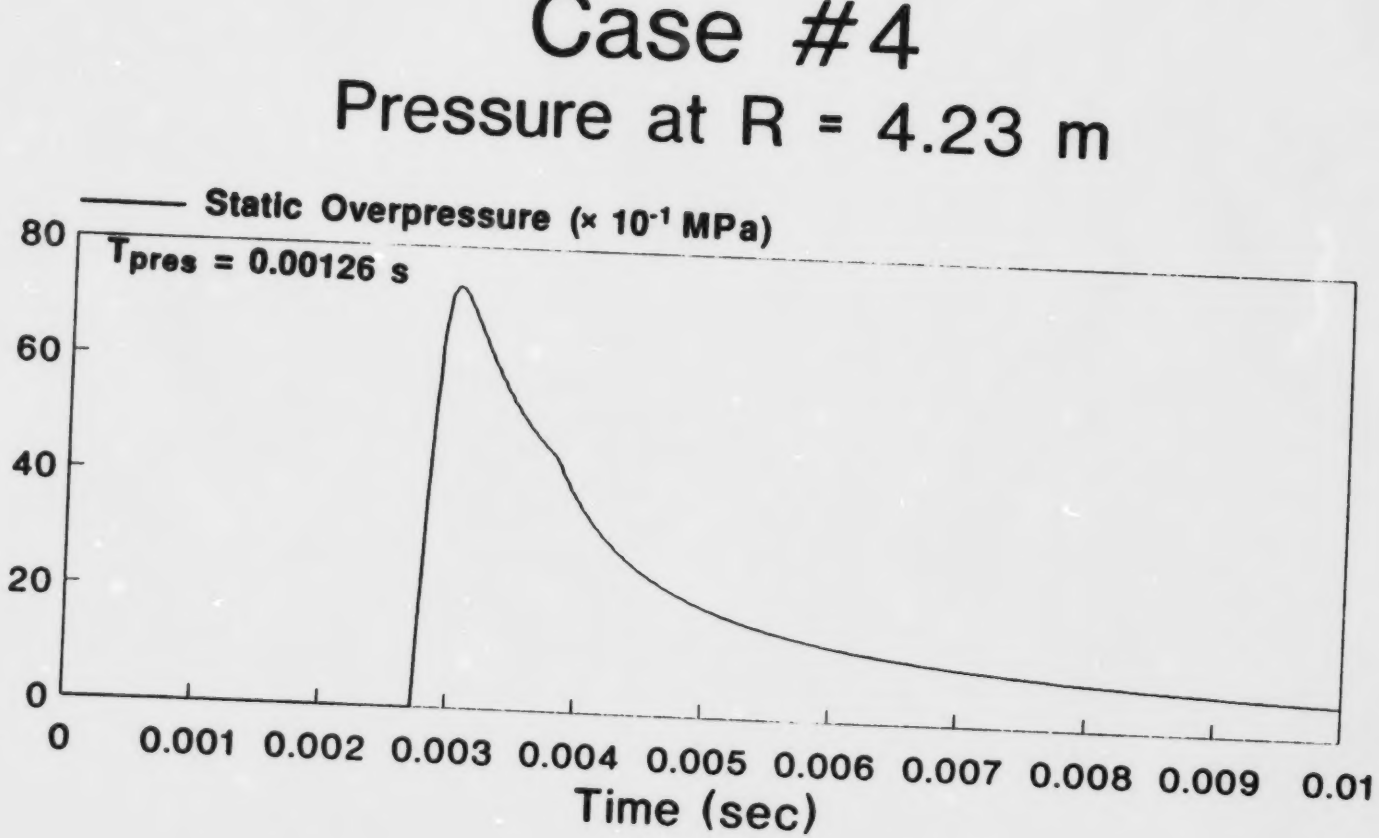

Fig. 19 **Static overpressure attained at the calandria wall (r = 4.23 m) as a function of time**

Case #7
Bubble Pressure and Radius

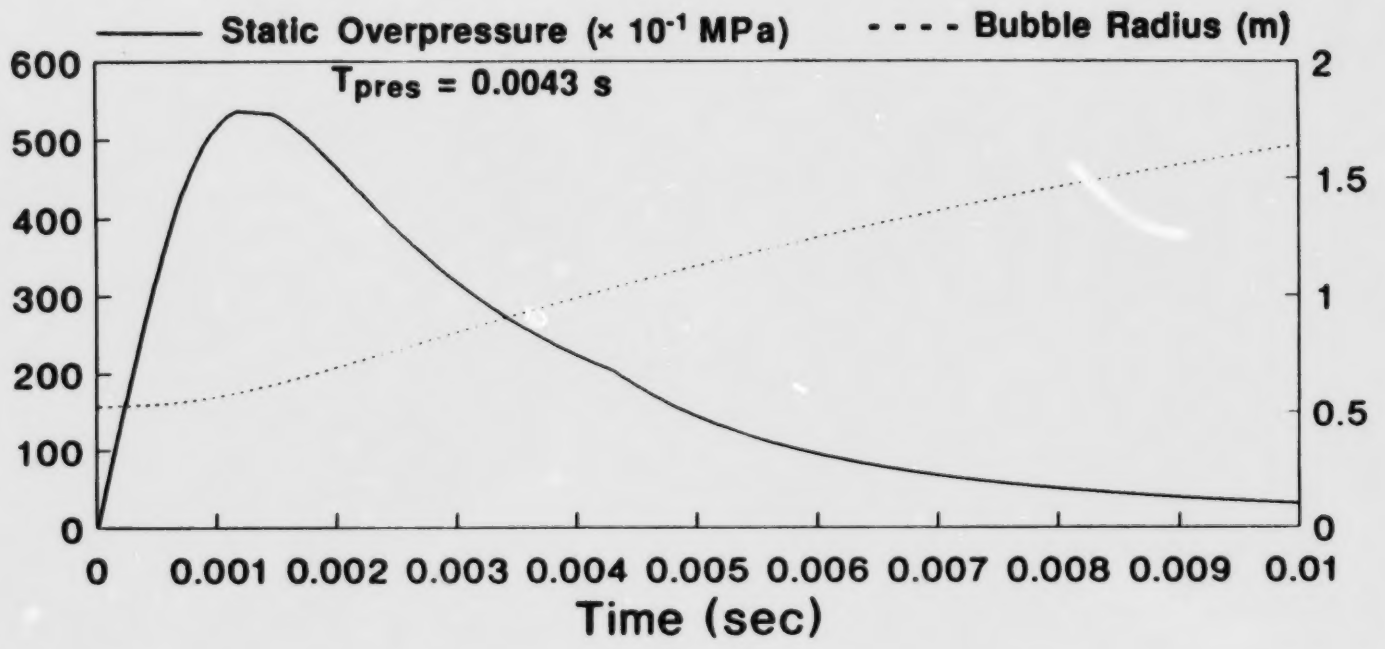

Fig. 20 **Bubble pressure and bubble radius as a function of time**

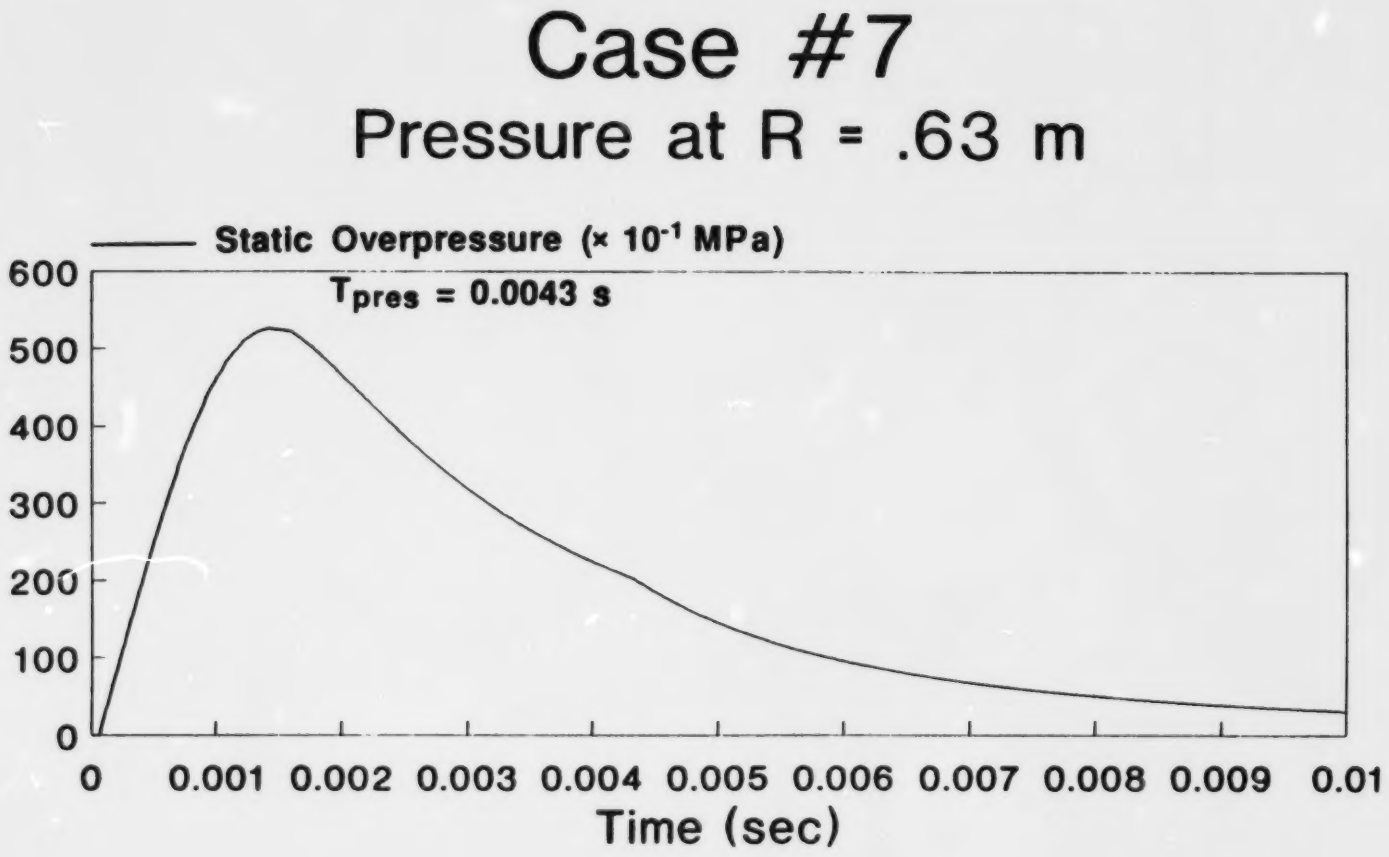

Fig. 21 Static overpressure transient in the moderator at r = 0.63 m from bubble center

Case #7
Pressure at R = 2.12 m

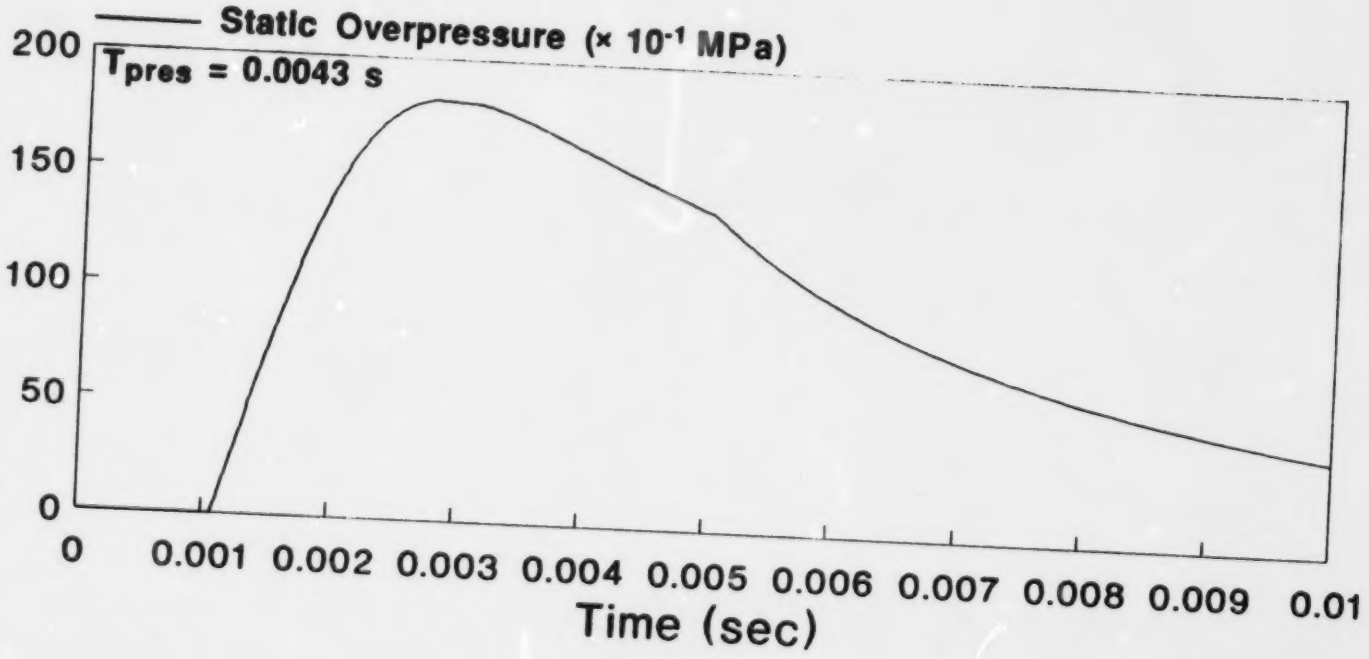

Fig. 22 Static overpressure transient in the moderator at r = 2.12 m from bubble center

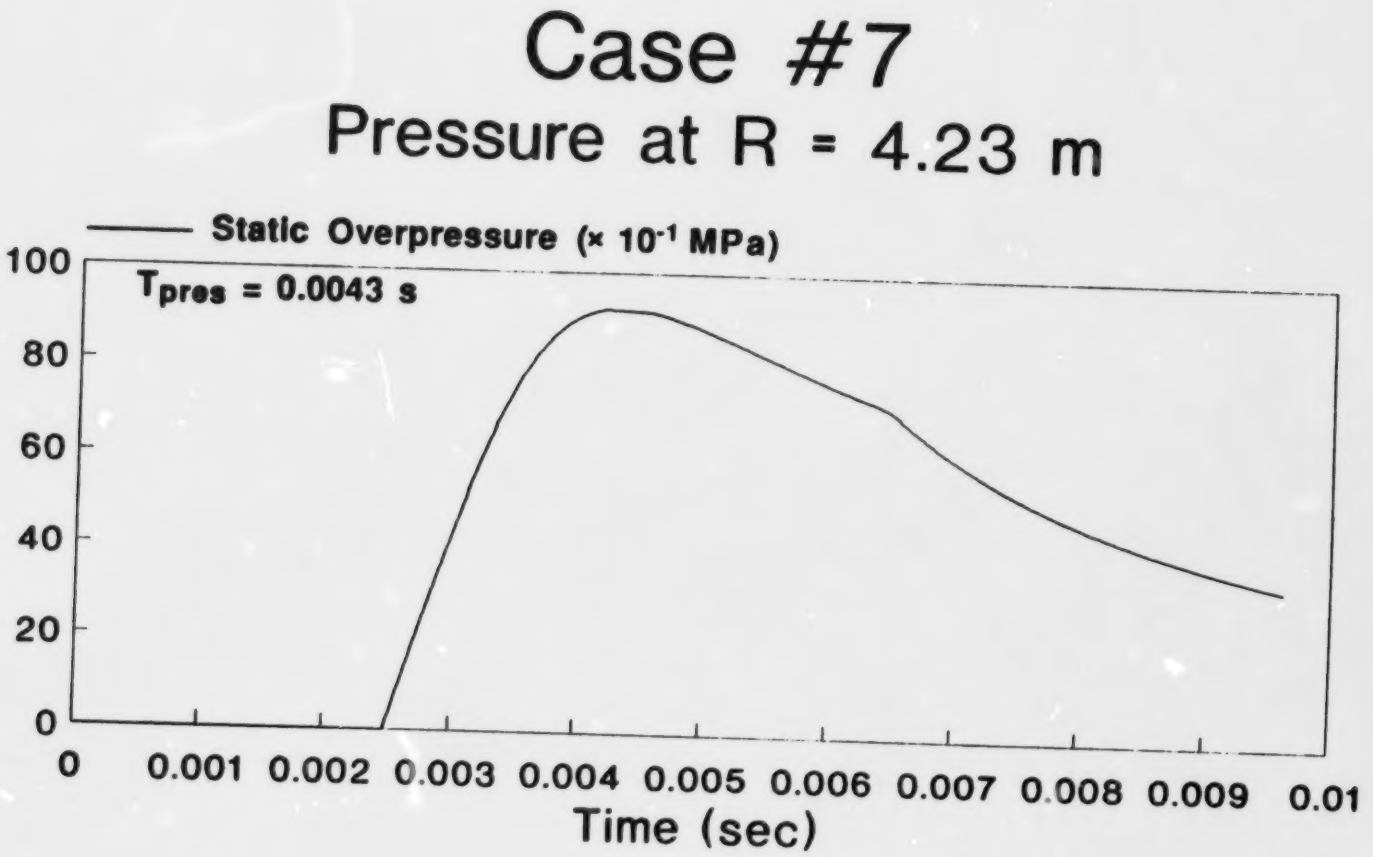

Fig. 23 **Static overpressure attained at the calandria wall (r = 4.23 m) as a function of time**

Case #8

Bubble Pressure and Radius

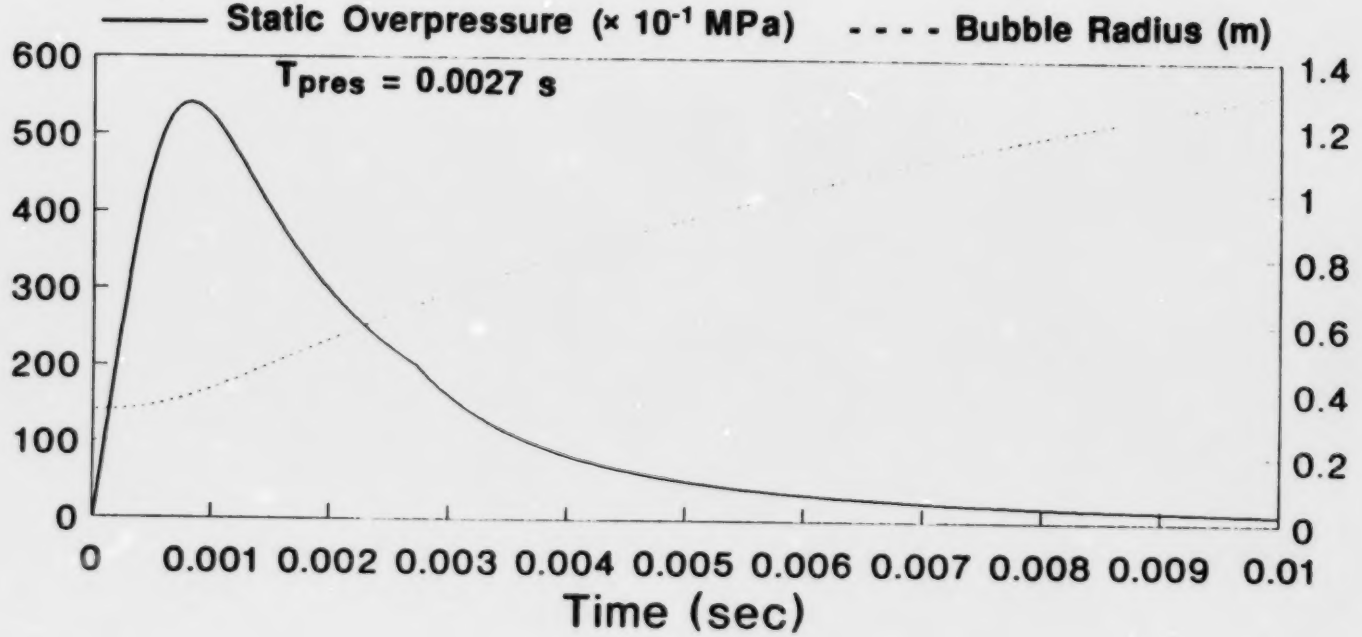

Fig. 24 **Bubble pressure and bubble radius as a function of time**

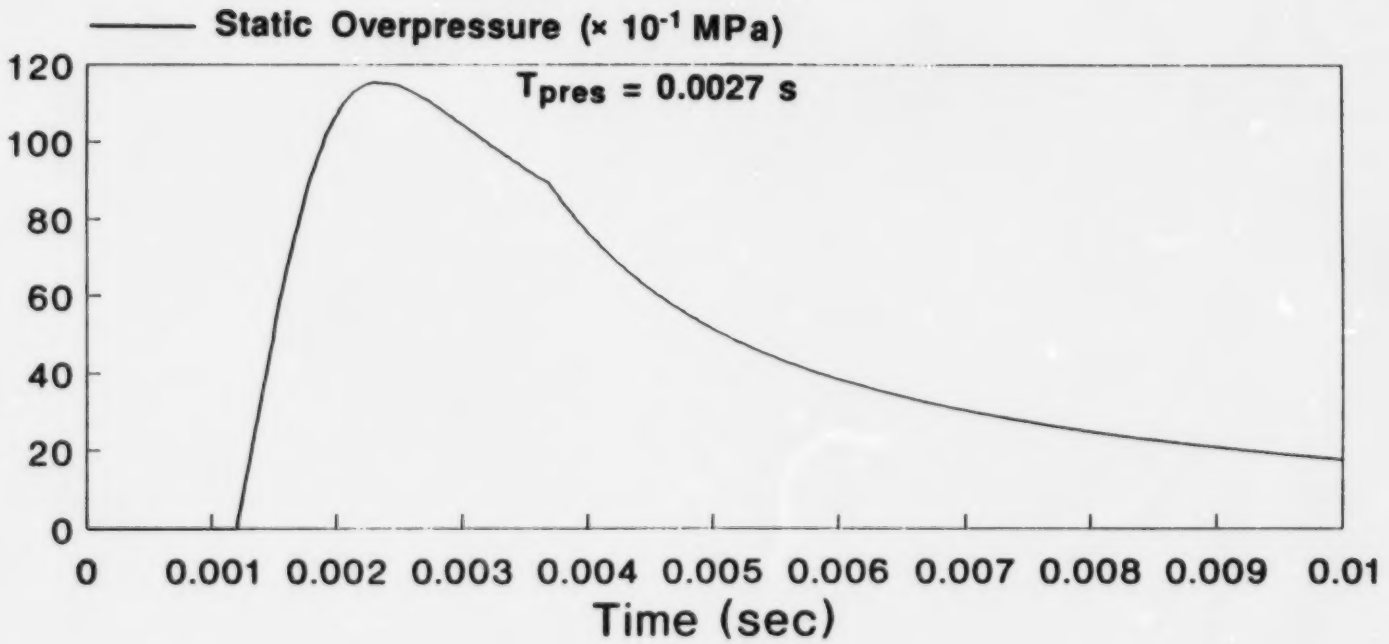

Fig. 25 **Static overpressure transient in the moderator at r = 2.12 m from bubble center**

Case #8
Bubble Pressure at R = 4.23 m

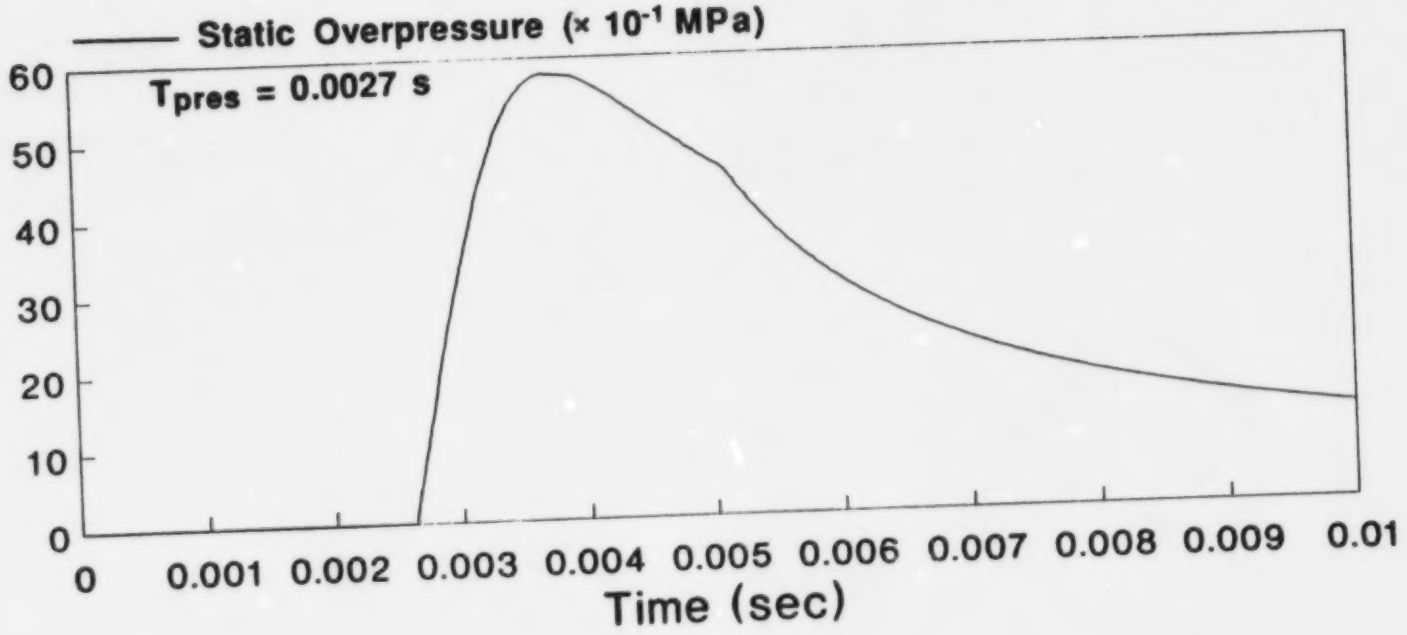

Fig. 26 Static overpressure attained at the calandria wall (r = 4.23 m) as a function of time

APPENDIX A

A REVIEW OF UNDERWATER EXPLOSIONS

(References cited are those listed in the main text)

A REVIEW OF UNDERWATER EXPLOSIONS

1 INTRODUCTION

A common scenario for a large-scale vapor explosion includes the four main stages shown schematically in Fig. A-1: (1) mixing, (2) triggering, (3) propagation, and (4) expansion. It is during the fourth stage that the high pressure vapor bubble expands rapidly, doing work on the environment. To assess the damage potential of such an explosion, it is therefore necessary to investigate the dynamics of the high pressure vapor bubble and the pressure field generated in the surrounding water. A brief review of previous work in the field of underwater explosions is given in the following.

Since the time of World War II, there has been a substantial amount of research carried out on underwater explosions. Throughout this review, vapor explosions and underwater explosions will be considered as two different phenomena. In general, the main objective of underwater explosion research is to determine the potential yield and efficiency of various types of solid explosives. As a result of this research, there have been many numerical models developed to describe the explosion phenomenon. Numerous large-scale experiments have been performed to investigate the mechanisms involved and at the same time provide data for code validation. Due to the relative similarity between the two phenomena (the difference being that in a vapor explosion the energy is derived from the thermal energy of the hot liquid whereas in underwater explosions the energy is derived from the chemical energy of the explosive through a detonation process), vapor explosion research can greatly benefit from the work carried out on underwater explosions.

In an underwater explosion, the initial mass of the explosive is converted into a bubble of very hot gas at tremendous pressure. As in the case of vapor explosion, the high pressure gas bubble expands doing work on the environment. The following is a general description of the dynamics of the high pressure bubble (gas or vapor) following the explosion, as depicted in Fig. A-2. Due to the imbalance of pressure inside the bubble and the environment, the bubble expands. The rapid initial expansion generates a shock wave which propagates radially outward. Initially, the shock wave propagates at a supersonic velocity, however it quickly decays to the speed of sound of water (approximately 1500 m/s). The expanding bubble also creates a convective radial flow ahead of it produced by the displaced water. The bubble expands past the equilibrium radius due to the inertia of

the outflowing water. The equilibrium radius defines a bubble volume where if such a bubble was initially at rest it would remain at rest. The bubble expands to a maximum radius and then begins to collapse due to a pressure deficiency within the bubble relative to the surrounding water. As the bubble collapses, compressive waves are sent inwards, causing the bubble pressure to rise. Behind the collapsing bubble an inflow of water is established. Once again, as in the expansion phase, the bubble overshoots the equilibrium radius. The bubble collapses to a minimum radius, corresponding to a maximum bubble pressure, and then rebounds. The rebound of the bubble coincides with the generation of a second shock wave. The bubble growth and collapse cycle continues with the amplitude of the pressure pulses decreasing with time due to dissipative effects.

Facilities at Nobel's Explosive Company Ltd. were used to perform some large-scale underwater explosions for assessing the explosive potential of different types of condensed explosives. Such tests are of great interest to both the military and explosive manufacturers. There is a great demand for information on explosives due to the increased interest in underwater blasting employed in offshore oil drilling and mining. Results and other experimental details concerning these experiments can be found in Paterson and Begg (1978). Explosive charges varying in size from 0.5 to 5 kg were detonated in an abandoned quarry flooded with water to a depth of 9 m, a width of 27 m and a length much longer. Measurements obtained during these experiments include detonation velocity (within the charge radius), maximum bubble radius, bubble period and pressure time histories at different distances from the charge (6 - 12 m). From the data collected Paterson and Begg (1978) calculated the distribution of the initial explosive energy into shock and bubble energies.

In general, large-scale experiments tend to be very expensive and time consuming compared with experiments done at small scale. However, the amount of small-scale test data available is limited because the scaling of underwater explosion results was not understood. Bjorno and Levin (1976) carried out some small-scale experiments (0.2 to 0.6 kg) to test the scaling of underwater explosion results. The experiments were performed in a water filled steel tank (2 × 3 × 2 m). Pressure measurements were taken at distances of 0.4 and 1.1 m from the charge. Bjorno and Levin (1976) demonstrated that their small-scale results agree well with values calculated using the scaling law developed by Hilliar (1919) for large-scale underwater explosions. They concluded that small-scale experimental results could be used to replace a number of costly large-scale experiments.

In general, the majority of underwater explosion research deals with the detonation of underwater condensed explosives. However, some work has also been done in investigating the performance of underwater gaseous explosives. Such experiments are performed in vertical tubes closed off at the top and open at the bottom and completely immersed in water. Balashkand et al. (1966 and 1977) experimentally measured the shock strength of propane-oxygen gaseous mixtures detonated in partially enclosed volumes at small water depths. Later, Kogarko et al. (1975) studied the detonation of hydrogen-oxygen gaseous mixtures at a depth of 80 m, in both partially enclosed and spherical geometries. An analytical treatment of the problem can be found in Kogarko et al. (1969).

A comprehensive account of the state-of-the-art of underwater explosion research up until the year 1946, which includes the war years when research was most active, is given by Cole (1948). A more recent review is given in Holt (1977). The following review on underwater explosions can in no way be considered complete, but must be taken as a general overview of the more important aspects of the phenomena which can be useful in vapor explosion modeling. The review will be divided into two sections, the first dealing with the primary shock wave and the second with the gas bubble motion. Reference will also be made to the explosion generated by a pressurized sphere and to cavitation bubble dynamics.

2 PRIMARY SHOCK WAVE

The task in underwater explosion modeling is to solve the continuity, momentum, and energy differential equations along with an appropriate equation of state. These equations are highly nonlinear and as a result assumptions must be made concerning the effects of, for example, viscosity and compressibility. There have been many numerical techniques developed to solve these equations such as finite difference and the method of characteristics. One of the main problems is that unlike the continuity, momentum, and energy equations, the equation of state is particular for a given liquid. Furthermore, since the equation of state is derived by curve fitting experimental data, it is considered to be accurate only within the experimental conditions (e.g., the pressure range). Since in an underwater explosion the water adjacent to the explosive is subjected to pressures ranging from 1 to over 20,000 MPa, the equation of state must be very versatile to accommodate this large range in pressure. Therefore, one of the main tasks was to obtain equations of state for water which are accurate at very high pressures.

Glass and Heuckroth (1963) solved explicitly the hydrodynamic shock tube problem. They considered a uniform cross section infinitely long tube with water in the driven section and high pressure gas in the driver section. In the analysis they used a modified form of the Tait equation for water, given as follows

$$p = B\,[(\rho/\rho_o)^n - 1] \tag{1}$$

where the constants are determined experimentally to be $n = 7.15$ and $B = 304$ MPa by Richardson et al. (1947) for salt water with a salinity of 0.04 gm per gm of water and $n = 7.25$ and $B = 293$ MPa for fresh water (Penny, 1950). Note that the experimental constant B as defined is a function of entropy, but Glass et al. (1963) assumed that since the pressure was not too high the change in entropy would be negligible. The constants n and B are quoted as being acceptable up to pressures of 2500 MPa. After manipulating the appropriate equations they derived the hydrodynamic shock tube formula which was then solved numerically using an IBM 650 computer. Fig. A-3 shows the results of the variation of the shock velocity (w), particle velocity (u_2), and sound speed (a_2) as a function of the shock pressure ratio p_{21}. Also plotted in Fig. A-3 are experimental results obtained by Rice and Walsh (1957). The numerical results calculated by Glass et al (1963) show good agreement with the experimental results. This illustrates the accuracy of using the isentropic Tait equation of state given by Eqn. (1) up to moderate pressures.

There exists an abundance of literature on numerical modelling of underwater explosions dating back to the times of World War II, when much of the work was done. The problem of an expanding bubble has been studied at different levels of complexity. The complexity enters the problem when the compressibility of the surrounding liquid is included in the calculations. Rayleigh's (1917) pioneering formulation of the problem can be considered the most approximate since it completely ignores compressibility of the surrounding liquid. Such an approach is equivalent to setting the sound speed to be infinite. As a result of this approximation, no pressure waves can emanate from the expanding bubble. At the other end of the spectrum, solving the three conservation equations using a finite-difference approach can be considered to be the most exact. There exist many such codes, however, the practicality of such an approach depends on the efficiency of the code and the speed of the computer employed. Calculations from such a code will be presented later on in the review.

Within the two extremes mentioned above there exist different levels of approximation which can be incorporated. A summary of two such approximate methods can be found in Lyuboshits and Pervushin (1972) who presented comparative calculations using a "quasi-acoustic" model and the more exact Kirkwood-Bethe (1942) theory. In the acoustic model pressure waves radiate out from the expanding bubble at a velocity equal to the sound speed of the surrounding liquid (which is taken to be constant). In comparison, the Kirkwood-Bethe model assumes that the waves travel at a velocity equal to the local liquid sound speed plus the liquid velocity. As a result, for lower initial bubble pressures (weaker shocks) the two models are comparable but for higher bubble pressures the Kirkwood-Bethe model is superior since the liquid velocity is not negligible. A more detailed description of the acoustic model is given in Appendix C of this report. A similar acoustic treatment of the problem can be found in Trilling (1952).

As mentioned above, there are many papers that are concerned with solving the expanding bubble problem using finite-difference techniques. The later papers can be considered relatively more accurate when compared to the literature from the 40's to the 60's, because of the availability of more accurate equations of state at high pressures and more sophisticated computers. Therefore, instead of reviewing many of the older papers it is believed that a review of one of the more credible recent papers is more in order. The following is a review of numerical results (which can be considered representative of many other papers written on this topic) obtained by Sternberg and Walker (1971). In general the results are very well documented and are supported by experimental data.

Sternberg and Walker (1971) modeled the underwater explosion of a spherical pentolite (50/50 TNT/ pentaerythritol tetranitrate) charge. The hydrodynamic calculations were done using the artificial viscosity "q" method. This is a finite-difference technique which solves the fluid flow equations in a Lagrangian space coordinate system. A total of 300 cells were adopted, with 50 in the gas bubble and 250 in the water. The calculations were carried out until the primary shock wave reached 100 charge radii from the center of the charge. In an earlier paper they carried out the calculations up to 19 charge radii (Walker and Sternberg, 1965).

An equation of state having the following form was implemented in the code,

$$p = \frac{F_1}{v} + \frac{F_2}{v} + \frac{F_3}{v} + \frac{F_4}{v} \qquad (2)$$

where p is pressure, v is specific volume, and F_1, F_2, F_3, and F_4 are lengthy polynomials in E (internal energy), fitted to experimental data. The above equation of state is accurate up to pressures of 25,000 MPa.

The primary results show that the shock velocity decreases from 6000 to 1600 m/s within the first ten charge radii. Beyond this distance the shock propagates at the sonic velocity of the water. Fig. A-4 shows how the shock pressure varies with distance. At first the shock pressure decays very rapidly, from 16,200 to 120 MPa after 10 charge radii. Beyond this distance the pressure drops off roughly inversely proportional with distance. Also included in Fig. A-4 are experimental results for 36 and 23 kg spherical pentolite charges obtained at Woods Hole in 1945, as described by Cole (1948). The numerical results agree well with the experimental results. In the earlier paper (Walker and Sternberg, 1965 using a similar code), the numerical results between 1 and 6.5 charge radii were compared with experimental data obtained by Coleburn (1962), again with good agreement. Fig. A-5 is a graph which superimposes six pressure-time histories at various charge radii. The vertical bar on the $R/R_o = 2$ trace (shown dotted) signifies the time when the gas bubble surface expands to 2 charge radii. Therefore, for times above this, the point $R/R_o = 2$ is inside the gas bubble. The several bumps seen on the trace are due to secondary shocks which reverberate within the bubble.

Fig. A-6 shows the calculated particle velocity of the water versus distance at times corresponding to 4, 10, 25, 50, and 100 charge radii. Once the shock reaches a distance of 25 charge radii, the particle flow velocity drops off as a function of the inverse square of distance, which means that the flow is essentially incompressible except in the vicinity of the shock wave.

Another aspect of interest is how the initial energy of the explosive is distributed. As the shock wave propagates, it heats the water. This dissipative energy can not be converted into useful work. The extent of energy lost to heating the water is determined by the strength of the shock, with the stronger the shock the more the water is heated. As a result, a large part of this dissipative energy is expended very close to the charge, where the shock is strongest. Sternberg and Walker's (1971) calculations show that the temperature of the water at the bubble surface at time $t = 0$ is increased to 1273K. When the shock wave reaches a distance of 1.1 charge radii the temperature at the front is 838K and the temperature of the water at the bubble surface is 913K. Eventually, when the shock

reaches two charge radii the temperature of the water at the shock is 358K and 588K at the bubble surface. Fig A-7 demonstrates how the water temperature decreases as a function of time at various positions.

A large part of the initial energy also goes into the kinetic energy of the water, both by the passage of the shock and by the piston effect of the expanding bubble. A typical breakdown of the initial energy in an underwater explosion is given by Fig. A-8, from Hicks (1968).

Included as Figs. A-9 and A-10 are two spark shadowgraphs of the explosion of a 5 cm diameter glass sphere containing air at an initial pressure of 2.76 MPa. Although it is not related in any way to an underwater or vapor explosion, it does demonstrate how the rapid expansion of a gas can produce an outward propagating shock wave. The wavy lines which are evident just inside the contact surface are due to the turbulence which is generated by the expanding gas and the remaining shattered glass.

3 GAS BUBBLE MOTION

Aside from the primary shock wave, the motion of the resulting bubble is also of interest. As discussed earlier, the high pressure gas bubble expands very rapidly at first and then slows down approaching a maximum. The maximum is then followed by a stage in which the bubble collapses. A series of photographs taken from a high speed film (Swift) of the bubble oscillation following the detonation of a 0.25 kg tetryl charge is shown in Fig. A-11. Shown in Fig. A-12 is the corresponding radius—time plot. The plot shows that the bubble undergoes three oscillations. Other experimental results show that as many as seven oscillations can occur.

The dynamics of pressurized bubbles has been investigated analytically by many different researchers. In general, it is assumed that the change in density of the water surrounding the bubble is negligible, and therefore the flow can be taken to be incompressible. This assumption is based on the fact that the pressure associated with bubble oscillations is fairly low, in fact during most of the growth/collapse cycle the pressure is below atmospheric. The incompressible assumption greatly reduces the complexity of the equations. Without getting too involved in the mathematics, the following expression, known as the Willis (1941) formula, relating the period of the bubble oscillation (T) to the ambient ambient

density (ρ_o), and pressure (p_o), and the total energy (E), has been derived by several writers

$$T = 1.14\,\rho_o^{1/2}\,\frac{E^{1/3}}{p_o^{5/6}} \tag{3}$$

Of course, as the bubble accelerates to a minimum (increasing the pressure) the incompressible assumption becomes less and less accurate. However, the assumption holds true for the majority of the cycle. Also neglected in the above analysis is the effect of buoyancy of the bubble. The net upward force due to buoyancy causes the bubble to migrate upwards as it oscillates.

A different phenomenon which to some degree is related to underwater explosion is cavitation. Cavitation occurs in a liquid when the pressure falls below atmospheric, thereby placing the liquid in tension. Due to the inability of a liquid to counteract tension, cavities filled with vapor and noncondensible gas form in the bulk of the liquid. When the pressure in the liquid is restored, the cavities (or bubbles) collapse. The main interest in cavitation bubble dynamics arises from the destructive forces generated by the collapse near a solid surface. One mechanism which has been identified as being the driving force behind cavitation damage is the shock wave which is radiated when the bubble reaches a minimum. Therefore, the main difference between the two phenomena is that in cavitation there is no primary shock wave produced although the subsequent bubble dynamics is similar.

As in the case of underwater explosion there exists a tremendous amount of literature on cavitation bubble dynamics. The first serious treatment of the problem was done by Rayleigh (1917). He derived the following differential equation which governs the motion of the bubble,

$$R\frac{d^2R}{dt^2} + \frac{3}{2}\left(\frac{dR}{dt}\right)^2 = \frac{p - p_a}{\rho_c} \tag{4}$$

where R and p are the radius and pressure of the bubble at time t, ρ_c is the incompressible coolant density, and p_a is the ambient pressure outside the bubble. This equation neglects viscosity, surface tension, and compressibility of the liquid surrounding the bubble. Furthermore, it assumes that the bubble is spherical at all times and that the ambient

pressure is uniform. Rayleigh also considered the case of the collapse of an empty cavity in a large mass of liquid.

There have been many modifications proposed to this basic building block formula. For example, Plesset and Prosperetti (1977) modified Eqn. (4) by including surface tension and viscosity effects. Fujikawa and Akamatsu (1980) further modified the Rayleigh equation by including compressibility of the surrounding liquid, nonequilibrium condensation within the bubble, and heat conduction and temperature discontinuity across the interface. They also obtained numerical solutions during the collapsing stage and the rebound where the pressure wave is generated. Initially the bubble contains either vapor or both vapor and noncondensible gas in an infinite sea of viscous compressible liquid. At time $t = 0$, the pressure of the surrounding liquid is increased instantly to a pressure above that inside the bubble. Using the appropriate continuity, momentum, energy, and state equations they analytically derived a lengthy and very elaborate differential equation describing the motion of the bubble. Details will not be included here but can be found in Fujikawa and Akamatsu (1980). The above mentioned equation was numerically integrated by Fujikawa and Akamatsu using the Runge-Kutta-Gill method on a FACOM M-190 digital computer.

The results of Fujikawa and Akamatsu (1980) include standard bubble radius, velocity, and bubble pressure versus time plots. It should be pointed out that it was assumed that the pressure in the bubble is uniform at all times. This assumption is valid as long as the radial velocity of the bubble is less than the sound speed of the vapor gas mixture inside the bubble. The results which are of most interest in keeping with the topic of this review is the pressure versus distance plots shown in Figs. A-13 and A-14. For this particular run the initial conditions are: bubble contains only vapor, bubble radius of 1 mm, vapor pressure of 0.002305 MPa, ambient pressure of 0.07025 MPa. Fig. A-13 shows the pressure buildup as the bubble contracts to a minimum and Fig. A-14 shows the formation of the outward propagating pressure wave which is generated by the expansion of the compressed gas. The results demonstrate that even though the bubble only contains vapor a pressure wave can be produced by its collapse. During the first half of the collapse stage the vapor condenses into liquid, so that the vapor pressures remains constant. However, during the final half of the collapse stage the bubble radius decreases so quickly that most of the vapor does not have time to condense. As a result the remaining vapor is compressed to a high pressure. Eventually the pressure builds sufficiently high to arrest the collapsing bubble and rebounds producing an outward propagating pressure wave, as shown in Fig. A-14.

4 CONCLUDING REMARKS

The primary objective of this review was to determine how the current state-of-the-art work in underwater explosion can be extended to the modeling of the expansion phase of a vapor explosion . As shown in the review, numerical hydrodynamic calculations (e.g., Sternberg and Walker) of the blast wave generated from an underwater explosion demonstrate good agreement with available experimental data. However, in extending the theory one must keep in mind that the pressures associated with underwater explosions (e.g., 20,000 MPa) far surpass the pressures generated during a vapor explosion (e.g., ~100's MPa). Because of the high pressures associated with underwater explosions it is necessary to develop sophisticated empirical equations of state for water which are valid under such extreme conditions. On the other hand, since vapor explosion pressures are considerably lower, it is sufficient to employ the Tait equation of state given in Eqn. (1).

As the calculations of Sternberg and Walker demonstrate, compressibility effects associated with the initial rapid expansion of the bubble diminish very rapidly. For example, the particle velocity approaches the incompressible solution (decays as a function of the inverse square of distance) after the primary shock has traveled 25 charge radii. Since the initial bubble pressure is considerably lower in a vapor explosion, the incompressible assumption becomes plausible for much earlier times (e.g., primary shock travels $<< 25\ R/R_o$). As discussed earlier, the incompressible assumption leads to the Rayleigh bubble equation which poses no difficulty in solving.

Summarizing, during the early stage of bubble expansion the radial bubble velocity is comparable to the speed of sound in the water, hence compressibility effects in the water cannot be ignored. However, calculations show that this stage in the bubble expansion is very short lived and also show that the primary shock wave rapidly decays to an acoustic wave. The remainder of the bubble expansion stage can satisfactorily be modeled using the incompressible Rayleigh theory, through Eqn. (4). Fig. A-15 shows how the primary shock wave and particle velocity profiles develop in time. During the early times (t_1), compressibility is important and the profiles do not correspond very well with the incompressible theory. At later time (t_2), the profiles fit perfectly the incompressible theory except very close to the shock wave which in general decays very rapidly. Further results can be found in Appendix C, in which results from a variety of analytical models are presented.

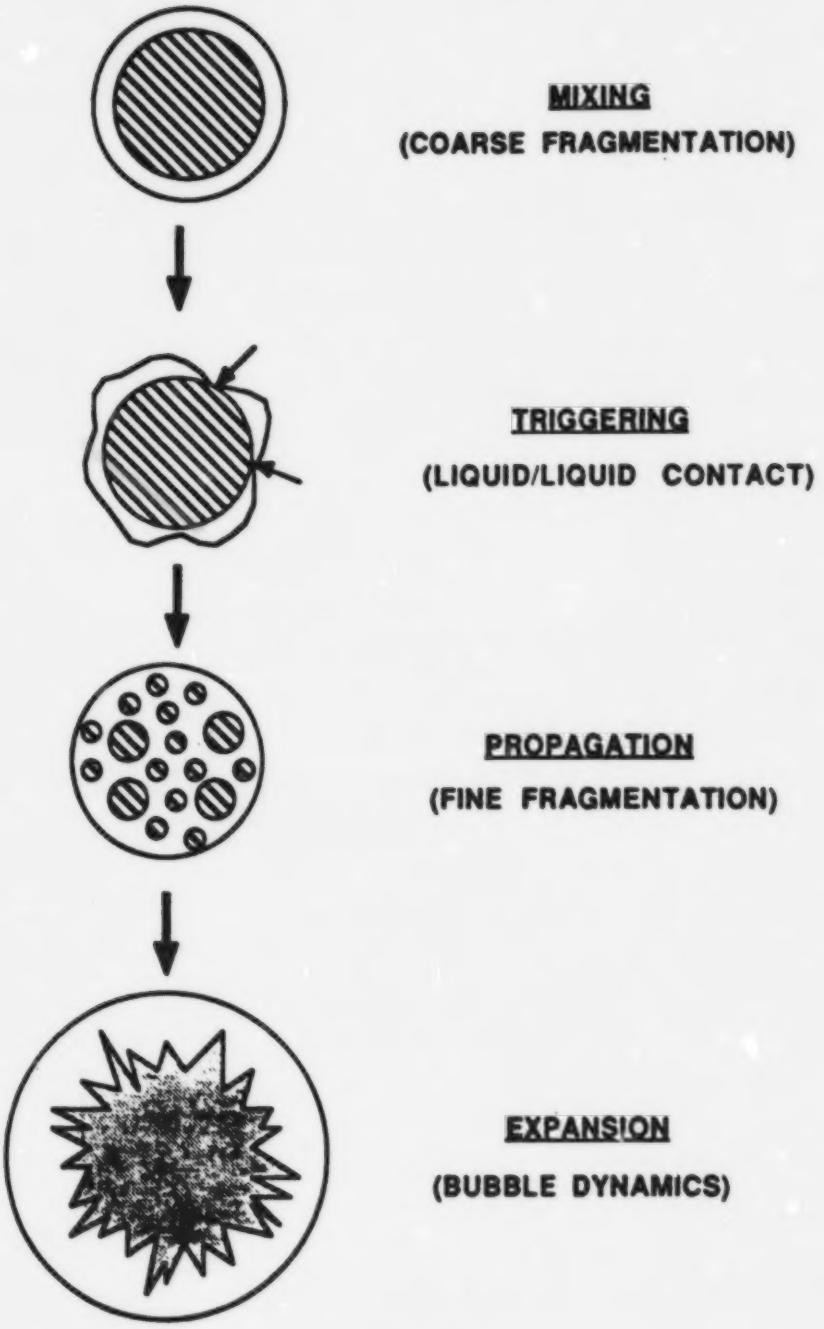

Fig. A-1 **Schematic of 4 stages in a vapor explosion**

BUBBLE DYNAMICS

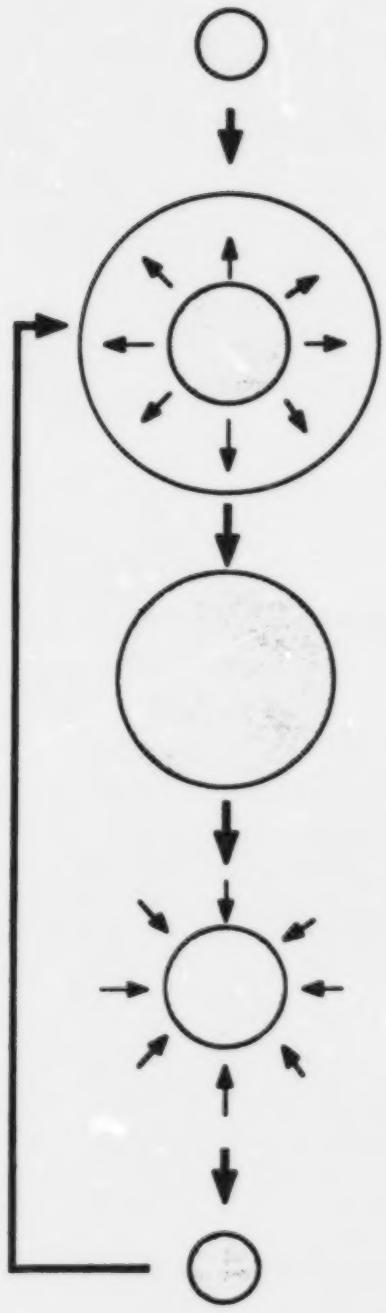

HIGH PRESSURE VAPOR BUBBLE IS FORMED AFTER EXPLOSIVE VAPORIZATION OF COOLANT

HIGH PRESSURE VAPOR EXPANDS GENERATING AN INITIAL SHOCK AND AN OUTWARD RADIAL COOLANT FLOW

VAPOR BUBBLE ACHIEVES A MAXIMUM DIAMETER

VAPOR BUBBLE COLLAPSES GENERATING AN INWARD RADIAL COOLANT FLOW

VAPOR BUBBLE REACHES A MINIMUM DIAMETER AND RESTARTS CYCLE

Fig. A-2 Schematic of bubble dynamics

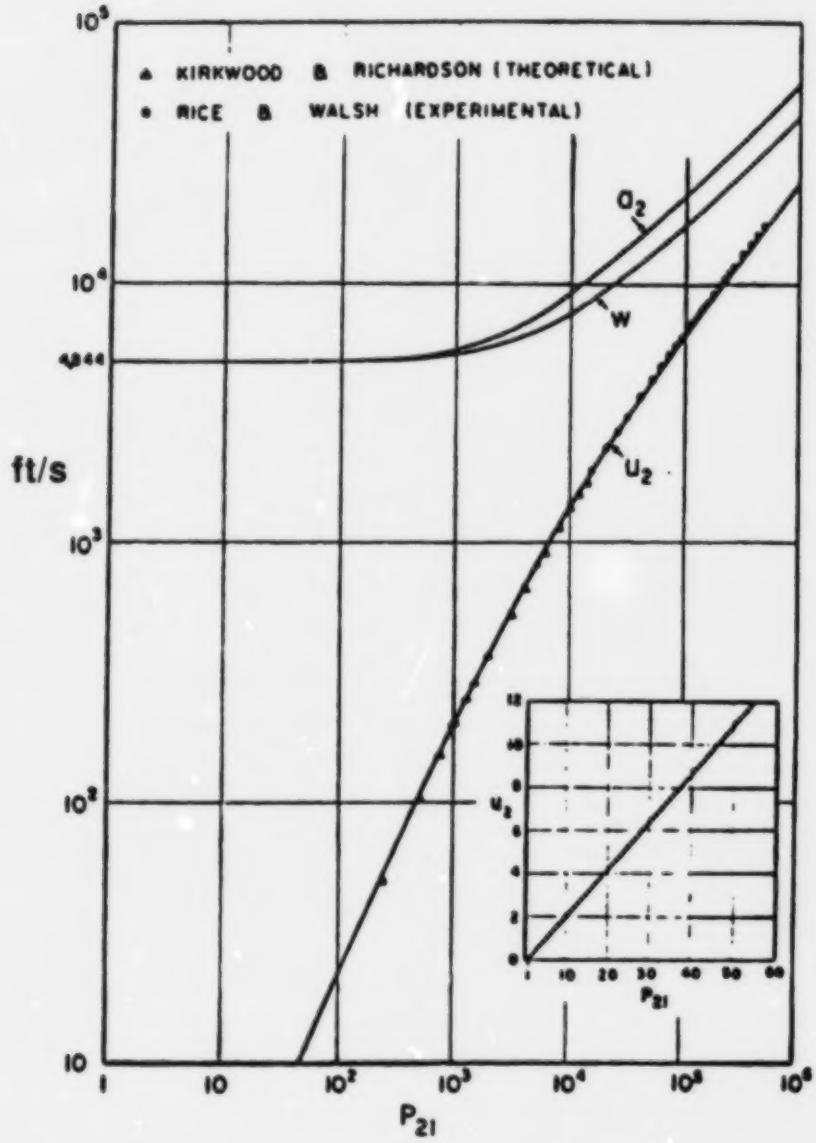

Fig. A-3 Variation of shock speed w, particle velocity u_2, and sound speed a_2 with shock pressure ratio p_{21} (Glass et al., 1963)

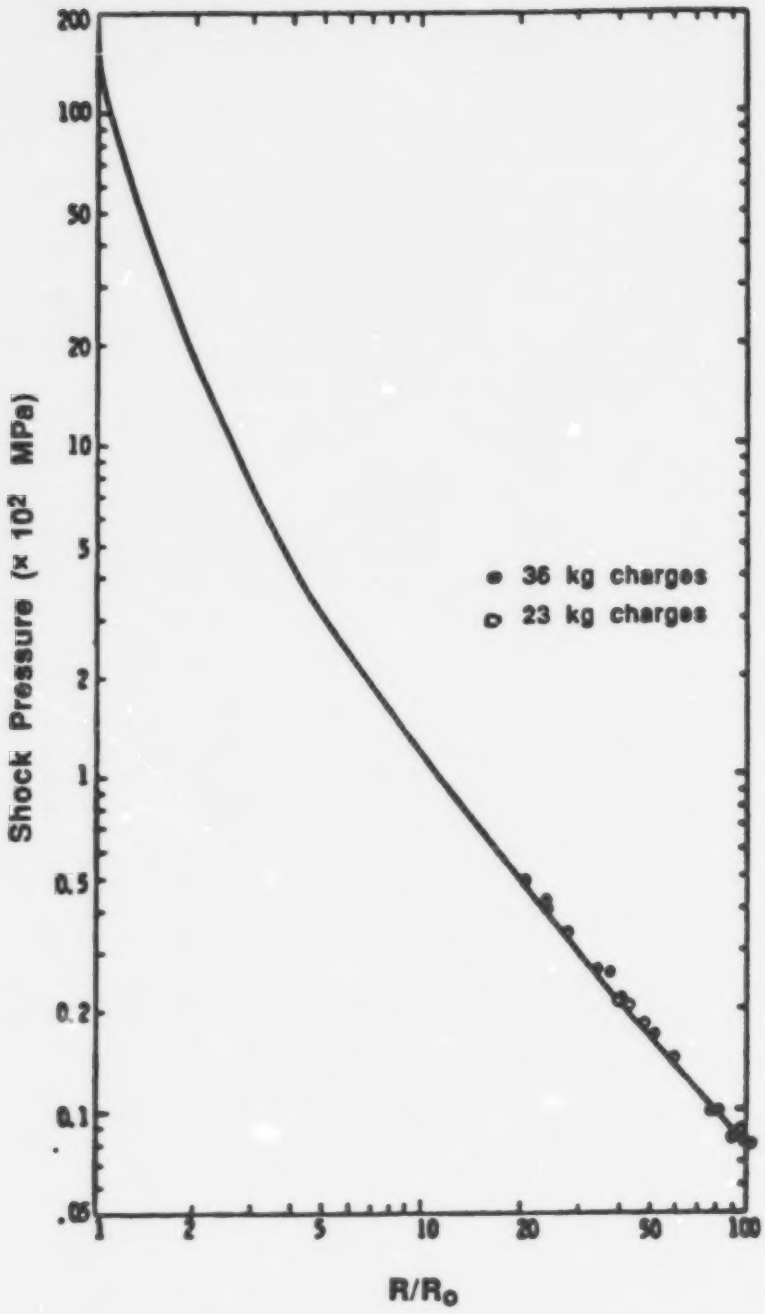

Fig. A-4 Calculated and experimental peak-pressures versus distance (Sternberg et al., 1971)

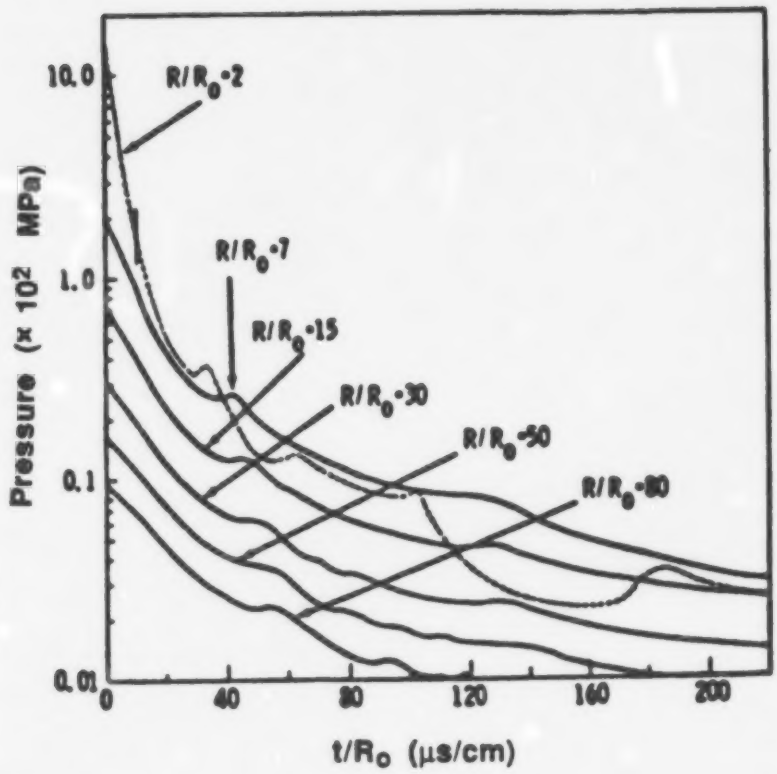

Fig. A-5 **Calculated pressure versus time at various charge radii (Sternberg et al., 1971)**

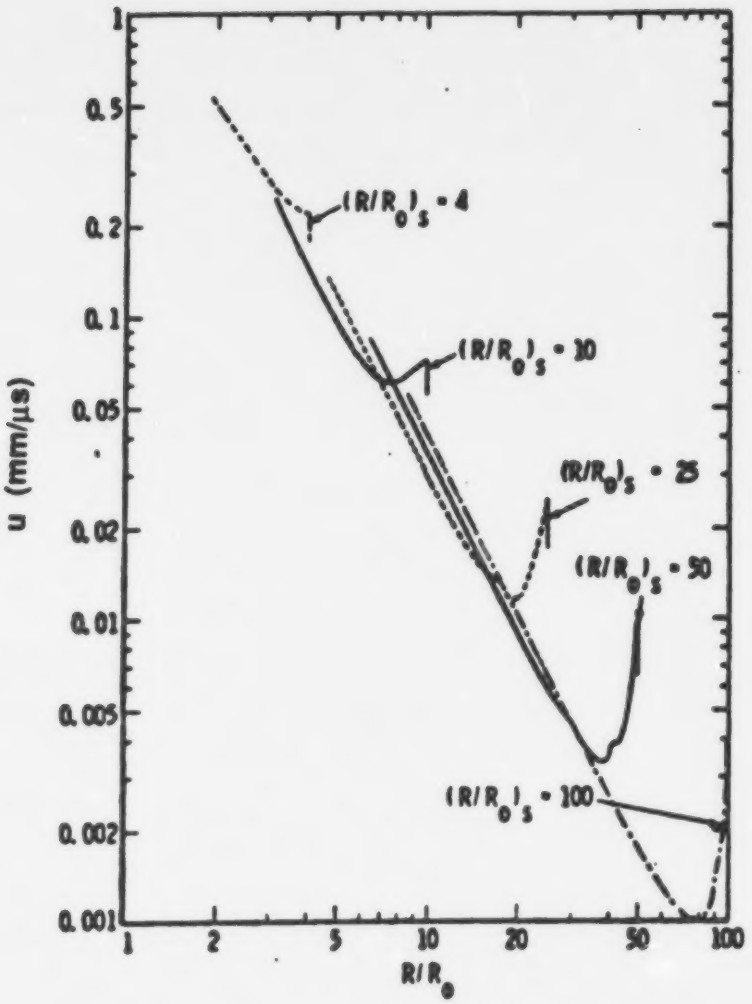

Fig. A-6 **Calculated particle velocity versus distance at times corresponding to various shock-front positions (Sternberg et al., 1971)**

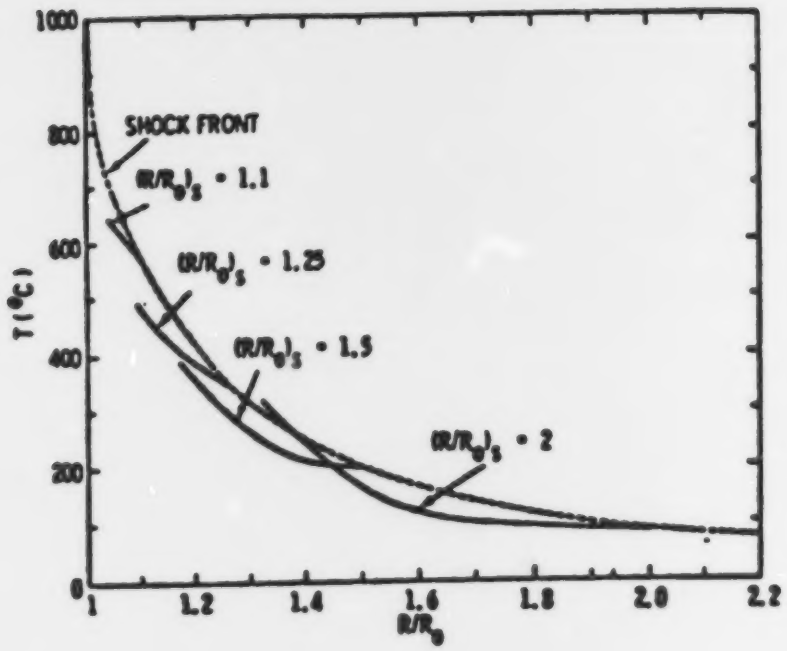

Fig. A-7 **Calculated temperature in the water versus distance at times corresponding to shock-front positions between 1 and 2 charge radii from center (Sternberg et al., 1971)**

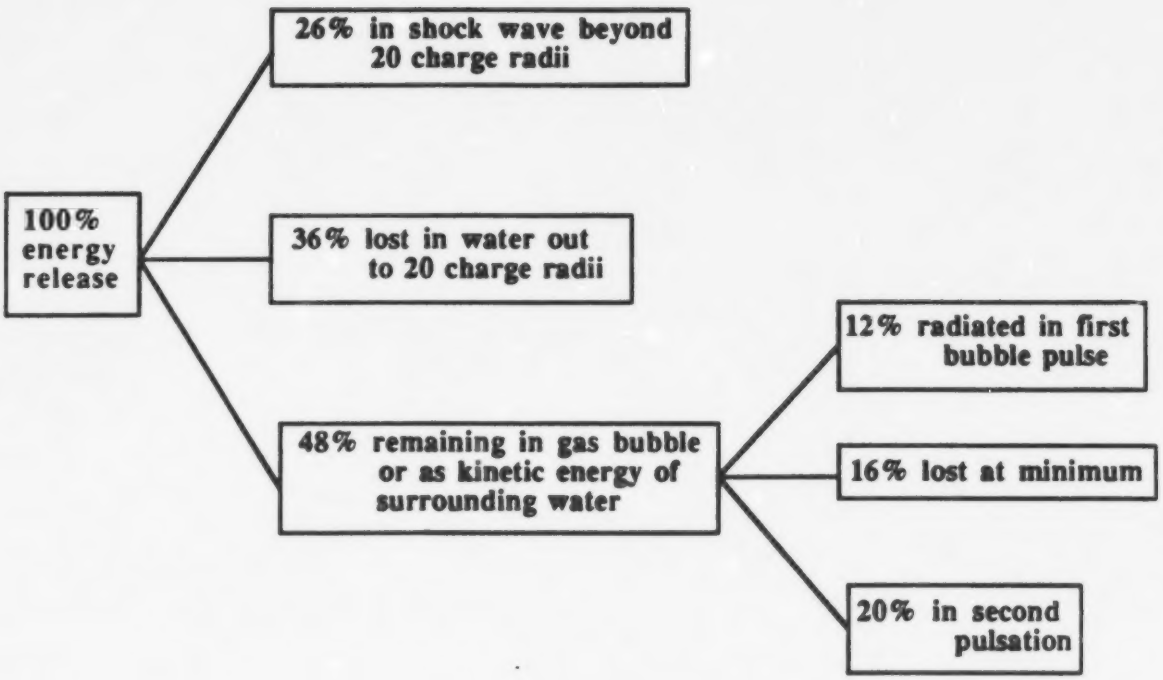
100% energy release
26% in shock wave beyond 20 charge radii
36% lost in water out to 20 charge radii
48% remaining in gas bubble or as kinetic energy of surrounding water
12% radiated in first bubble pulse
16% lost at minimum
20% in second pulsation

Some of shock wave energy crossing 20 charge radii is later transformed into bubble energy, so accounting for the apparent 110% total energy

Fig. A-8 Energy distribution from an underwater explosion (Hicks, 1968)

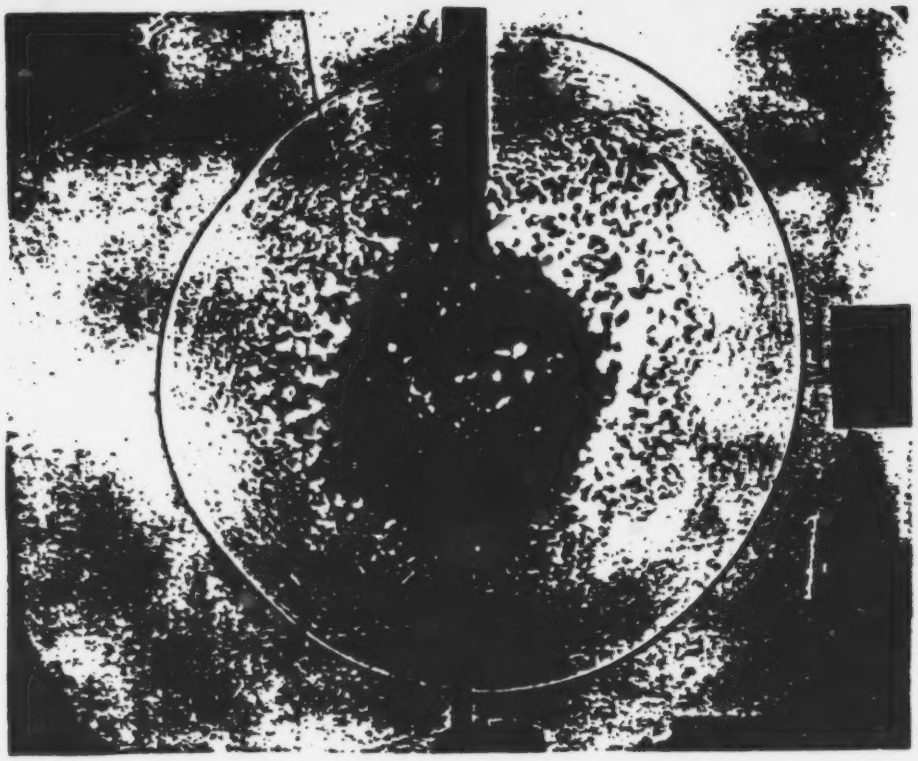

Fig. A-9 Spark shadowgraph of the explosion of a 5 cm diameter sphere of air, initial pressure = 2.76 MPa, time delay 300 μs (Boyer, 1960)

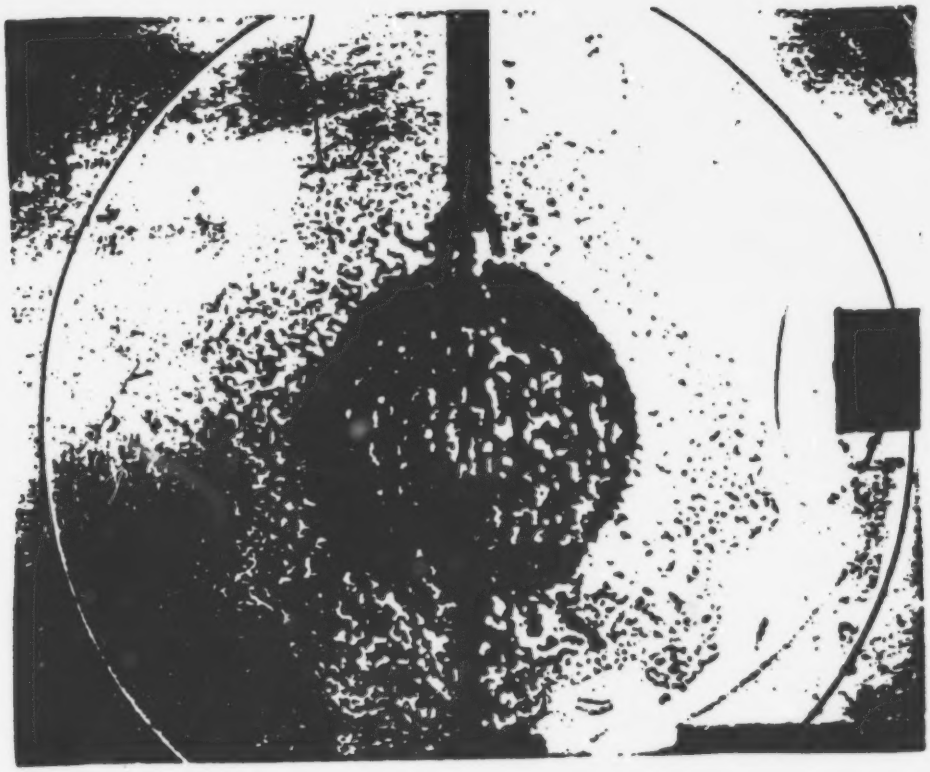

Fig. A-10 Spark shadowgraph of the explosion of a 5 cm diameter sphere of air, initial pressure = 2.76 MPa, time delay 320 μs (Boyer, 1960)

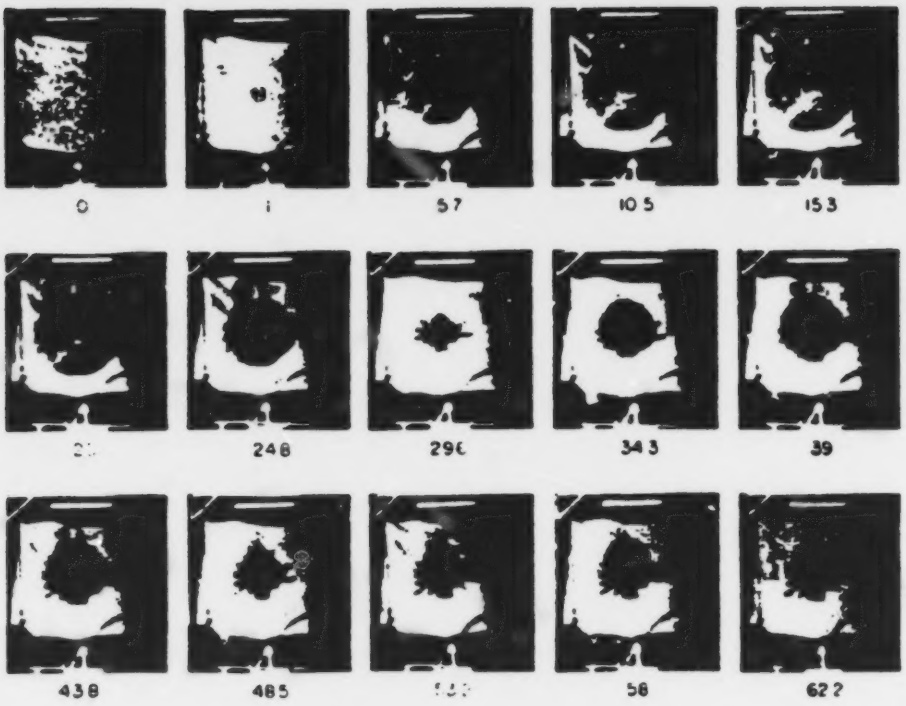

Fig. A-11 Pulsation of gas products from a 0.25 kg Tetryl charge 91 m below surface, with times shown in ms (Cole, 1948)

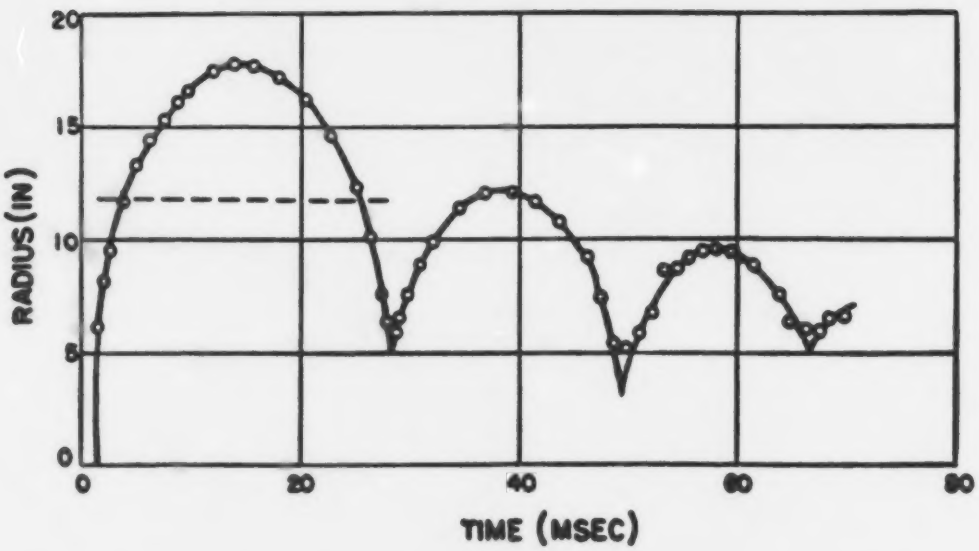

Fig. A-12 Radius versus time plot of trial shown in Fig. 11 (Cole, 1948)

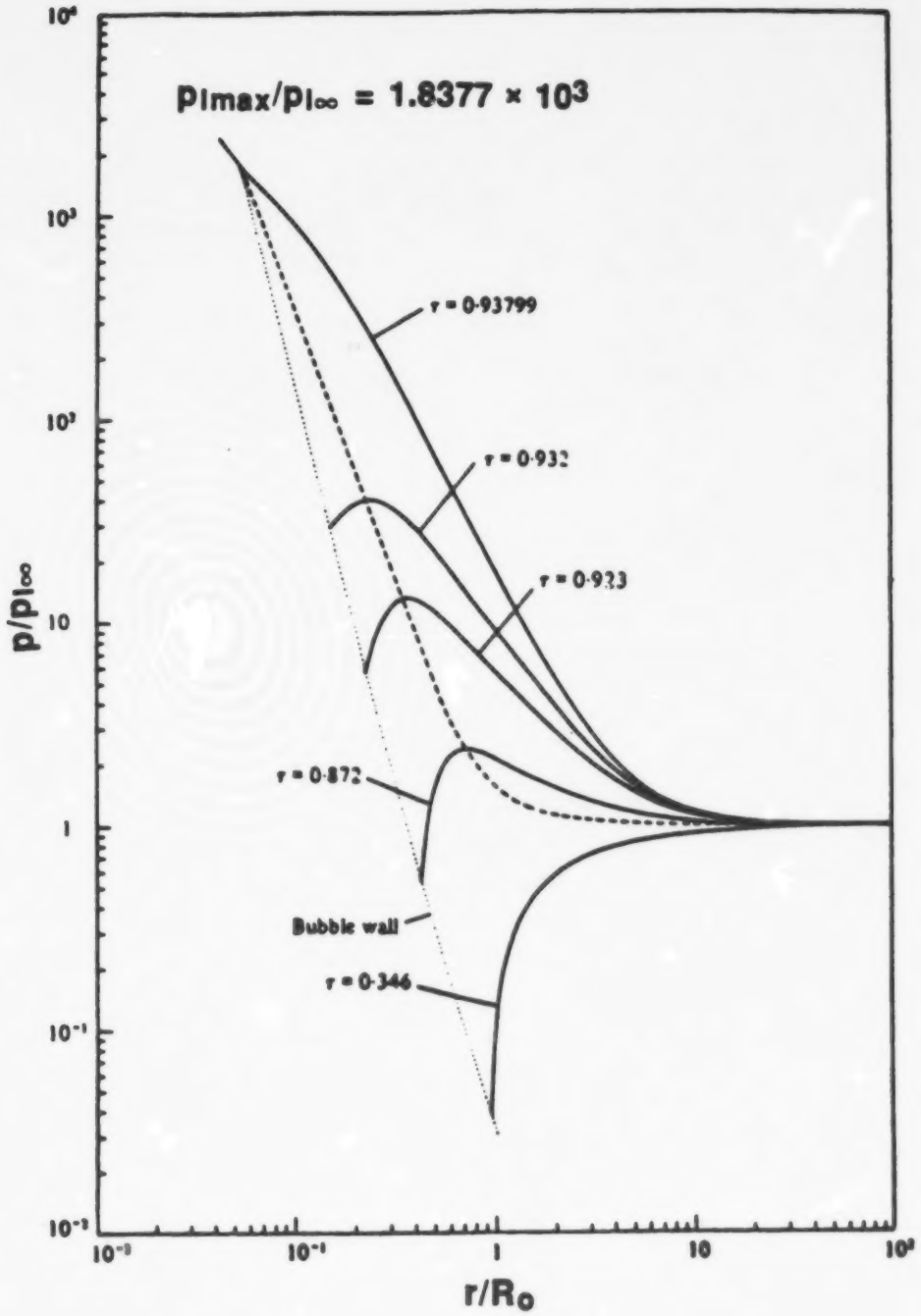

Fig. A-13 Pressure distribution in a liquid before the collapse of a pure vapor bubble with an initial radius of 1.0 mm (Fujikawa et al., 1980)

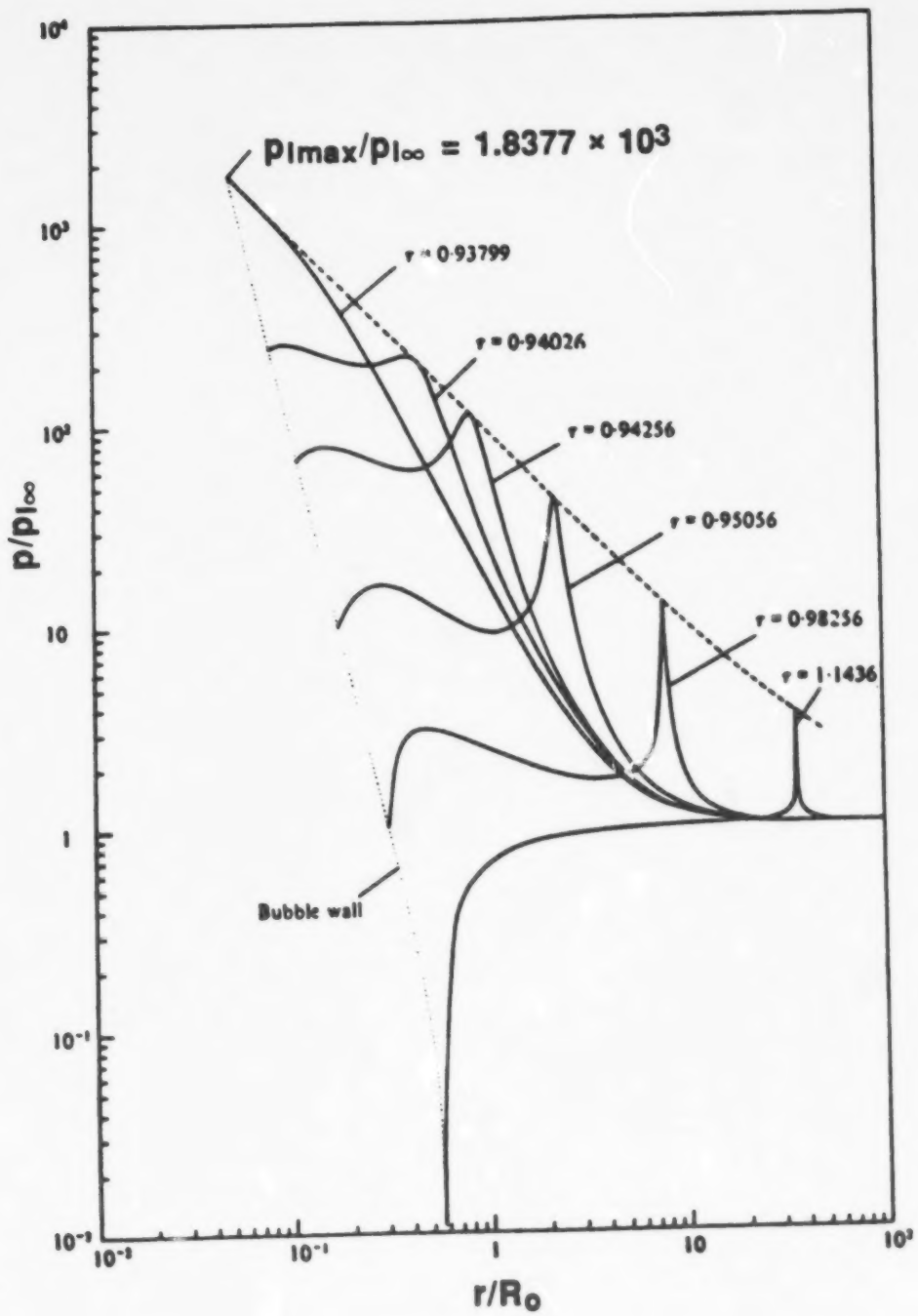

Fig. A-14 **Pressure distribution in a liquid after the collapse of a pure vapor bubble with an initial radius of 1.0 mm (Fujikawa et al., 1980)**

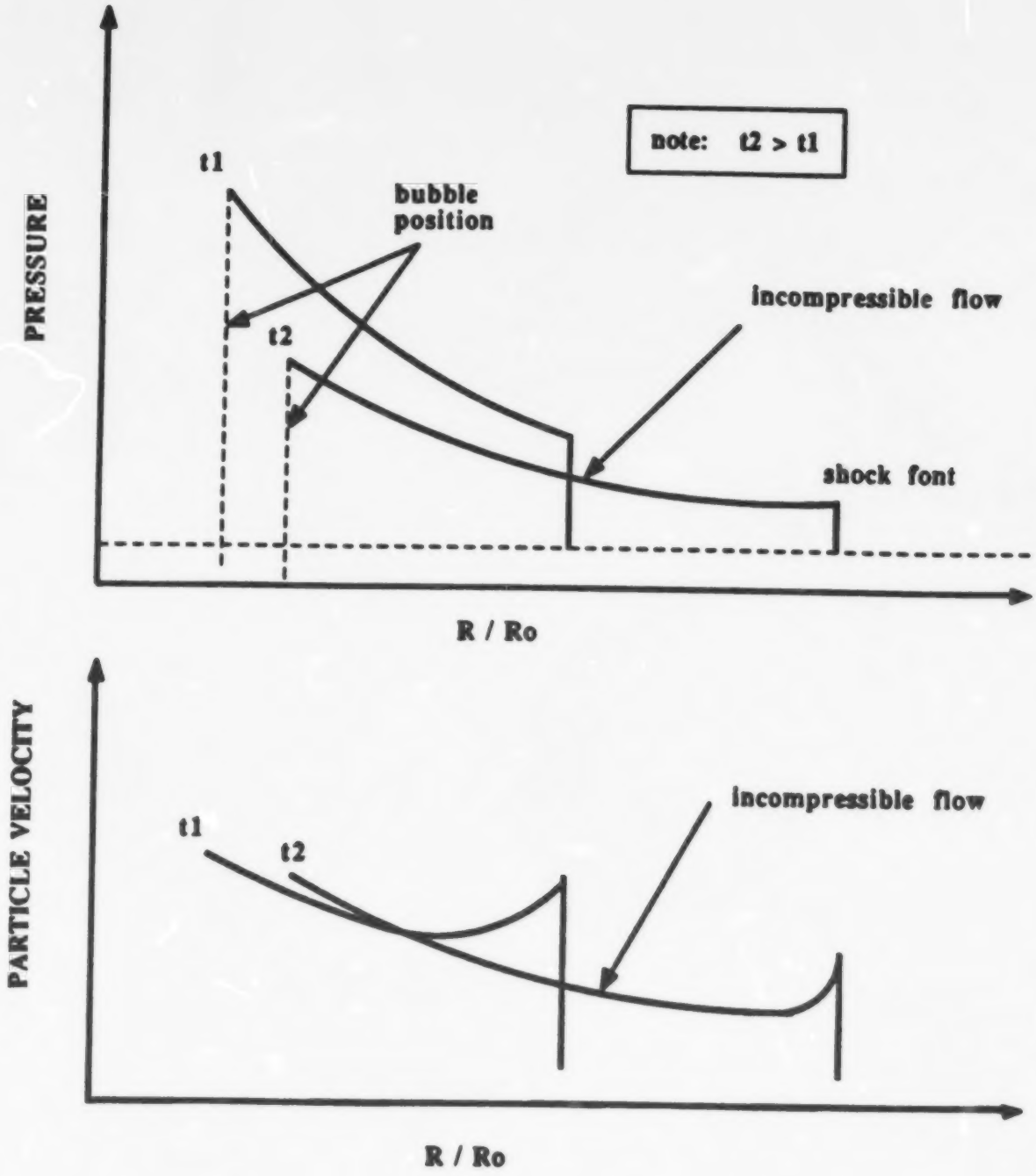

Fig. A-15 Schematic of variation of pressure and particle velocity with distance, for times t_1 and t_2

APPENDIX B

SIMPLIFIED HENRY MODEL

(References cited are those listed in the main text)

SIMPLIFIED HENRY MODEL

In view of the unknown quantities and the numerous arbitrary assumptions inherent in the Henry model, it was felt that it can greatly be simplified, and yet retain its essence, to facilitate the use of the model itself. In the detailed Henry model, two discharge scenarios are analyzed. The stratified flow mod[illegible]sumes that the hydrogen and the molten fuel are separated, with the hydrogen occupying the upper half of the ballooned pressure tube and the molten fuel occupying the lower half. In the dispersed flow model, the hydrogen and molten fuel are mixed homogeneously throughout the cross section of the pressure tube and flow toward the break at the same speed. We feel that the main heat source is the molten fuel in view of its high temperature and heat capacity and we therefore neglect the contribution from the hydrogen. This dispenses with the need to analyze a two phase heat source. The simplified core melt efflux scenario and growth of the steam bubble are illustrated schematically in Fig. B-1.

The core melt efflux velocity U_F is taken to be given by the Bernoulli relation

$$U_F = \sqrt{\frac{2[P_o - P_b(t)]}{\rho_F}} \tag{1}$$

where P_o is the pressure tube driving pressure, $P_b(t)$ is the steam bubble pressure and ρ_F is the core melt density. In the simplified model we disregard the acoustic considerations used by Henry.

The pressure tube rupture area follows that used by Henry namely that it is of fish scale diamond shape and that it grows to a maximum size in time t_o. Thus $A(t) = \frac{1}{2}w\ell$, geometrically, where w is the width and ℓ is the length of the diamond-shaped rupture. $A(t) = A_{max}(\frac{t}{t_o})^2$, temporally where $A_{max} = 2A_o$ and $A_o = \frac{\pi D^2}{4}$ is the cross-sectional tube area.

Thus

$$A(t) = A_{max}(\frac{t}{t_o})^2 \quad \text{for} \quad 0 < t < t_o \tag{2}$$

$$A(t) = A_{max} \quad \text{for} \quad t \geq t_o \tag{3}$$

The molten mass efflux rate is given by

$$\dot{m}_F = \rho_F U_F A(t) \tag{4}$$

from which

$$m_F(t) = \int_o^t \rho_F U_F A(t) dt \tag{5}$$

$$\text{or} \quad m_F(t) = \sum_o^t \dot{m}_F \Delta t \tag{6}$$

The rate of heat release by the molten fuel can be written as

$$\Delta Q_F = \dot{m}_F [h_F + C_F(T_F - T_b)] \Delta t \tag{7}$$

which is the same as that in the Henry model except that it neglects the time of flight t_b across the bubble and the relaxation factor R_{tb}, which was totally arbitrarily assigned by Henry. The parameters above are: h_F, the heat of fusion of the core melt; T_F, the temperature of the core melt; T_b, the bubble steam saturation temperature and C_F, the specific heat of the core melt.

The simplified model disregards the steam recondensation at the bubble surface. We feel that, at this stage, this is a non-essential second-order effect especially that reliable quantitative data is not available.

The heat flux from the core melt ΔQ_F goes into vaporization of steam in the bubble ΔQ_s.

In difference form

$$\Delta Q_s = \{m_s(t-\Delta t)[h_s(t)-h_s(t-\Delta t)] \tag{8}$$

$$+\frac{\Delta m_s}{\Delta t}[h_s(t)-h_\ell]\}\Delta t \tag{9}$$

and $\Delta Q_s = \Delta Q_F$ in the same time interval Δt. This is identical to the Henry formalism. From this, the rate of steam generation can be determined as

$$m_s(t) = m_s(t-\Delta t) + \Delta m_s \tag{10}$$

$$\text{or} \qquad m_s(t) = m_s(t-\Delta t) + \dot{m}_s \Delta t \tag{11}$$

where

$$\dot{m}_s = \frac{\Delta Q_F - m_s(t-\Delta t)[h_s(t)-h_s(t-\Delta t)]}{[h_s(t)-h_\ell]\Delta t} \tag{12}$$

Again this is identical to the Henry formalism except that we neglect the efflux of hydrogen into the bubble. The bubble pressure can now be determined from the moles of steam in the bubble. Thus

$$N_s(t) = N_s(t-\Delta t) + \frac{\dot{m}_s}{M_s}\Delta t \tag{13}$$

$$\text{and} \qquad P_b(t) = \frac{ZN_s(t)RT_b}{V_b} \tag{14}$$

where N_s is the number of moles of steam in the bubble and M_s is the molecular weight of steam, $Z = 1$ and T_b and V_b are the bubble steam temperature and volume, respectively.

The bubble growth and pressure field outside the bubble can now be determined from the Rayleigh model, identical to that used by Henry. Thus,

the bulk radial flow of liquid

$$\frac{1}{r^2} = \frac{\partial(r^2 u)}{\partial r} = 0 \qquad - - - \text{mass conservation} \tag{15}$$

$$\text{or} \qquad r^2 u = R^2 U_b = \text{constant} \tag{16}$$

$$\frac{\partial u}{\partial t} + u\frac{du}{\partial r} = -\frac{1}{\rho}\frac{\partial P}{\partial r} \qquad - - - \text{momentum conservation} \tag{17}$$

$$\text{since} \qquad u = \frac{R^2 U_b}{r^2} = \frac{R^2 \dot{R}}{r^2} \tag{18}$$

$$\text{then} \qquad \tilde{R}(\frac{R}{r})^2 + \frac{2\dot{R}^2 R}{r^2} - \frac{2\dot{R}^2 R^4}{r^5} = -\frac{1}{\rho}\frac{\partial P}{\partial r} \tag{19}$$

Integrating from $R \rightarrow r$

$$P(R) - P(r) = P_b - P(r) \tag{20}$$

$$P(R) - P(r) = -\rho\left[(\tilde{R}R^2 + 2\dot{R}^2 R)(\frac{1}{r} - \frac{1}{R}) + 2\frac{\dot{R}^2 R^4}{4}(\frac{1}{R^4} - \frac{1}{r^4})\right] \tag{21}$$

Assuming $\tilde{R} = 0$ and transforming $y = \frac{R}{r}$

$$P(r) = [P(R) - P_\infty]\left[\frac{4}{3}y - \frac{y^4}{4}\right] + P_\infty \tag{22}$$

$$\text{and} \qquad \dot{R} = U_b = \sqrt{\frac{2}{3}(\frac{P_b - P_\infty}{\rho_\ell})} \tag{23}$$

The simplified Henry formalism was used to carry out calculations of steam bubble growth and pressure field in the moderator coolant. Two core melt temperatures were chosen to represent the heat source term, namely

$T_f = 2473\,K$ and $T_f = 3273\,K$. The rupture time t_o was taken arbitrarily, as was done by Henry, to be $t_o = 1\ m$. The pressure field was calculated for the unbounded coolant environment (the so-called infinite sea model). The results from the simplified analysis are compared to those available in the report of the detailed Henry model calculations at different radial positions. Figs. B-2 and B-3 show the pressure field as a function of time at $r = 0.292m$ and $r = 0.635m$, respectively. The qualitative trend of the results for the simplified and detailed Henry model is similar. The simplified Henry calculations give peak pressures about twice that of the detailed Henry calculation. However, it must be pointed out that the curves extracted from the Henry report do not specify what T_f was used in the calculations nor any other pertinent details. In spite of this, since the simplified model neglects mitigative effects such as steam recondensation, relaxation factors and core melt transit time considerations, then the higher values are not too surprising. These effects as used in the detailed Henry model are accounted for on an entirely arbitrary basis. The more important reassuring conclusion is that the simplified model is qualitatively correct and thereby provides a convenient means to carry out a range of calculations using a variety of input parameters.

Figs. B-4 and B-5 show pressure-time profiles at three different radial positions namely $r = 0.2m$, $r = 0.5m$ and $r = 4.23m$. Fig. B-4 corresponds to a core melt temperature $T_f = 2473\,K$, while Fig. B-5 is for $T_f = 3273\,K$. It is to be pointed out that the peak pressure is equivalent to the steam bubble pressure. The decay of the steam bubble pressure with time, as the bubble grows, is shown in Fig. B-6 for two values of T_f of $2473\,K$ and $3273\,K$. The peak bubble pressure is $10MPa$ which corresponds to the pressure tube pressure $P_o = 10MPa$. Obviously, if the bubble pressure exceeded that level then this would choke off the core melt efflux. Finally,

the spatial pressure distribution and bubble interface position are shown in Figs. B-7 and B-8 at different times for T_F of 2473 K and 3273 K, respectively. The bubble pressure is constant corresponding to the flat initial portion of each curve. Thereafter, the pressure field decays asymptotically to P_∞ as $r \rightarrow \infty$.

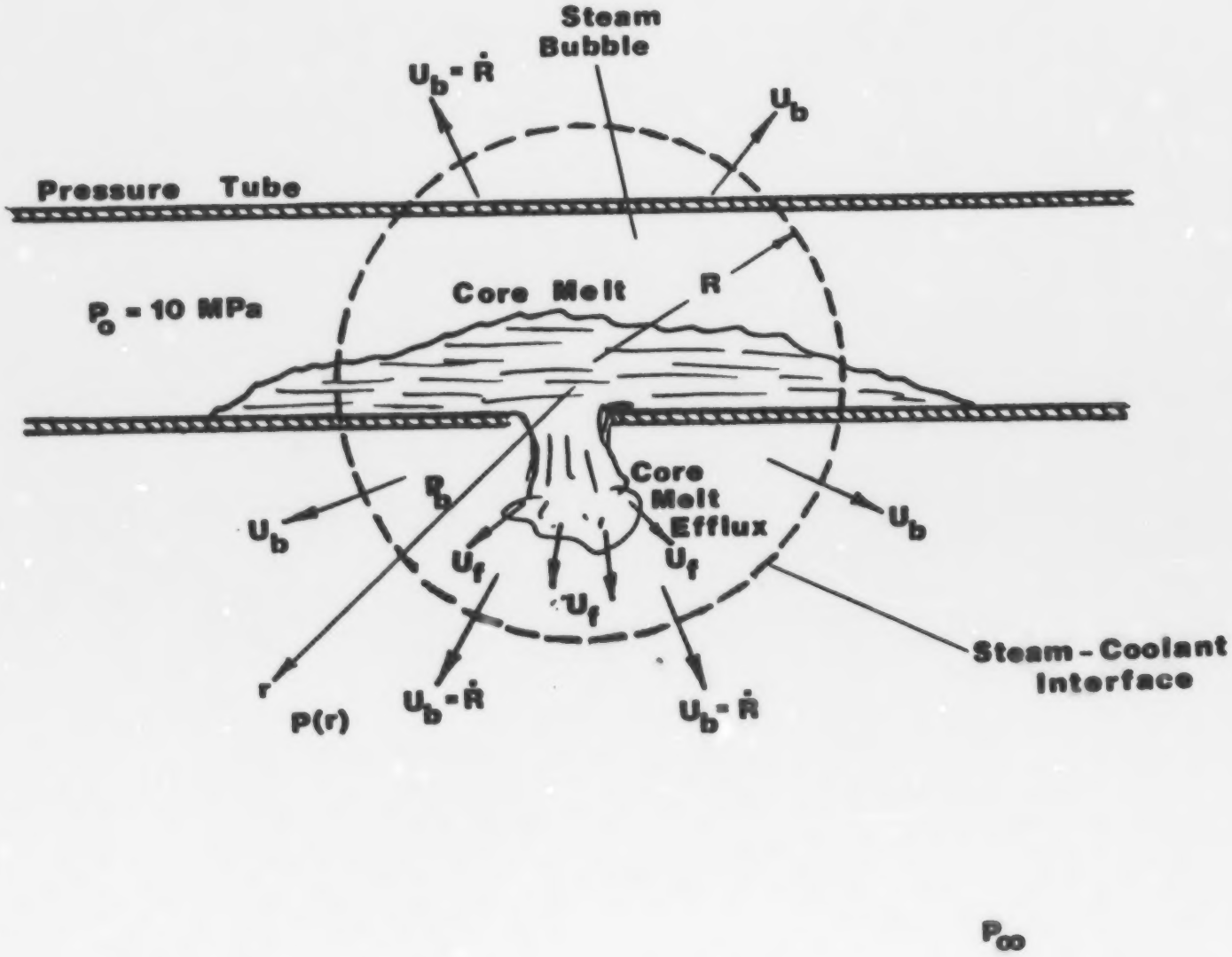

Fig. B-1 Schematic of core melt efflux scenario

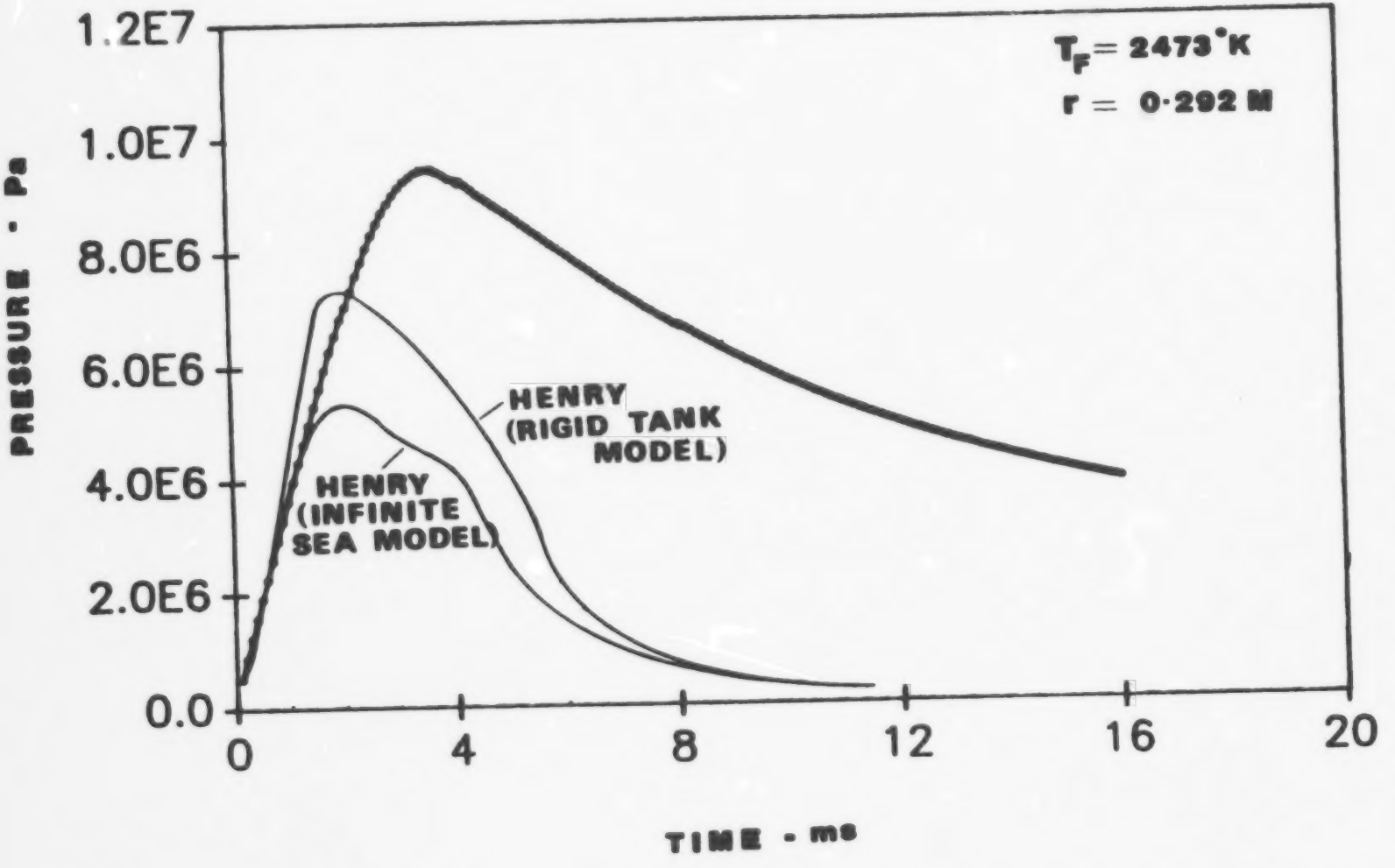

Fig. B-2 Pressure field as a function of time at r = 0.292 m

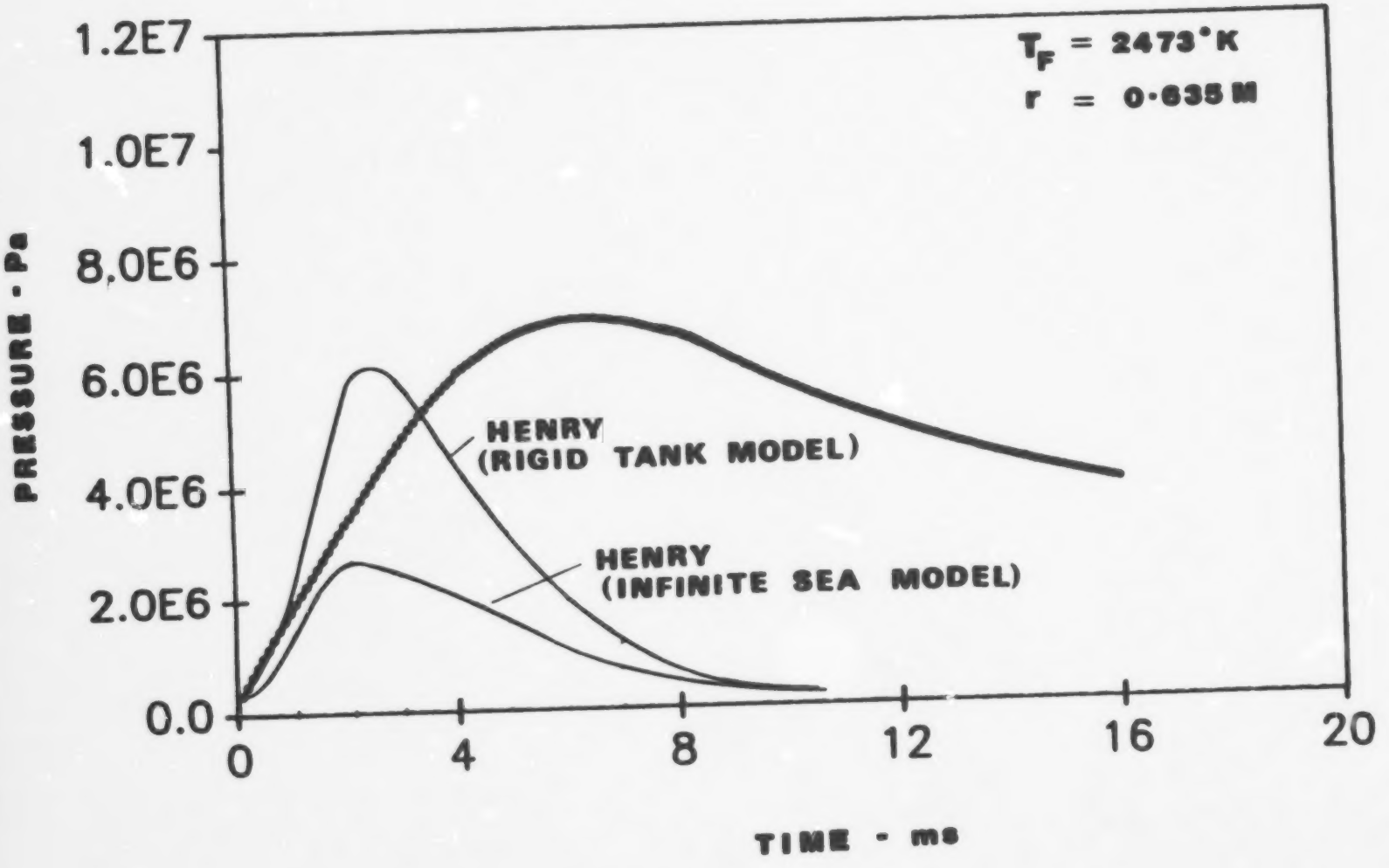

Fig. B-3 Pressure field as a function of time at r = 0.635 m

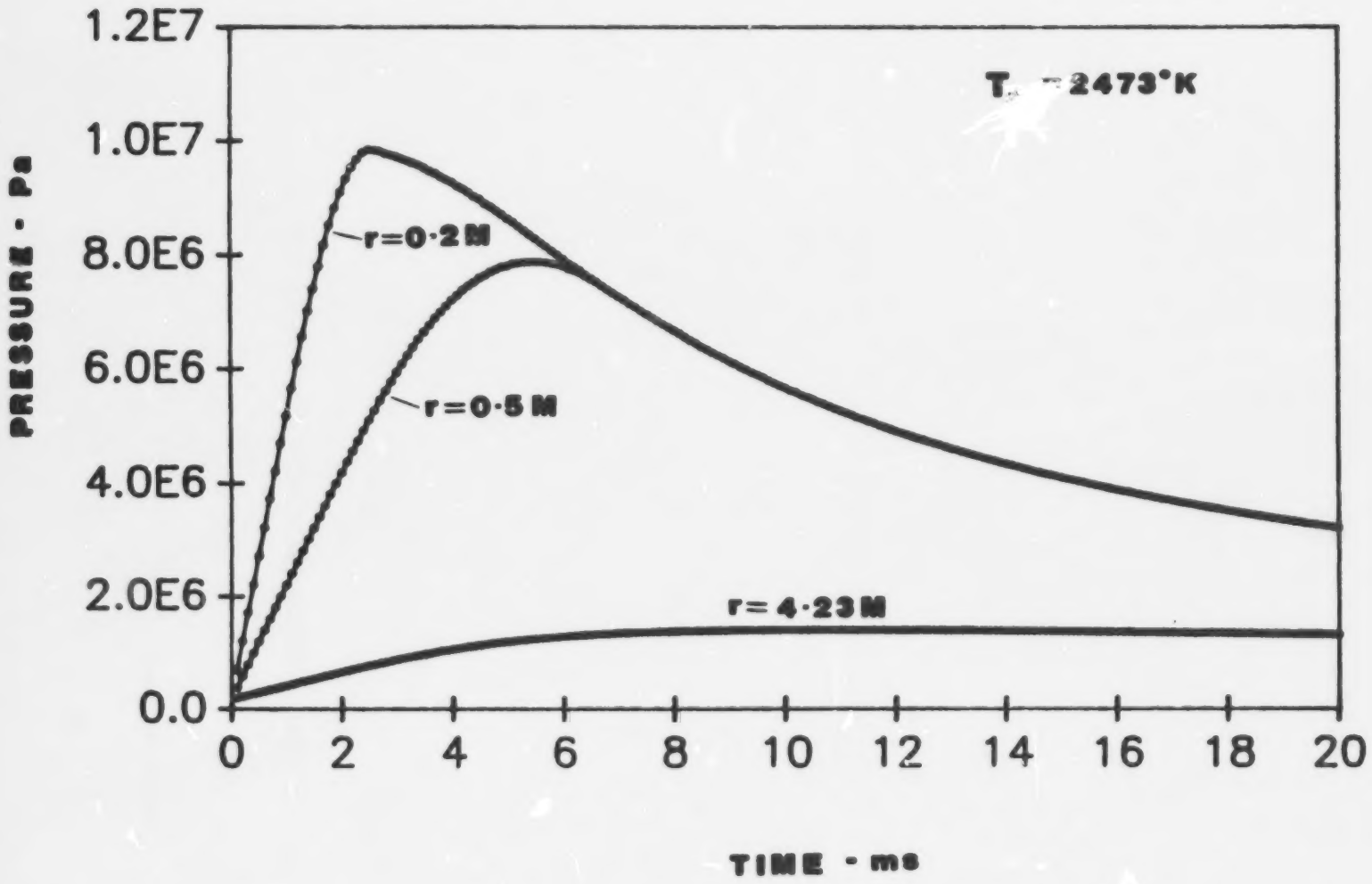

Fig. B-4 Pressure-time profiles at three radial positions for T_F = 2473K

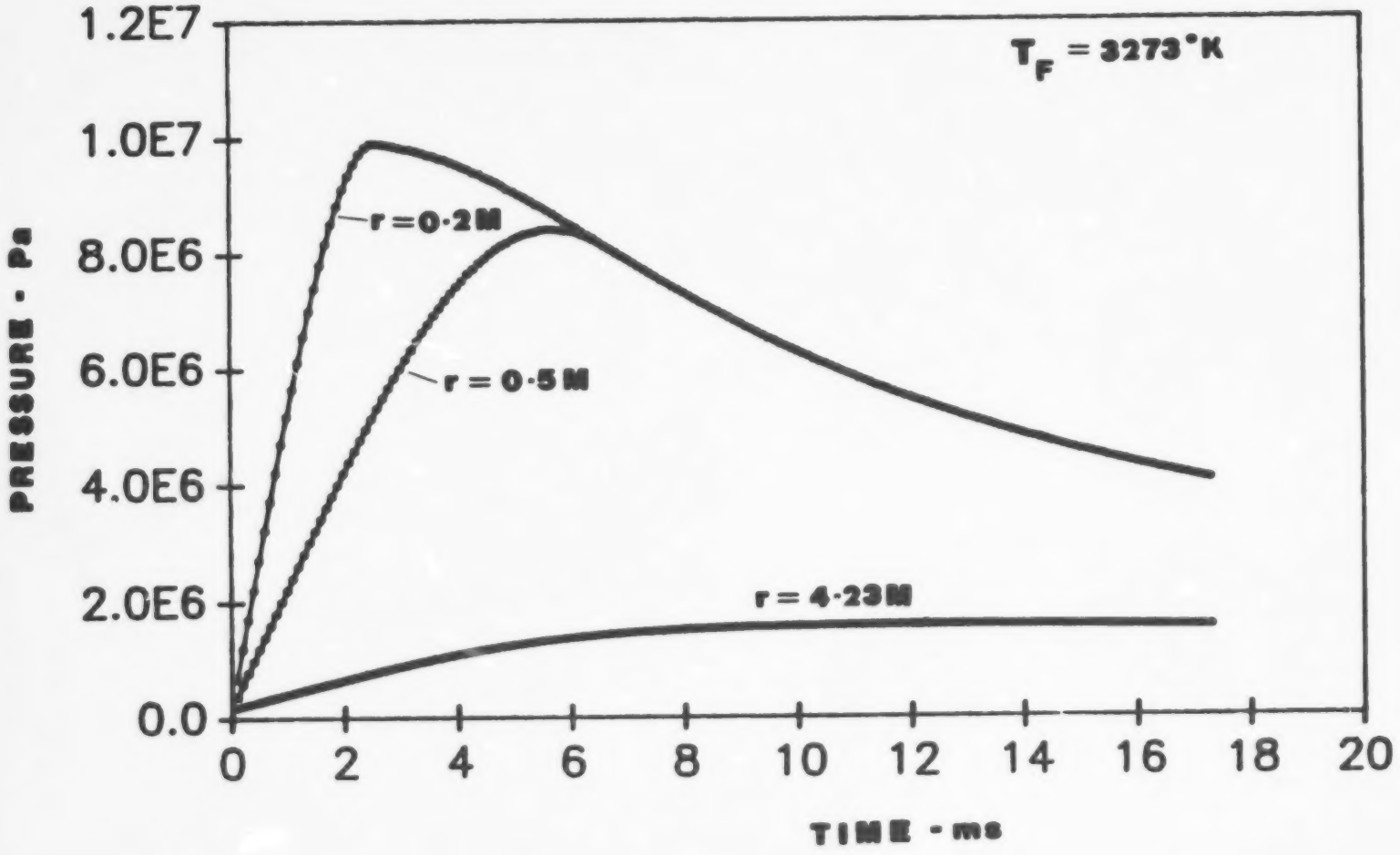

Fig. B-5 Pressure-time profiles at three radial positions for T_F = 3273K

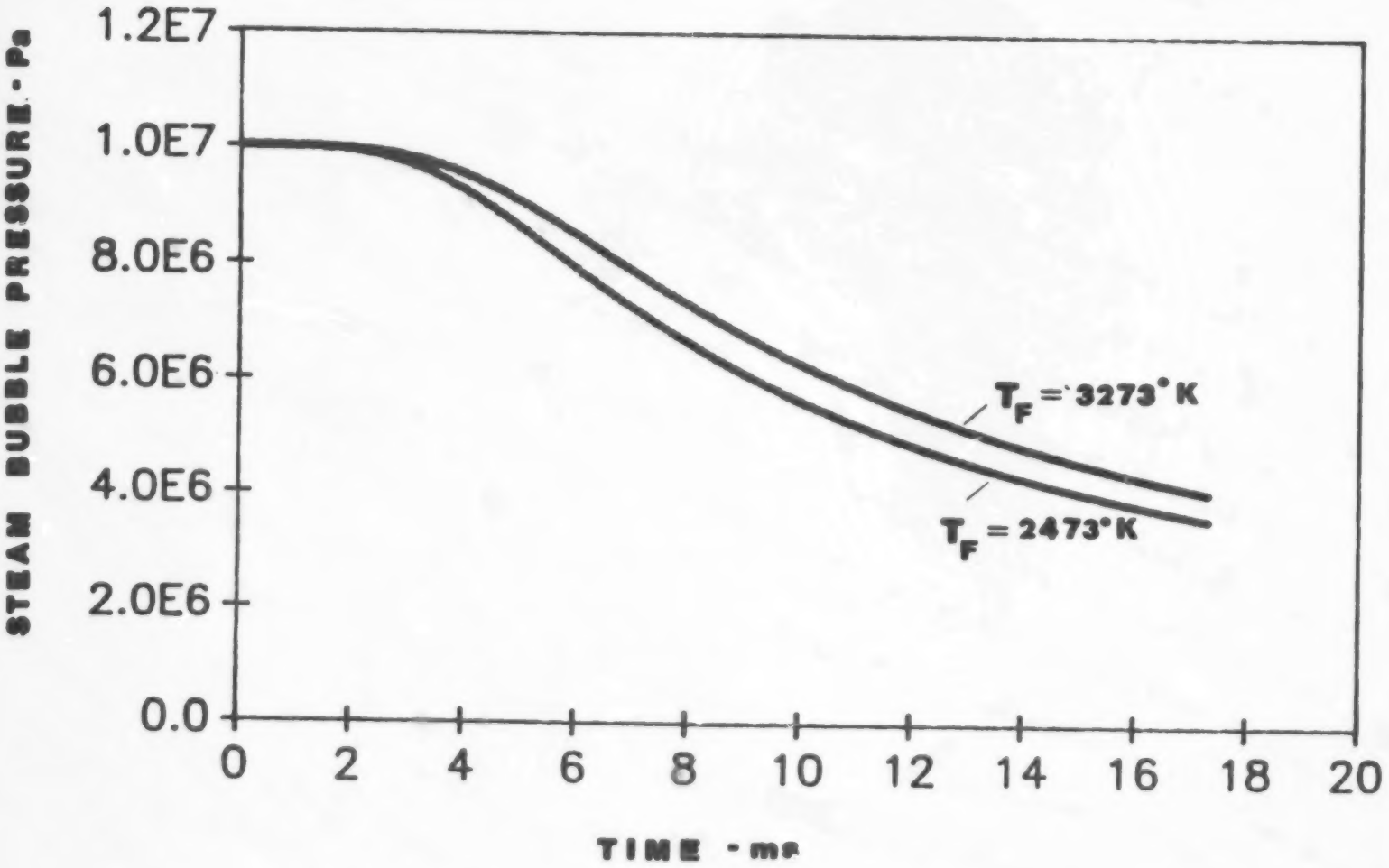

Fig. B-6 Decay of steam bubble pressure

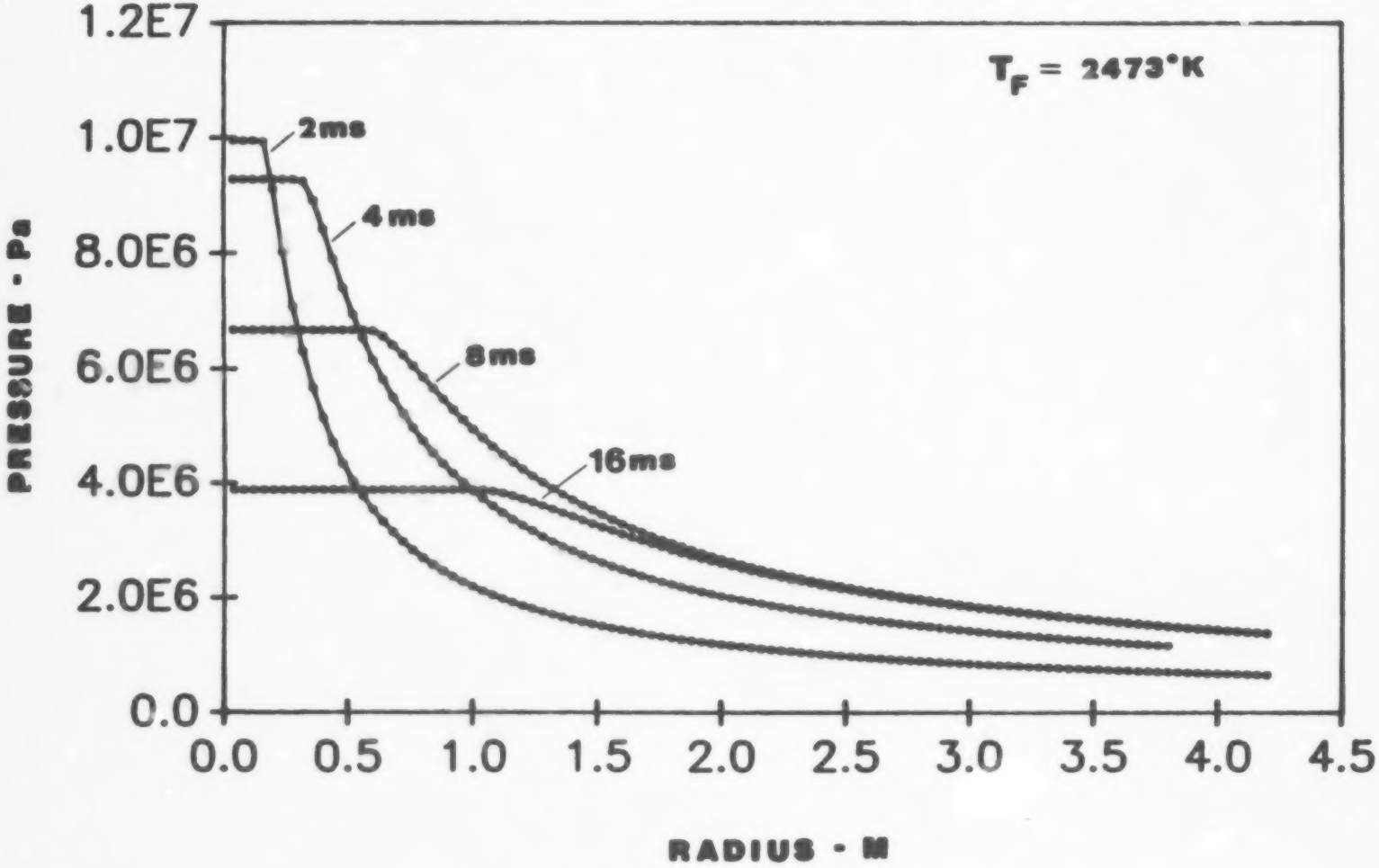

Fig. B-7 Spatial pressure profiles at various times for T_F = 2473K

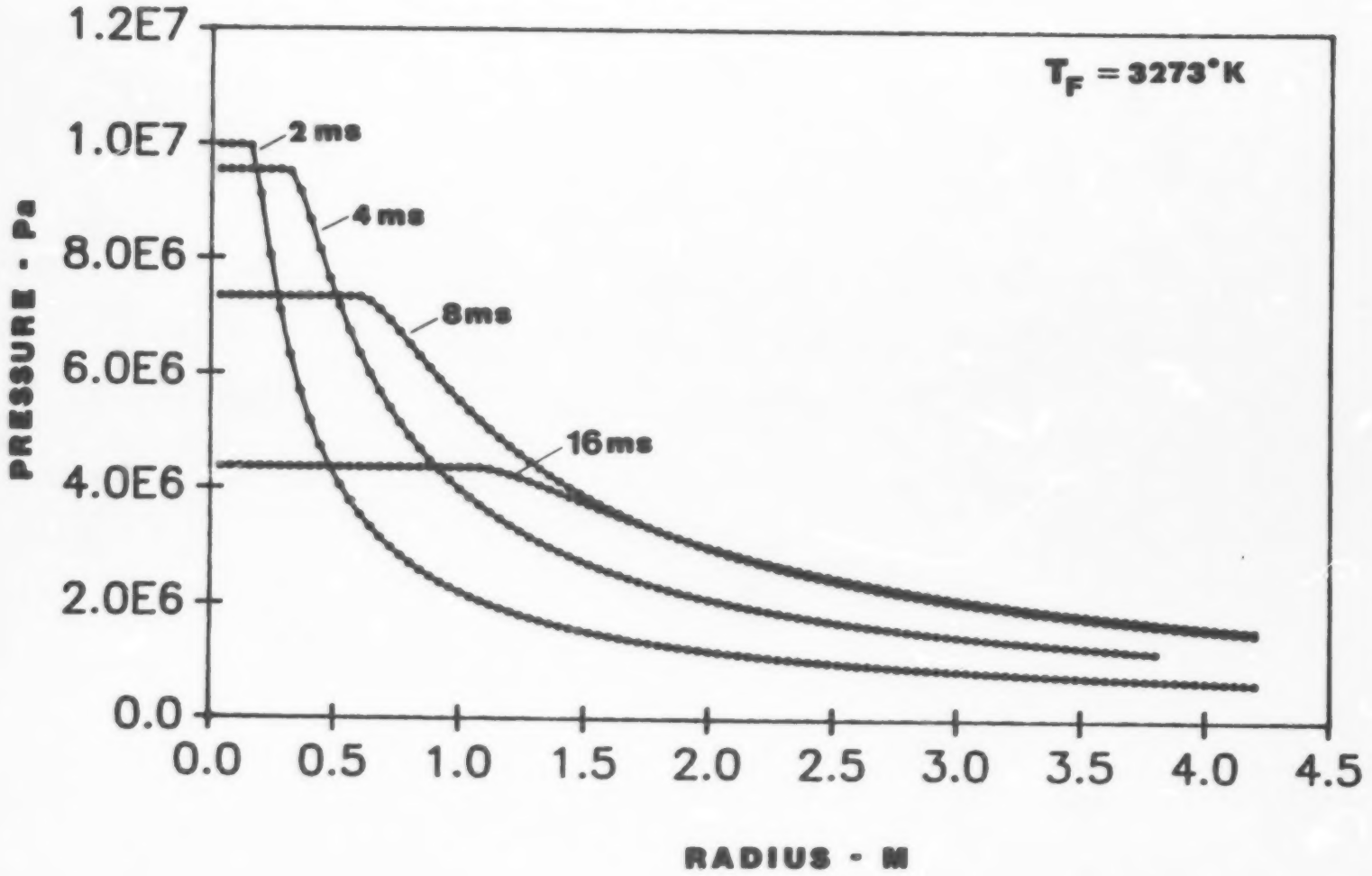

Fig. B-8 Spatial pressure profiles at various times for T_F = 3273K

APPENDIX C

NUMERICAL SIMULATION OF UNDERWATER EXPLOSIONS

(References cited are those listed in the main text)

1 INTRODUCTION

The blast properties of underwater explosions have been investigated by numerous investigators for a wide variety of explosives ranging from condensed explosives, electric discharges, collapsing vapour bubbles and fuel-oxygen detonations. From a qualitative point of view, underwater explosions differ considerably from their air blast counterpart due to the numerous phases and time scales involved. The initial stage of the process essentially involves the sudden release of energy resulting in the formation of a primary shock and acoustic oscillations in the gas bubble. The relatively short time scales associated with this phase are essentially controlled by the initial size and pressure of the exploding charge along with the acoustic impedance inside and outside of the bubble. This process is followed by relatively long oscillations of the bubble-water complex which are controlled by the size, pressure and compressibility of the bubble, and the density of the surrounding liquid. Since the pressure impulses generated by these oscillations can be as important as that produced by the primary shock, a complete blast analysis must somehow take into account both the short and long time scale processes. This report presents such an analysis for the particular case of an underwater explosion generated by a gas bubble initially pressurized at 28.0 MPa.

2 NUMERICAL MODELS FOR BUBBLE OSCILLATIONS

The relatively slow bubble oscillations which are observed following an underwater explosions are due to the "spring" action of the compressible gas and the inertia of the neighboring fluid. Most models assume an ideal gas inside the bubble which is further assumed to expand and compress isentropically such that

$$P(R) = P_b (R_b/R)^{3\gamma} \tag{1}$$

where P_b and R_b denote the initial bubble pressure and radius respectively.

The modelling required to describe the liquid essentially depends on whether the explosion is sufficiently violent that compressibility effects in the liquid itself must be taken into account. A good summary of the various levels of approximation involved can be found in the paper by Lyoboshits and Pervushin (1972) who present comparative calculations using the fully compressible model of Kirkwood and Bethe (1942), the "quasi-acoustic" model which assumes constant sound speed in the liquid, and finally the initial formulation of

Rayleigh (1917) which considers the limit of an incompressible liquid. When compression effects are taken into account, the models are usually based on the Tait equation of state

$$P = B\left[\left(\frac{\rho}{\rho_o}\right)^n - 1\right], \tag{2}$$

where B = 304 MPa, n = 7.15, and which is found to be typically valid for pressures as high as 2500 MPa (Cole, 1948).

Generally speaking, the bubble oscillation equation may be obtained by integrating the momentum equation for the liquid between the bubble surface to ambient conditions at infinity.

$$\int_R^\infty \left[\rho\frac{\partial u}{\partial t} + \rho u\frac{\partial u}{\partial r} + \frac{\partial P}{\partial r} = 0\right] dr \tag{3}$$

For an incompressible flow, this integration is quite easily performed using the flow velocity relation $u = (R/r)^2\dot{R}$ obtained from conservation of mass whereby one obtains the well known Rayleigh bubble oscillation equation

$$R\ddot{R} + 1.5\,\dot{R}^2 = \frac{P(R) - P_o}{\rho_o} \tag{4}$$

where R, $\dot{R}$, $\ddot{R}$ and P(R) denote the bubble radius, velocity, acceleration and pressure, respectively; where P_o represents the ambient pressure in the liquid. For very small bubble pressures, the Rayleigh equation may then be linearized to

$$\ddot{z} + \frac{3\gamma P_o}{\rho_o R_a^2} z = 0 \tag{5}$$

where $z = R - R_a$, $R_a = R_b(P_b/P_o)^{1/3\gamma}$ = equilibrium position, which results in simple harmonic motion with a period

$$\tau = 2\pi\left[\frac{\rho_o R_a^2}{3\gamma P_o}\right]^{1/2} \tag{6}$$

The Rayleigh equation provides a good description of the oscillation process provided that the initial pressure is sufficiently small that the bubble velocity remains much smaller than the sound speed, c_o, in the liquid. This equation is also limited by the fact that the assumption of incompressible flow prevents any acoustic wave energy transfer from the gas to the surrounding water. Consequently, in spite of its non-linear form, the oscillations obtained from this equation are always undamped.

The inclusion of compressibility effects into the analysis essentially prevents a direct integration of the momentum equation since the velocity field can only be obtained by a simultaneous solution of both the mass and momentum equations. For the case of weakly compressible flow, the velocity field may be derived from the velocity potential ϕ which, in turn, may be assumed to obey the spherical acoustic wave equation

$$\left[\frac{\partial}{\partial t} + c_o\frac{\partial}{\partial r}\right] r\phi = 0 \; ; u = -\frac{\partial \phi}{\partial r} \tag{7}$$

Trilling (1952) has shown that the inclusion of this additional equation and the exclusion of all terms of the order of $(u/c_o)^2$ or higher, where c_o is the ambient liquid sound speed, results in the following acoustic bubble oscillation equation

$$R\ddot{R}\left\{1 - \frac{2\dot{R}}{c_o}\right\} + 1.5\dot{R}^2\left\{1 - \frac{4\dot{R}}{3c_o}\right\} = \frac{P(R) - P_o}{\rho_o} + \frac{R\dot{P}}{\rho_o c_o} \tag{8}$$

which reduces to the Rayleigh equation when $\dot{R} << c_o$. For small oscillations, this equation may once again be linearized to

$$\ddot{z} + \frac{3\gamma P_o}{\rho_o c_o R_a}\dot{z} + \frac{3\gamma P_o}{\rho_o R_a^2} z = 0 \tag{9}$$

which now admits a damped harmonic oscillation solution.

The intrinsic assumption in the above acoustic equations is that the pressure waves, radiated from the bubble, travel at the sound speed of the liquid which is assumed to be constant. Naturally, as the initial bubble pressure is increased, the wave trajectory is determined by the velocity u + c where both the fluid velocity, u, and the local sound

speed, c, become time dependent variables which must also be determined as part of the overall solution. A relatively complex bubble oscillation equation taking these effects into account was in fact derived by Kirkwood and Bethe (1942).

Calculations performed by Lyuboshits and Pervushin (1972) for initial bubble pressures $P_b/P_o < 200$ indicate that the bubble oscillation amplitudes and frequencies obtained from the acoustic approximation are virtually identical to that obtained from the more accurate Kirkwood and Bethe equation.

In order to further investigate the relative merits of the various models, we have performed a series of calculations using the Rayleigh (incompressible), Trilling (acoustic), Kirkwood and Bethe (non-linear acoustic) as well as the linearized acoustic equation over a bubble pressure range of 0.01 - 1000 MPa. As expected, the models show very good agreement at low initial pressure with the exception that the Rayleigh equation fails to describe properly the acoustic oscillation decay. The acoustic effects also result in a reduction in the maximum bubble radius during the first oscillation and decrease in the overall oscillation period. It is also interesting to note that the acoustic model of Trilling, which assumes constant wave propagation velocity, leads to bubble oscillation trajectories which are very close to the more complex Kirkwood and Bethe model for bubble pressures up to approximately 100 MPa.

3 INITIAL SHOCK FORMATION

In order to describe the initial phase of the underwater blast process the properties of the shock wave generated by the sudden pressure release must first be determined. The instantaneous shock generation may be described by solving the classical shock tube problem for the particular case of a gas-water interface. This involves the simultaneous solution of the isentropic flow equation in the ideal gas and the shock hugoniot in the liquid on the basis of the Tait equation of state so as to match the velocity and pressure across the interface. This problem has been solved by Glass and Heuckroth (1963) who have shown that the transmitted shock pressure, P_s, is virtually equal to the initial bubble pressure P_b for $P_b < 50$ MPa. In this regime, one may also obtain a good estimate of initial fluid velocity, u_s, behind the shock transmitted using the simple acoustic relation

$$u_s = \frac{P_s - P_o}{\rho c_o} = \frac{P_b - P_o}{\rho c_o} \qquad (10)$$

4 INITIAL SHOCK DECAY

Generally speaking, the blast decay process may be described by simultaneously solving the mass and momentum equations for a spherical coordinate system

$$\frac{\partial \rho}{\partial t} + \frac{1}{r^2}\frac{\partial \rho u r^2}{\partial r} = 0 \tag{11}$$

$$\frac{\partial \rho u}{\partial t} + \frac{1}{r^2}\frac{\partial \rho u^2 r^2}{\partial r} + \frac{\partial P}{\partial r} = 0 \tag{12}$$

in conjunction with the Tait equation of state. Due to the non-linear nature of these equations, an exact solution requires the use of a finite difference code capable of handling sharp pressure gradients occurring at the shock front without excessive instabilities or artificial diffusion. One algorithm which has a very good track record in the simulation of transient compressible flows is the Flux Corrected Transport (FCT) method of Boris (1976) which is particularly noted for its relatively low level of artificial diffusion.

An alternate approach to the problem is to seek approximate solutions to the above equations which can describe both the compressible flow near the shock front, along with the nearly incompressible flow in the vicinity of the bubble. Due to the relatively good accuracy of the acoustic approach in describing the bubble oscillation and the initial transmitted shock strength, it would seem reasonable to attempt a similar analysis for the subsequent pressure decay outside the bubble. In the acoustic approximation, the time dependent pressure and velocity fields outside the bubble may be derived from the time history of the bubble oscillation. Appropriate methods for calculating the external flow field have been presented by Trilling (1952), Keller and Kolodner (1956) and Lyuboshits and Pervushin (1972). Following the analysis of the latter, the calculation may be performed by assuming $G(r,t) = r\partial\phi/\partial t$ obeying the acoustic wave equation

$$\frac{\partial G}{\partial t} + c_o \frac{\partial G}{\partial r} = 0 \tag{14}$$

where G may be expressed through the momentum equation as

$$G(r,t) = r[h(r,t) + \tfrac{1}{2}u(r,t)^2] \tag{15}$$

where $h = \int dP/\rho$ and u denote the enthalpy and fluid velocity, respectively. Since in the linear acoustic limit, the enthalpy $h = (p - p_o)/\rho_o$ the characteristic equation approximately states that the total pressure (i.e., static + stagnation) in the liquid decays at a rate proportional to 1/r along the straight characteristic emanating from the bubble surface and corresponding to the wave velocity in the ambient fluid. Furthermore, in this acoustic approximation, the velocity of the fluid may be estimated as

$$u(r,t) = \dot{R}(R/r)^2 + \frac{G(r,t)}{rc_o}\left[1 - \frac{R}{r}\right] \tag{16}$$

which consists of an incompressible flow term near the bubble surface and an acoustic decay term in the far-field.

On the basis of the above equations, and the acoustic bubble oscillation equation, the pressure and velocity for any radius r and time t may thus be obtained as follows

1) Determine the time at which a wave reaching the position r at time t was initially radiated from the bubble surface. This time is given by

$$c_o(t - t_b) = r - R(t_b) \tag{17}$$

where $R(t_b)$ denotes the bubble radius obtained from the solution of the bubble oscillation equation.

2) Evaluate $G(r,t) = G(R(t_b))$ from the enthalpy and velocity at the bubble surface at a time $t = t_b$

$$G(r(t_b)) = R(t_b)\{h(R(t_b) + \dot{R}(t_b)^2/2\} \tag{18}$$

(h may be evaluated through the relation $h = (c^2 - c_o^2)/(n - 1)$ where n is the exponent in the Tait equation of state, and c is the local sound speed $c = \{dp/d\rho\}_s^{1/2}$ obtained by differentiating the Tait equation of state. In the linear approximation, one could also use the simpler relation $h = (p - p_o)/\rho_o$).

3) Compute the flow velocity and the dynamic pressure

$$u(r,t) = \dot{R}(R/r)^2 + [G(r,t)/rc_o](1 - R/r) \quad (19)$$

$$p_o(r,t) = \rho_o u(r,t)^2/2 \quad (20)$$

4) Compute the local enthalpy and sound speed

$$h(r,t) = G(r,t)/r - 1/2\, u(r,t)^2 \quad (21)$$

$$c^2(r,t) = h(r,t)(n - 1) + c_o^2 \quad (22)$$

5) Compute local pressure using, once again, the Tait equation of state and the sound speed definition.

5 COMPUTATIONAL RESULTS

In order to investigate the relative performance of the acoustic model in terms of the finite difference FCT solution, computations were performed for the particular case of an initial bubble pressure of 28.0 MPa and $\gamma = 1.327$. These values were suggested to us as typical values which may be expected to occur as the result of a vapour explosion. For both calculations, the motion of the bubble interface was derived by solving Trilling's acoustic bubble oscillation equation with an initial bubble velocity of 19.1 m/s which was obtained from the linear acoustic relation for the fluid velocity behind the transmitted shock. The peak bubble velocity is approximately 74 m/s and occurs at a time of 5 ms which is considerably shorter than 1.7 s period of the bubble oscillations. The bubble radius trajectories are shown in Figures C-1 to C-4 and compared to those obtained with the more approximate Rayleigh equation for incompressible flow and the more accurate Kirkwood and Bethe equation. As previously state, the Trilling and Kirkwood and Bethe models yield virtually identical results over this pressure range whereas the Rayleigh equation remains valid only in the very early phase of the oscillations.

The pressure and velocity profiles derived from the acoustic and FCT calculations are compared in Figures C-5 - C-6 respectively for the case of a bubble with an initial radius of 1 m. In the FCT calculations, the flow inside the bubble was also calculated in order to estimate the magnitude of the gasdynamic oscillations occurring due to the sudden pressure

release from the bubble. The initial gas temperature for this particular calculation was 900 K which may, in fact, be lower than that expected from a vapour explosion (~ 1200 K). The extent of the bubble on the pressure profiles can be seen from the flat portion of the acoustic calculation which assumes uniform conditions inside the bubble. It is clear from both the pressure and velocity profiles that the solutions obtained outside the bubble are virtually identical for both methods. Inside the bubble, the FCT calculation shows relatively small gasdynamic oscillations which are amplified near the centre of the bubble due to focussing effects. Near the interface, the pressure remains very close to that obtained assuming uniform isentropic expansion in the bubble. The velocity profiles inside the bubble are, of course, highly non-uniform due to the no-flow conditions at the centre. The FCT calculations also show a sharp "spike" in pressure at the interface which is due to a very slight error in the density at this point which is greatly amplified by the 7.15 power in the Tait equation of state. Overall, the performance of the acoustic model is excellent for this pressure range and results in profiles which are, in fact, better resolved near the shock than the FCT calculation which was performed using 100 computations cells inside the bubble and nearly 4000 cells outside. Considering that computational times for these FCT and acoustic calculations were 10 hrs and 1.5 min respectively on a machine with a computational power similar to the VAX 780, it would appear that the acoustic model represents the most appropriate model for pressure levels encountered in vapour explosions. Since the Trilling oscillation equation is also based on the acoustic approximation, and is in very close agreement with the more general Kirkwood and Bethe equation for pressures less than 100 MPa, it would seem that the use of this equation is preferable to using a complete finite difference analysis to solve for the motion of the bubble interface. Indeed due to the very large gradients which are observed near the interface, and the constant compromises made in finite difference codes to resolve both stability and artificial diffusion problems, we have found that the use of such codes to predict the gas-water interface motion is probably considerably less accurate than bubble oscillation equations which are derived from integral methods and not susceptible to computational errors near the interface.

Due to the short run times associated with acoustic calculations, the above calculations which describe the very early blast decay were extended so as to obtain pressure and velocity profiles at larger times, as well as static pressure and dynamic pressure histories for the initial shock decay and subsequent bubble collapses. The calculations were performed for a total time of 6.6 seconds which was sufficient to accommodate 4 oscillation cycles. The pressure profiles shown in Figures C-7 and C-8 show the initial

monotonic profile which eventually separates into a compressible region near the shock and an incompressible region near the bubble surface. Near the bubble surface, there exists a very sharp pressure gradient which is associated with the deceleration phase of the bubble. This deceleration eventually leads to a flow reversal and the collapse of the bubble (Figure C-9, 1st and 2nd frame), the sudden re-pressurization of the bubble, and to the formation of the second pulse (Figure 9, 3rd frame). The static and dynamic pressure pulses produced by the initial shock and the first two bubble collapses are shown in Figures C-10 - C15 for positions 2 m, 5 m, 10 m, 20 m, 50 m and 100 m downstream, respectively. The pressure histories at 2 m reveal a gradual increase in dynamic pressure as the bubble surface approaches that position. This steady ramp is abruptly terminated when the bubble surface crosses this point and the relatively low density inside the gas bubble results in a negligible dynamic pressure which, in these calculations, is set to zero. During the bubble collapse, the dynamic pressure histories at this position reveal two ramps which are associated with the compression and expansion phases. The fact that the dynamic pressure in the compression phase is larger than that for the expanding phase is a consequence of the compressibility of the liquid which results in the formation of a compression wave which acts to permanently remove energy from the fluid in the vicinity of the bubble. This acoustic energy transfer results in a damping of the oscillations which, in this pressure regime, is sufficiently severe that the amplitude of the static pressure pulses decreases significantly for each subsequent cycle.

The damping of the pressure pulses, which is observed at all locations, results in a first collapse pressure pulse which is typically 55% that of the initial shock, and a subsequent pulse with a further pressure reduction of 35%. On the other hand, the pressure pulse generated by the bubble collapse is significantly longer in duration than for the initial shock. Consequently, although the largest pressure is encountered behind the incident shock, the strongest impulse occurs on the first bubble collapse. The peak pressure and impulse data for the initial shock and three bubble collapses are summarized in Figure C-16. It is evident from these plots that the peak pressure rapidly assumes a 1/r decay law as predicted from simple far-field acoustic theory. A similar far-field decay behaviour is also observed for positive phase impulses at distances larger than 10 m (i.e., 10 bubble radii for this case).

6 CONCLUSIONS

The present study has demonstrated the importance of compressibility effects in the pressure pulses generated by pressurized gas bubbles which could occur as the result of a vapour explosion. These effects are clearly observed not only in the leading shock but also in the subsequent bubble collapses where energy is repeatedly removed from the oscillations through the formation of compression waves. This accounts for the pressure reduction of 45% between the static pressure generated by the leading shock and the first bubble collapse. The validity of the acoustic model to describe the flow has been demonstrated through comparisons with detailed finite difference calculations. In fact, for the pressure level of 28.0 MPa considered in the calculations, it would appear that the lack of artificial diffusion in the acoustic solutions results in highly resolved profiles and a CPU time reduction of 2-3 orders of magnitude.

In spite of its accuracy in describing the inviscid flow field generated by a suddenly pressurized sphere, some issues should be addressed in order to assess the full relevance of the above calculations to actual vapour explosions. Firstly, the calculations have been performed assuming no heat or mass transfer, or any time dependent phase changes inside the bubble during the explosion process. Secondly, pressurization of the gas bubble has been assumed instantaneous or, at least, occurring on a time scale which is much shorter than the characteristic time of the oscillations. Preliminary calculations have shown that, in order for the predicted oscillations to be accurate, the pressurization time should be smaller than that required for the bubble to reach its maximum velocity. For the bubble pressure of 28.0 MPa, this peak velocity is achieved very early at a time which is more than two orders of magnitude shorter than the bubble oscillation period. If the pressurization is significantly longer than this time, the pressure oscillations can easily be reduced by an order of magnitude. On the other hand, if condensation occurs inside the bubble, the collapse pressure could be significantly higher than expected assuming a single gas phase during the oscillation process. Finally instabilities occurring at the bubble interface during the bubble rebound could induce very rapid mixing and a secondary vapour explosion. These effects are clearly beyond the real of the present investigation and should be considered in future studies.

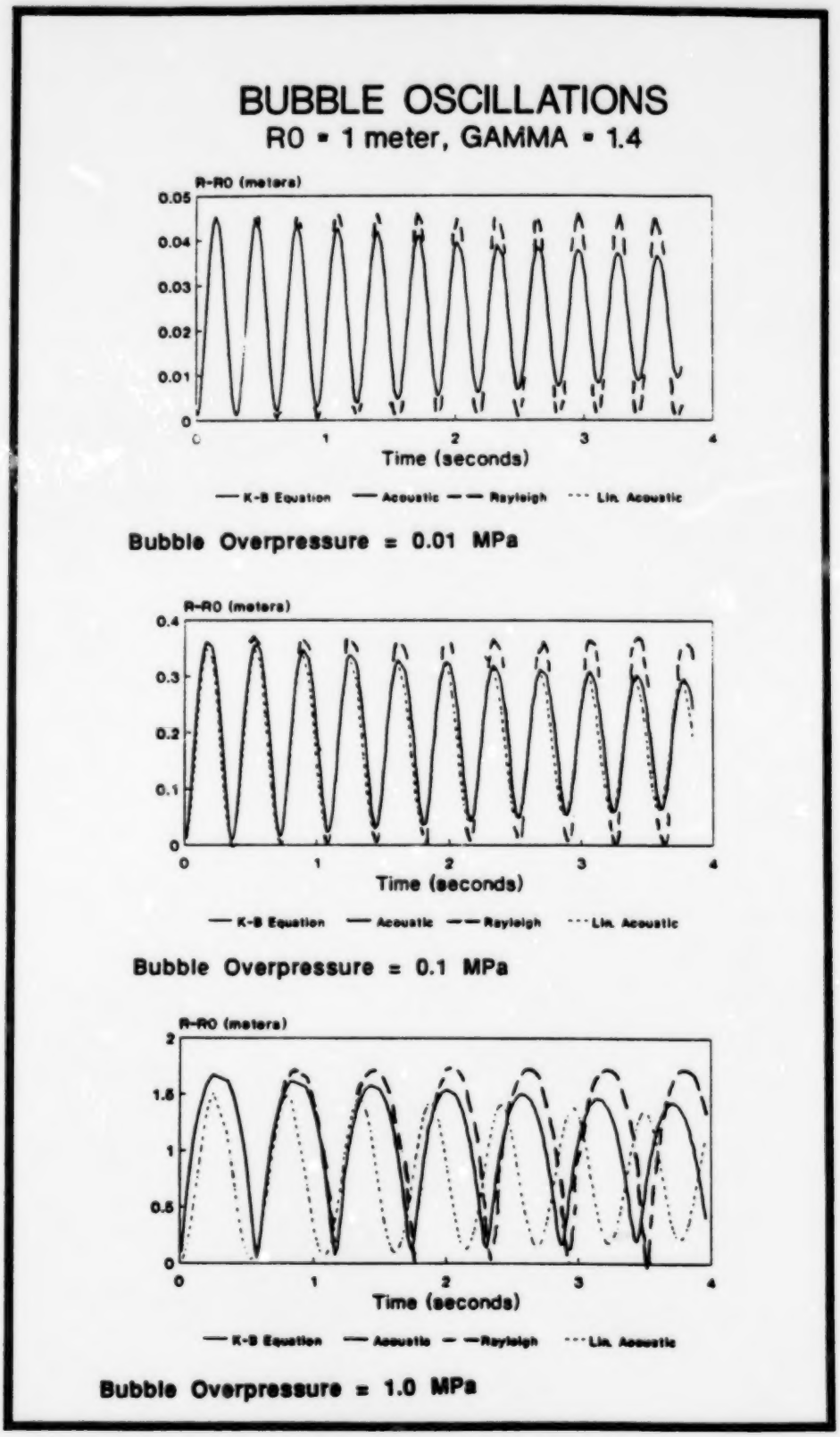

Fig. C-1 **Bubble oscillations computed using various numerical models with initial bubble overpressures ranging from 0.1 to 10 atm**

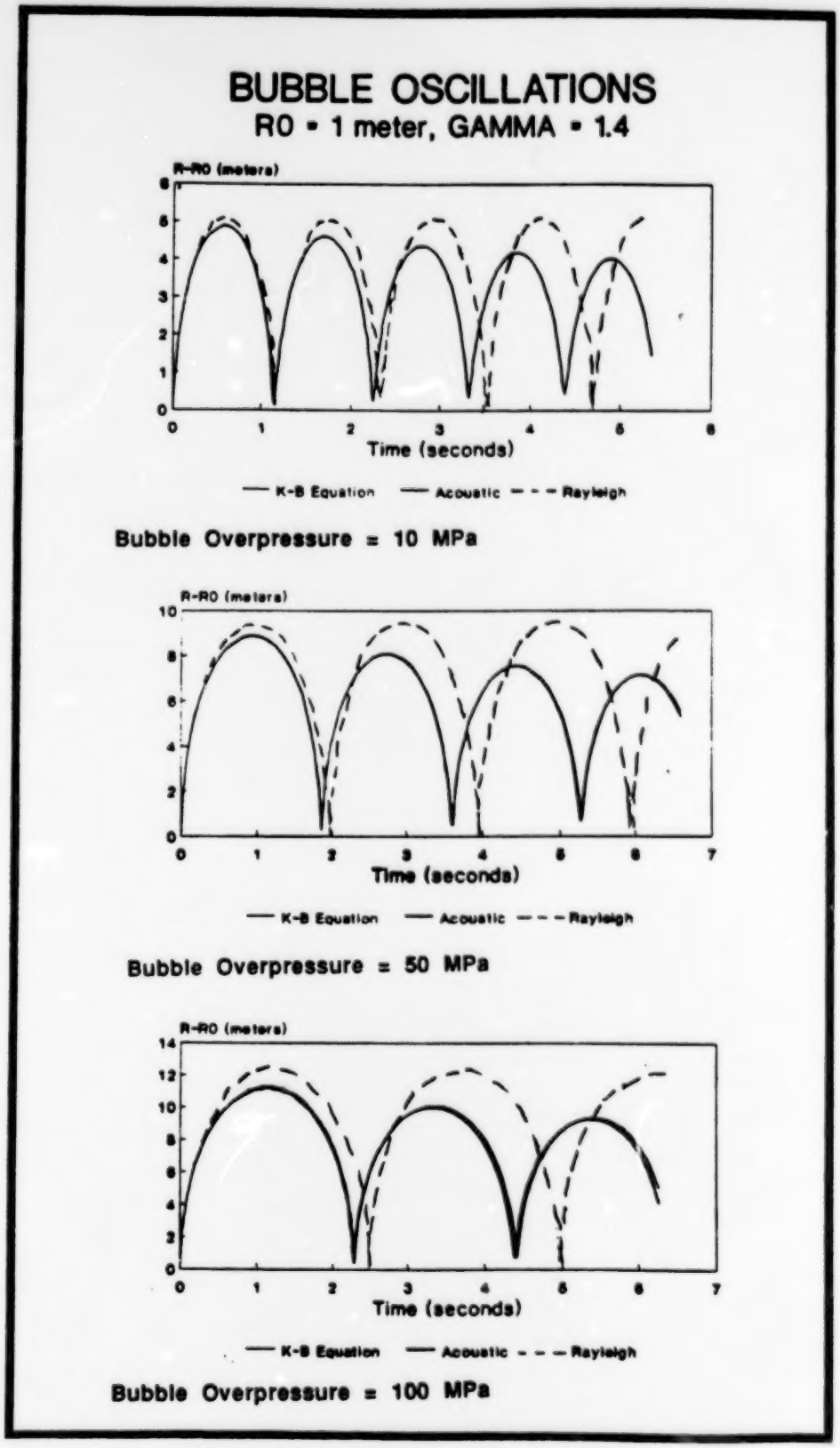

Fig. C-2 **Bubble oscillations computed using various numerical models with initial bubble overpressures ranging from 10 to 100 MPa**

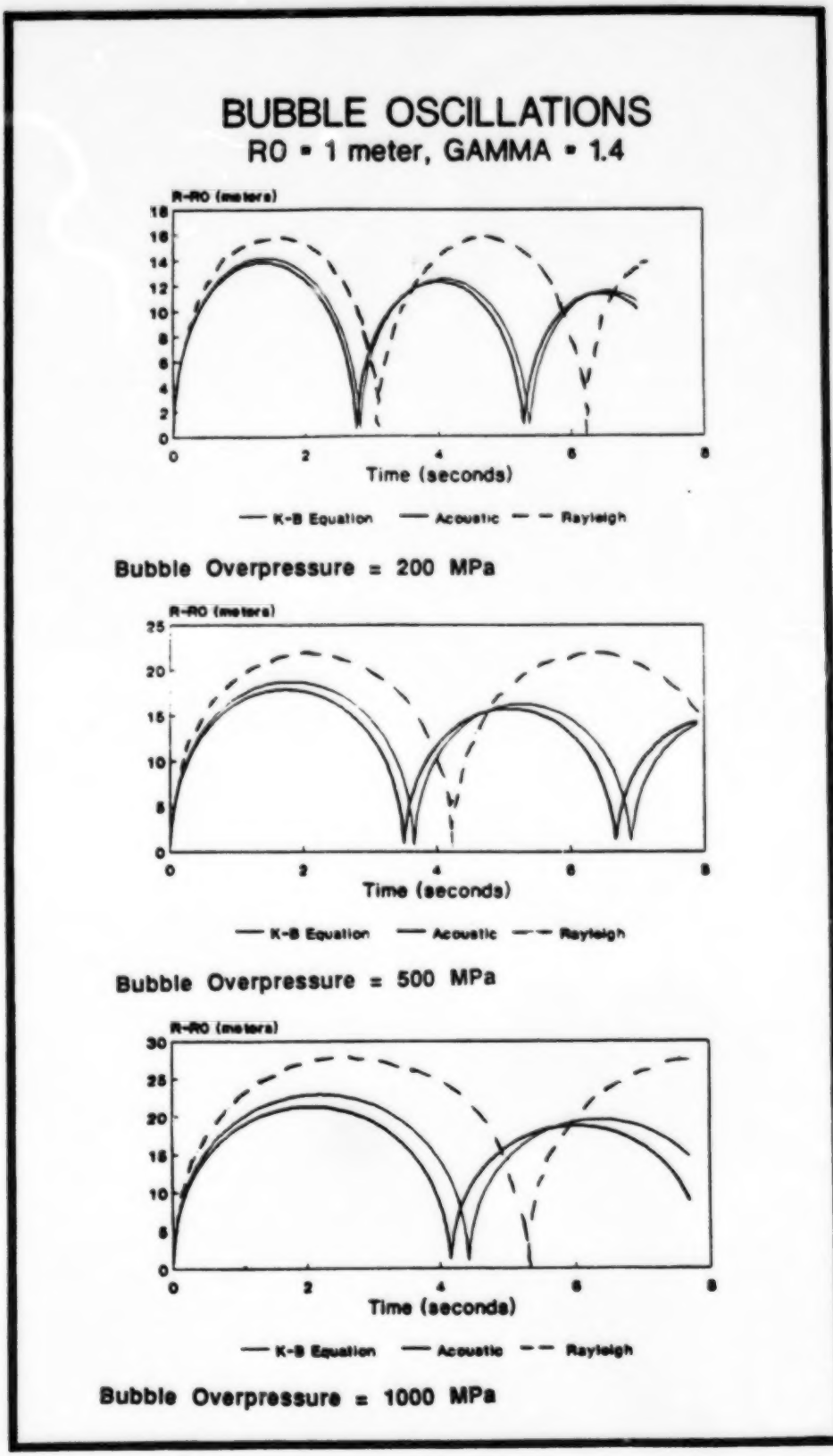

Fig. C-3 **Bubble oscillations computed using various numerical models with initial bubble overpressures ranging from 200 to 1000 MPa**

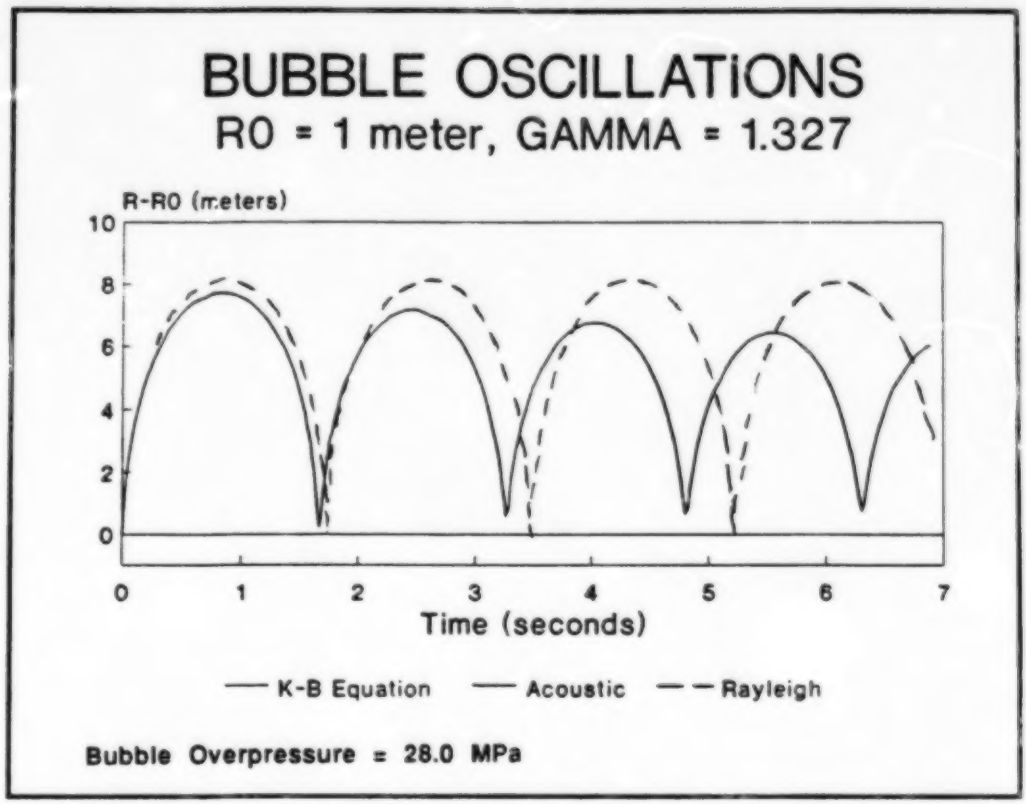

Fig. C-4 **Bubble oscillations computed using various numerical models with initial bubble overpressure 28.0 MPa**

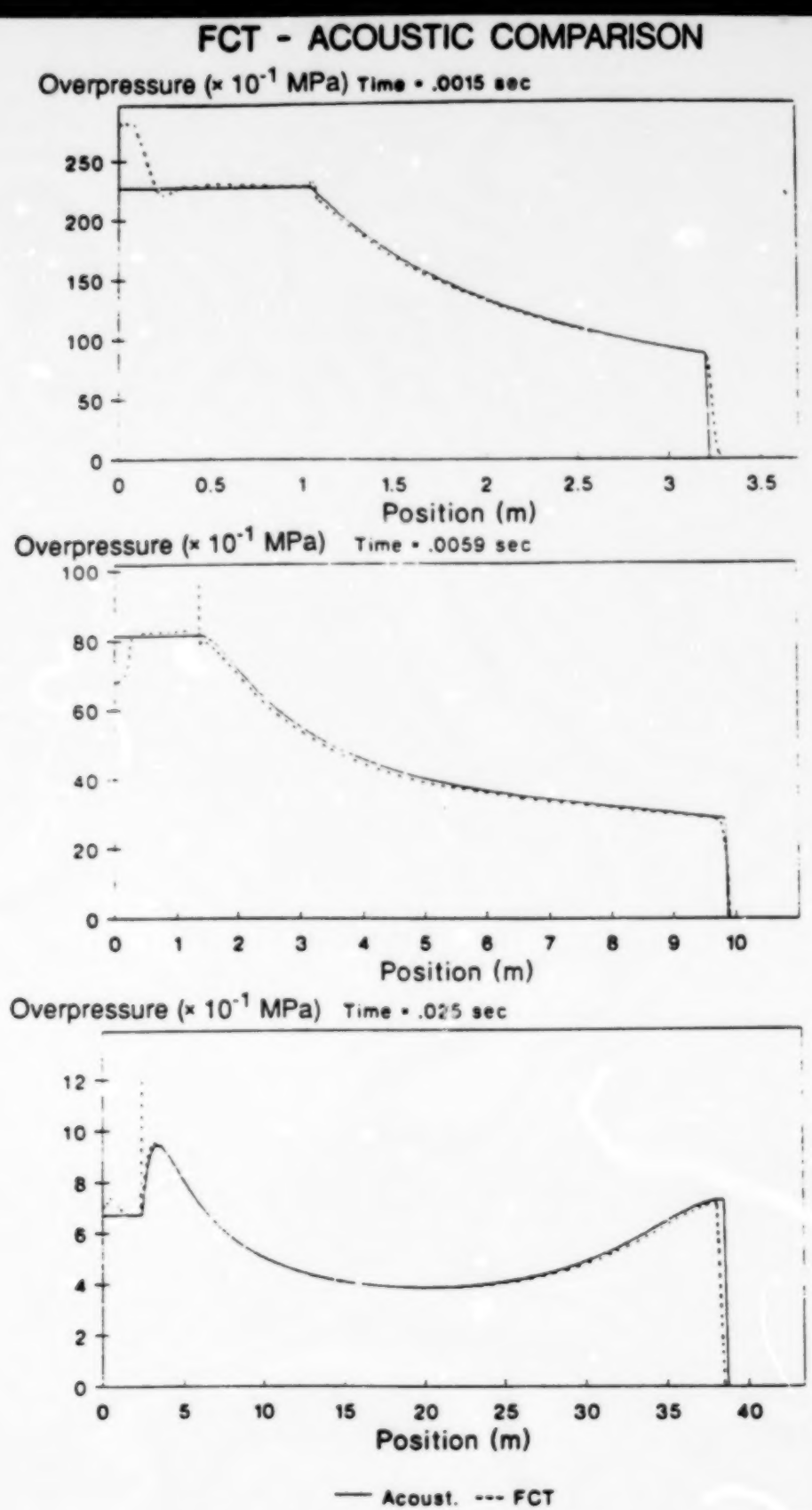

Fig. C-5 **Pressure profiles computed using the acoustic model and the FCT numerical code at various times**

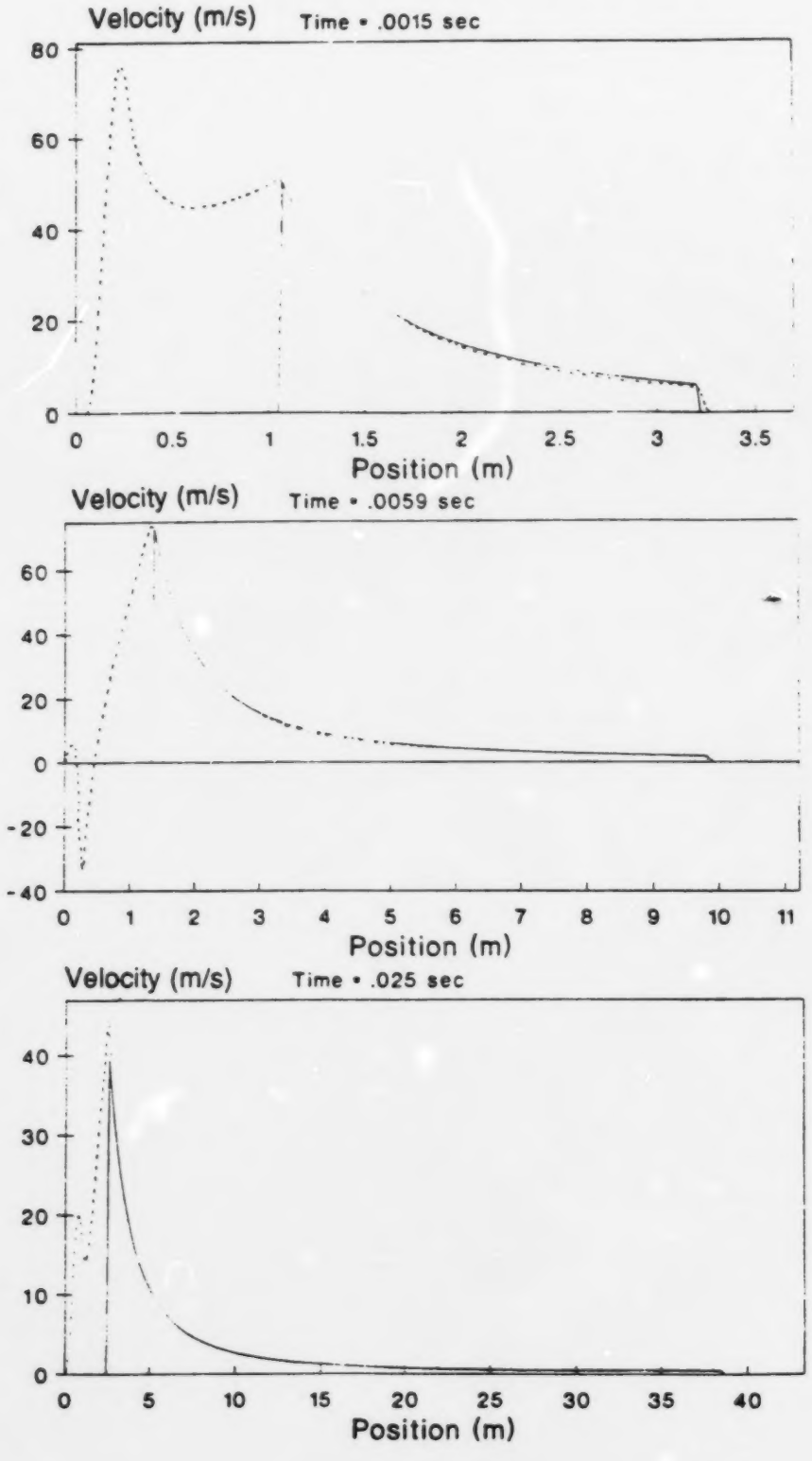

Fig. C-6 **Liquid velocities computed using the acoustic model and the FCT numerical code at various times**

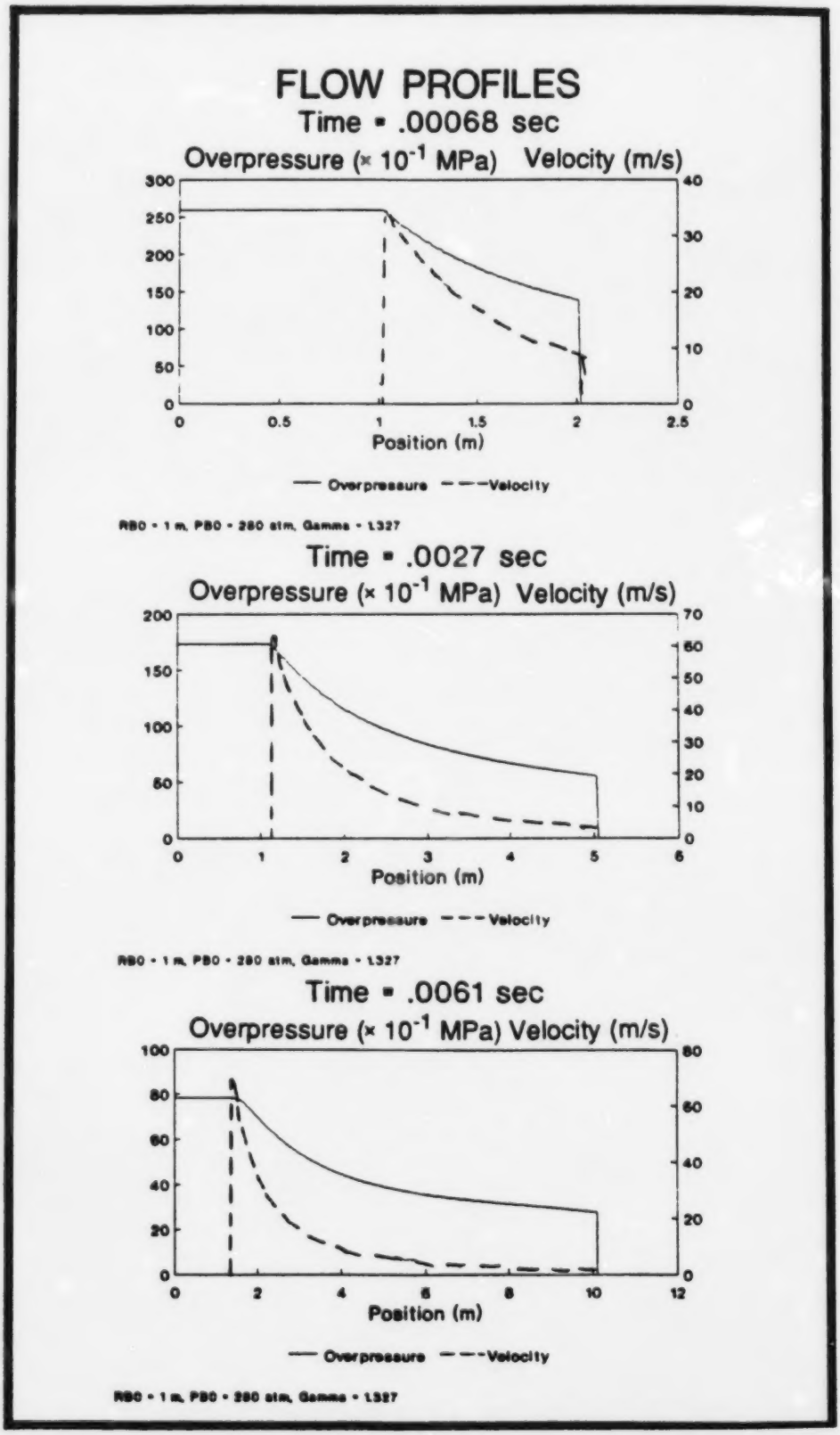

Fig. C-7 **Overpressure and velocity profiles computed using the acoustic model at 0.68, 2.7 and 6.1 ms**

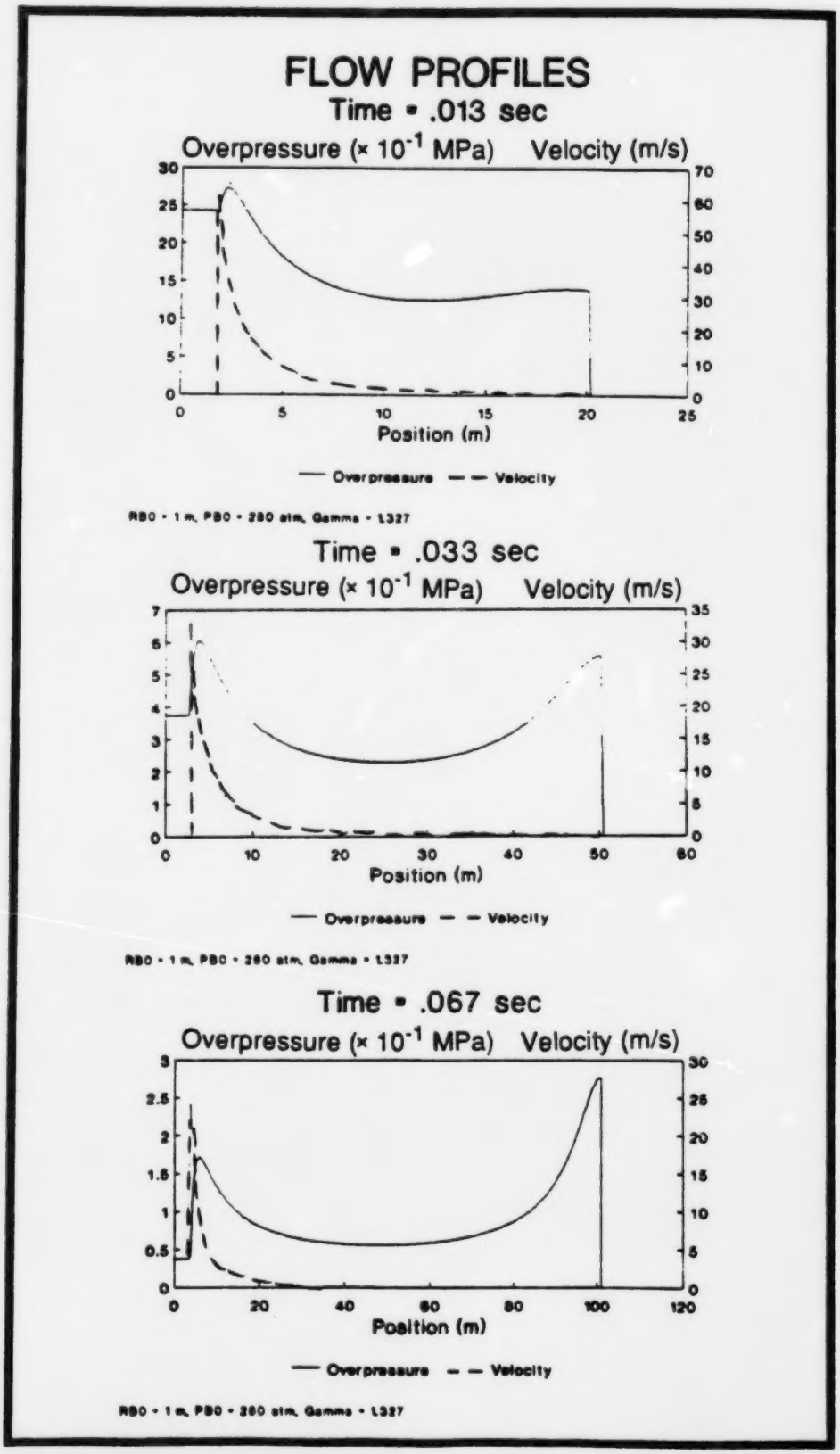

Fig. C-8 **Overpressure and velocity profiles computed using the acoustic model at 13, 33 and 67 ms**

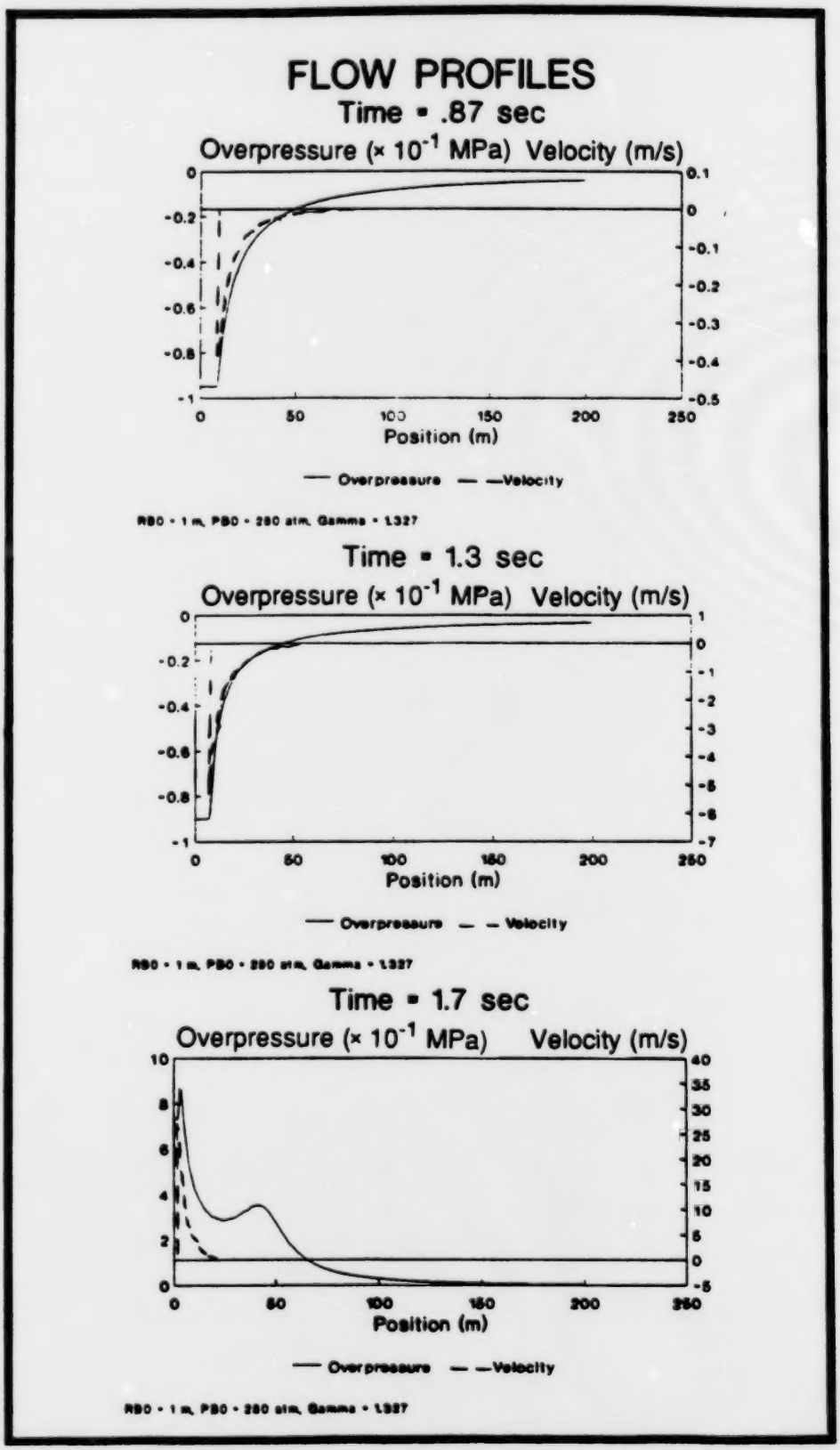
FLOW PROFILES
Time = .87 sec
Overpressure (× 10^-1 MPa) Velocity (m/s)
Position (m)
Overpressure
Velocity
RBO = 1 m, PBO = 280 atm, Gamma = 1.327
Time = 1.3 sec
Overpressure (× 10^-1 MPa) Velocity (m/s)
Position (m)
Overpressure
Velocity
RBO = 1 m, PBO = 280 atm, Gamma = 1.327
Time = 1.7 sec
Overpressure (× 10^-1 MPa) Velocity (m/s)
Position (m)
Overpressure
Velocity
RBO = 1 m, PBO = 280 atm, Gamma = 1.327

Fig. C-9 Overpressure and velocity profiles computed using the acoustic model at .87, 1.3 and 1.7 s

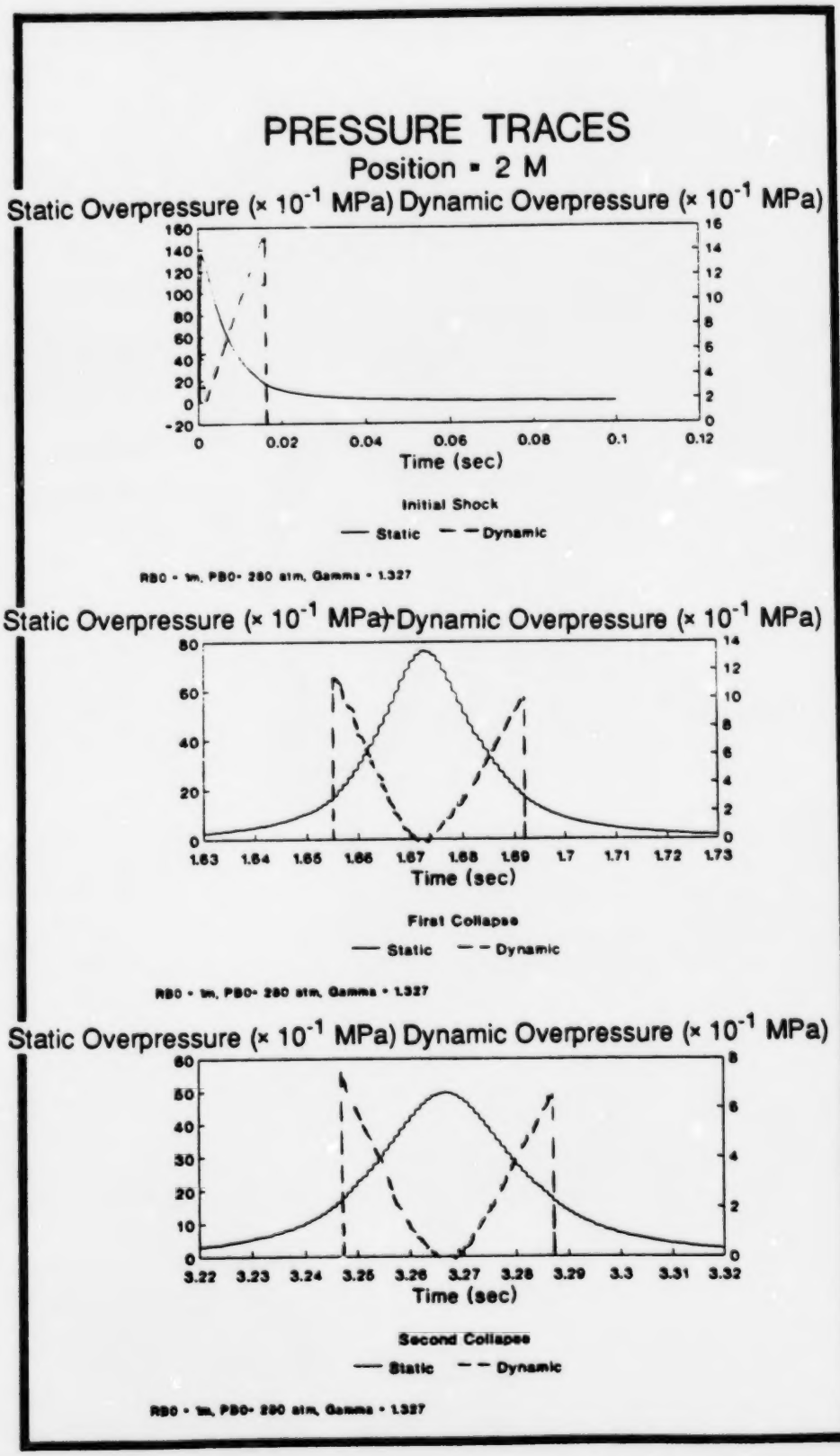

Fig. C-10 Static and dynamic pressure transients at a radial position of 2 m showing initial shock and subsequent bubble pulses during bubble collapses

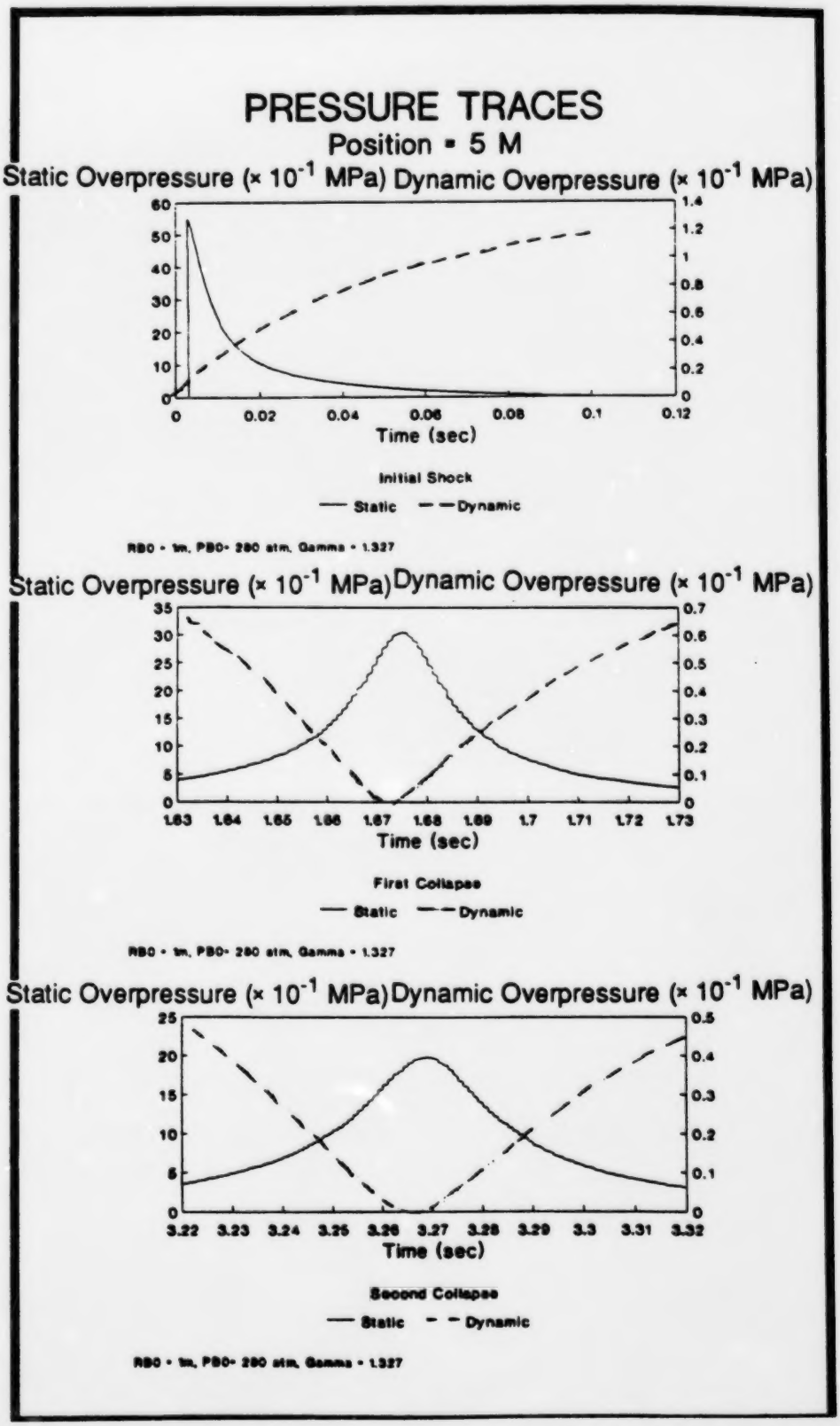
PRESSURE TRACES
Position = 5 M
Static Overpressure (× 10^-1 MPa) Dynamic Overpressure (× 10^-1 MPa)
Time (sec)
Initial Shock
Static
Dynamic
RB0 = 1m, PB0= 280 atm, Gamma = 1.327
Static Overpressure (× 10^-1 MPa) Dynamic Overpressure (× 10^-1 MPa)
Time (sec)
First Collapse
Static
Dynamic
RB0 = 1m, PB0= 280 atm, Gamma = 1.327
Static Overpressure (× 10^-1 MPa) Dynamic Overpressure (× 10^-1 MPa)
Time (sec)
Second Collapse
Static
Dynamic
RB0 = 1m, PB0= 280 atm, Gamma = 1.327

Fig. C-11 Static and dynamic pressure transients at a radial position of 5 m showing initial shock and subsequent bubble pulses during bubble collapses

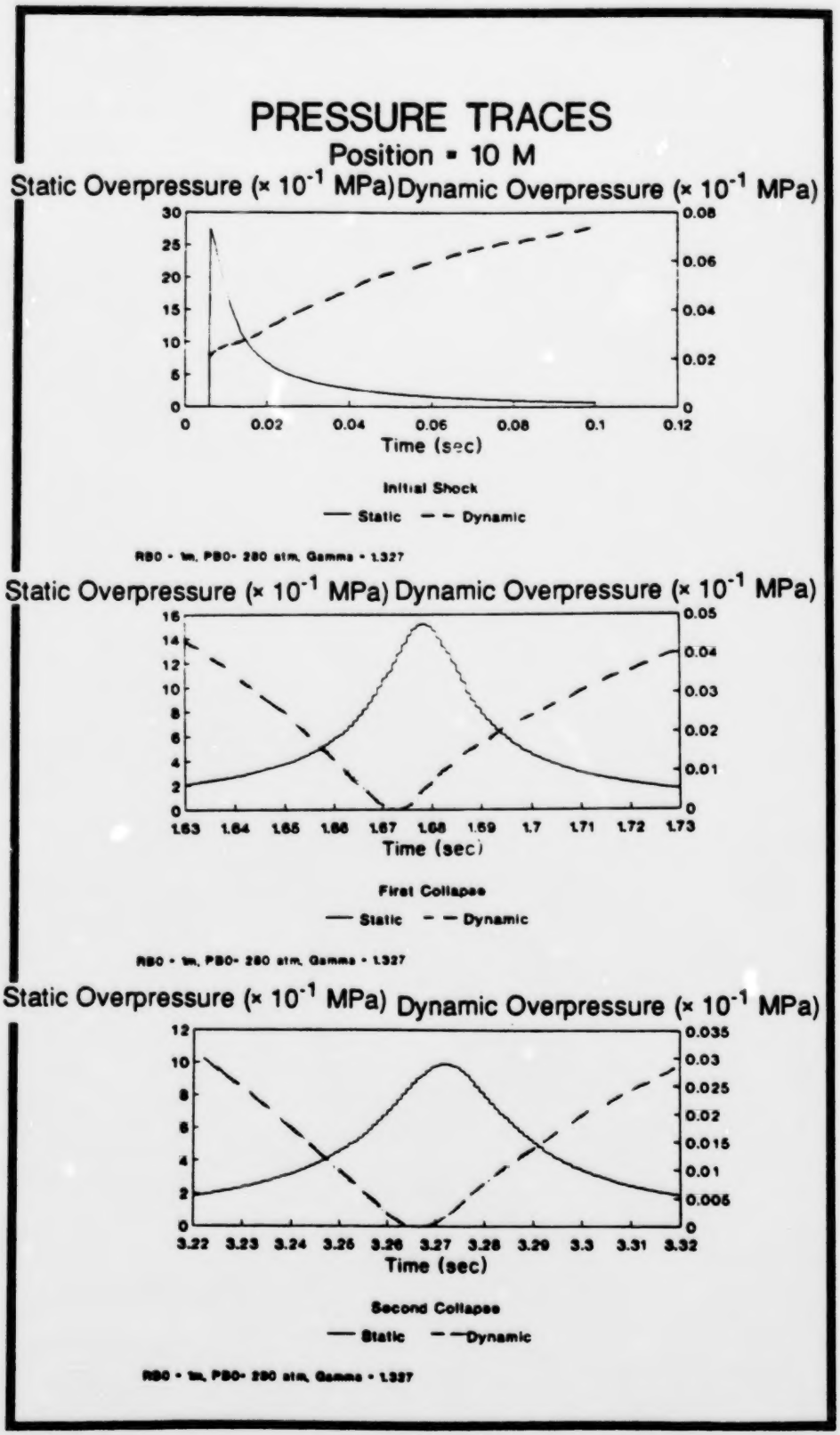

Fig. C-12 Static and dynamic pressure transients at a radial position of 10 m showing initial shock and subsequent bubble pulses during bubble collapses

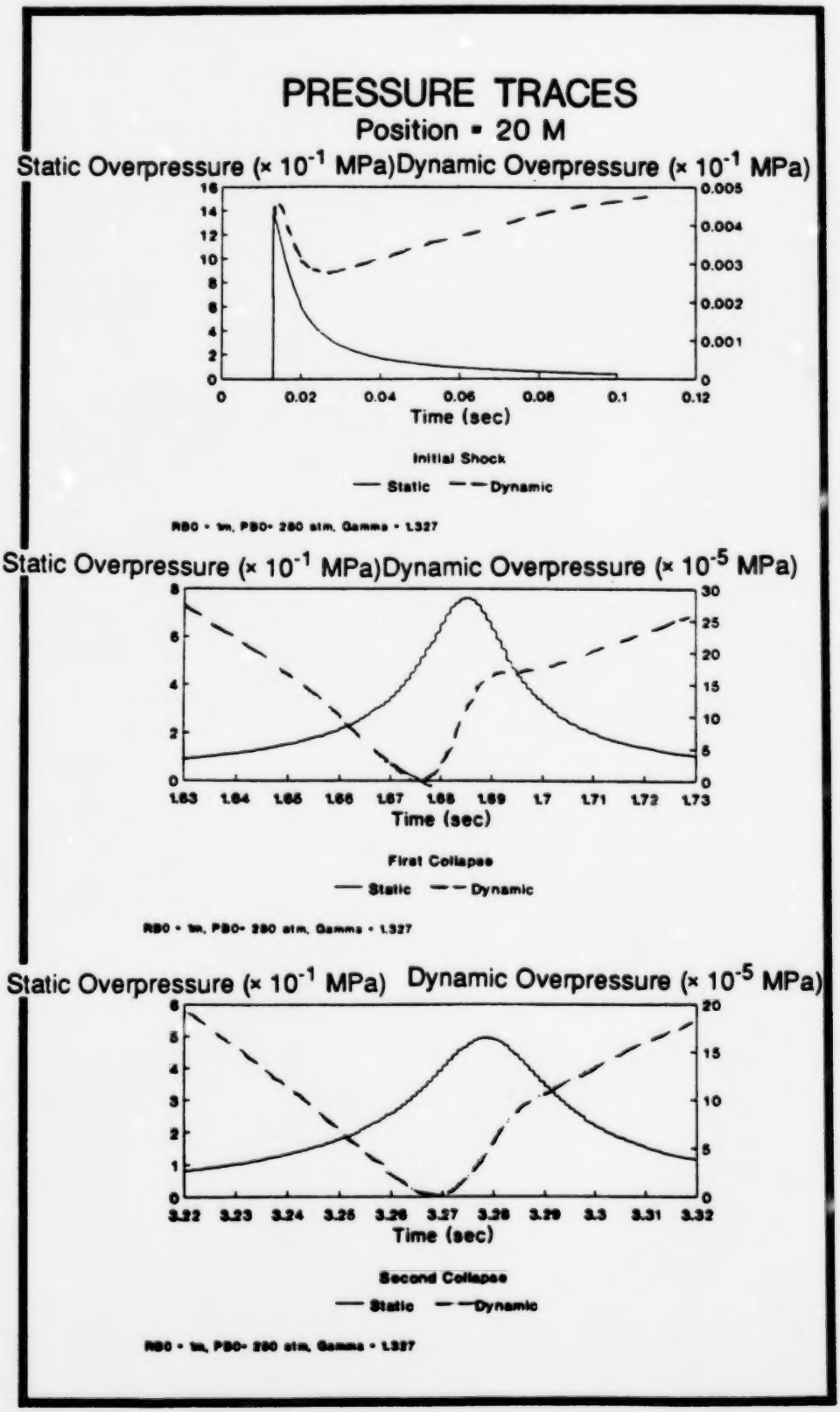
PRESSURE TRACES
Position = 20 M
Static Overpressure (× 10^-1 MPa)Dynamic Overpressure (× 10^-1 MPa)
Time (sec)
Initial Shock
Static
Dynamic
RBO = 1m, PBO= 280 atm, Gamma = 1.327
Static Overpressure (× 10^-1 MPa)Dynamic Overpressure (× 10^-5 MPa)
Time (sec)
First Collapse
Static
Dynamic
RBO = 1m, PBO= 280 atm, Gamma = 1.327
Static Overpressure (× 10^-1 MPa) Dynamic Overpressure (× 10^-5 MPa)
Time (sec)
Second Collapse
Static
Dynamic
RBO = 1m, PBO= 280 atm, Gamma = 1.327

Fig. C-13 Static and dynamic pressure transients at a radial position of 20 m showing initial shock and subsequent bubble pulses during bubble collapses

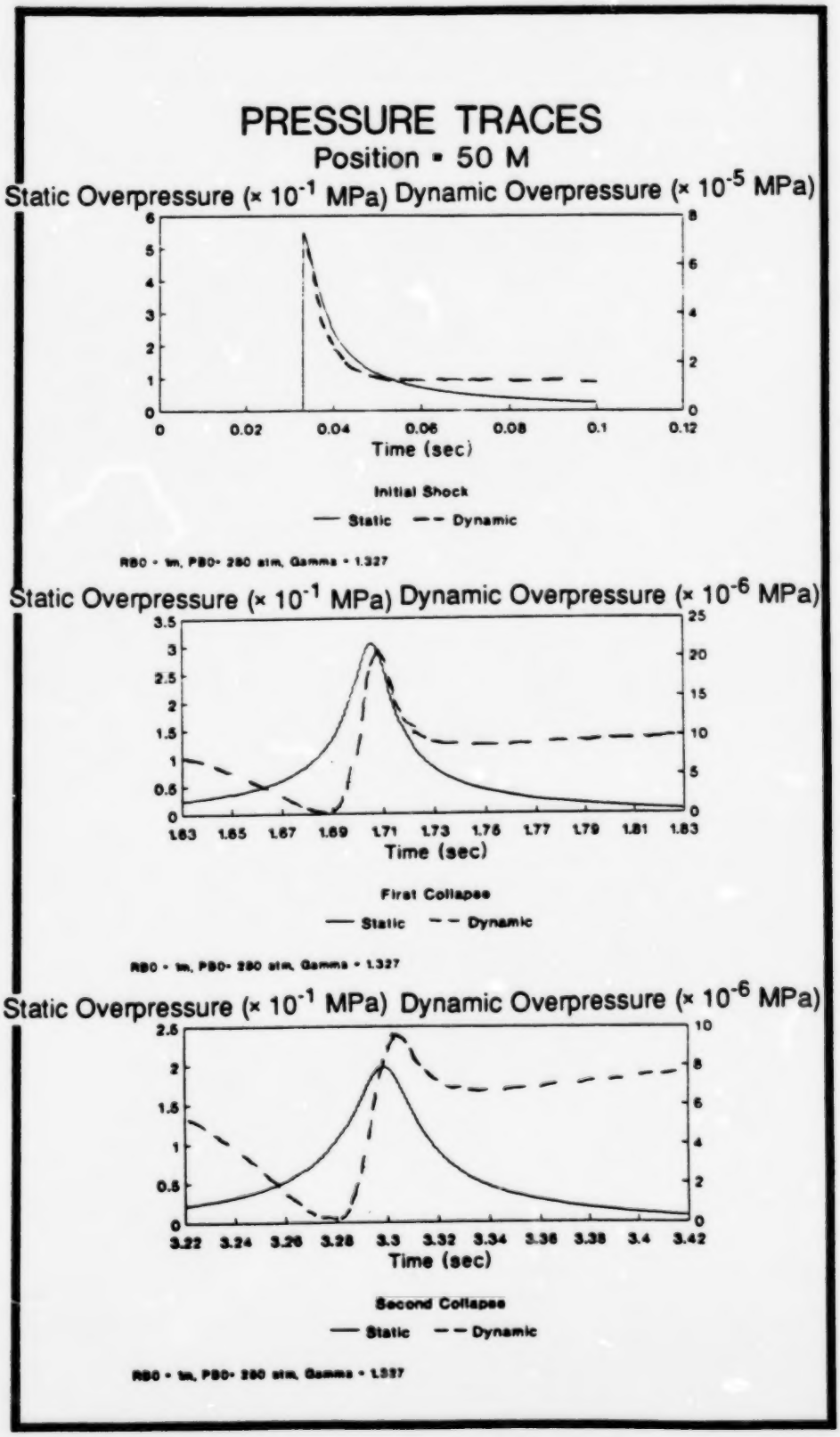
PRESSURE TRACES
Position = 50 M
Static Overpressure (× 10-1 MPa) Dynamic Overpressure (× 10-5 MPa)
Time (sec)
Initial Shock
Static
Dynamic
RBO = 1m, PBO= 280 atm, Gamma = 1.327
Static Overpressure (× 10-1 MPa) Dynamic Overpressure (× 10-6 MPa)
Time (sec)
First Collapse
Static
Dynamic
RBO = 1m, PBO= 280 atm, Gamma = 1.327
Static Overpressure (× 10-1 MPa) Dynamic Overpressure (× 10-6 MPa)
Time (sec)
Second Collapse
Static
Dynamic
RBO = 1m, PBO= 280 atm, Gamma = 1.327

Fig. C-14 **Static and dynamic pressure transients at a radial position of 50 m showing initial shock and subsequent bubble pulses during bubble collapses**

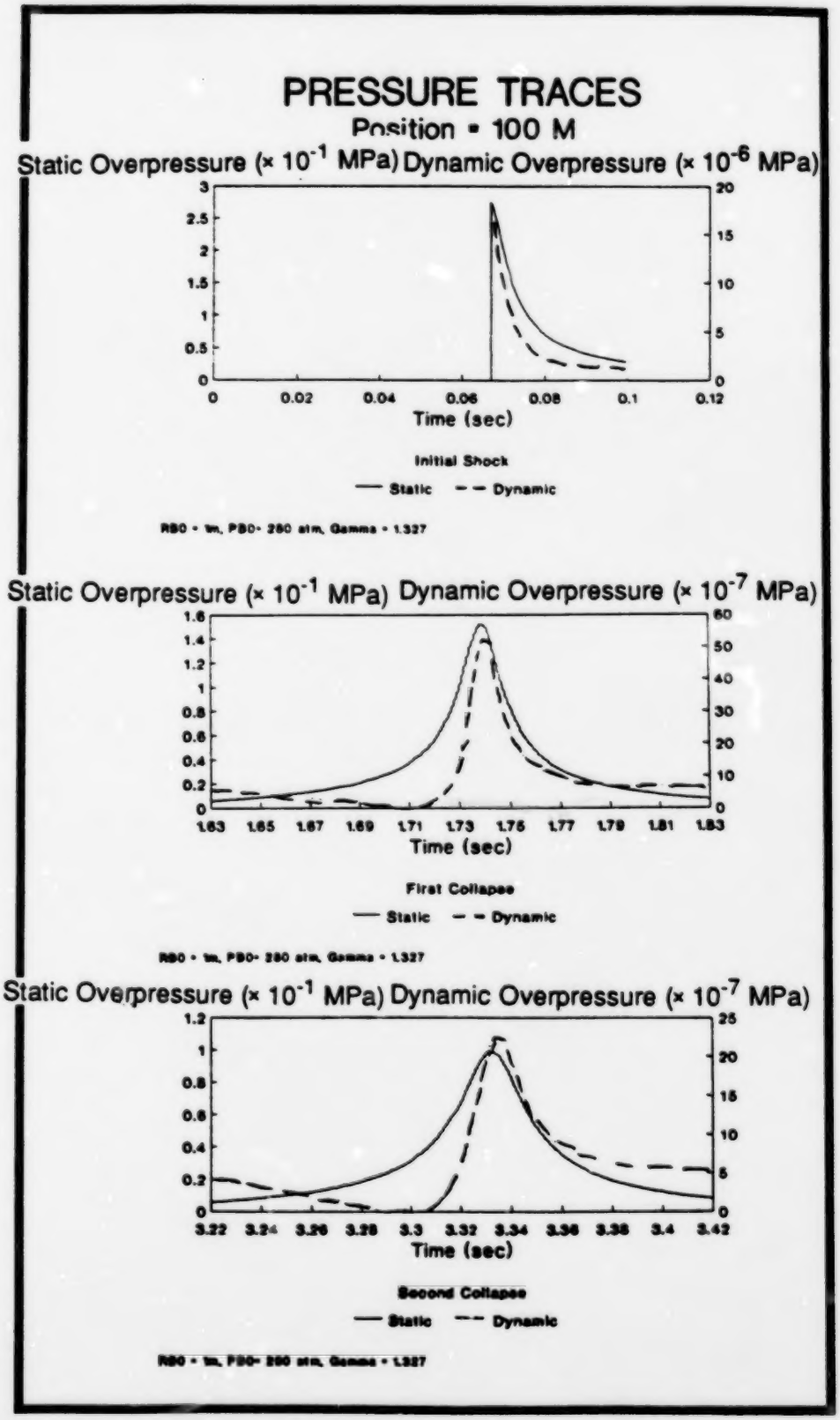
PRESSURE TRACES
Position = 100 M
Static Overpressure (× 10^-1 MPa) Dynamic Overpressure (× 10^-6 MPa)
Time (sec)
Initial Shock
Static
Dynamic
RBO = 1m, PBO= 280 atm, Gamma = 1.327
Static Overpressure (× 10^-1 MPa) Dynamic Overpressure (× 10^-7 MPa)
Time (sec)
First Collapse
Static
Dynamic
RBO = 1m, PBO= 280 atm, Gamma = 1.327
Static Overpressure (× 10^-1 MPa) Dynamic Overpressure (× 10^-7 MPa)
Time (sec)
Second Collapse
Static
Dynamic
RBO = 1m, PBO= 280 atm, Gamma = 1.327

Fig. C-15 **Static and dynamic pressure transients at a radial position of 100 m showing initial shock and subsequent bubble pulses during bubble collapses**

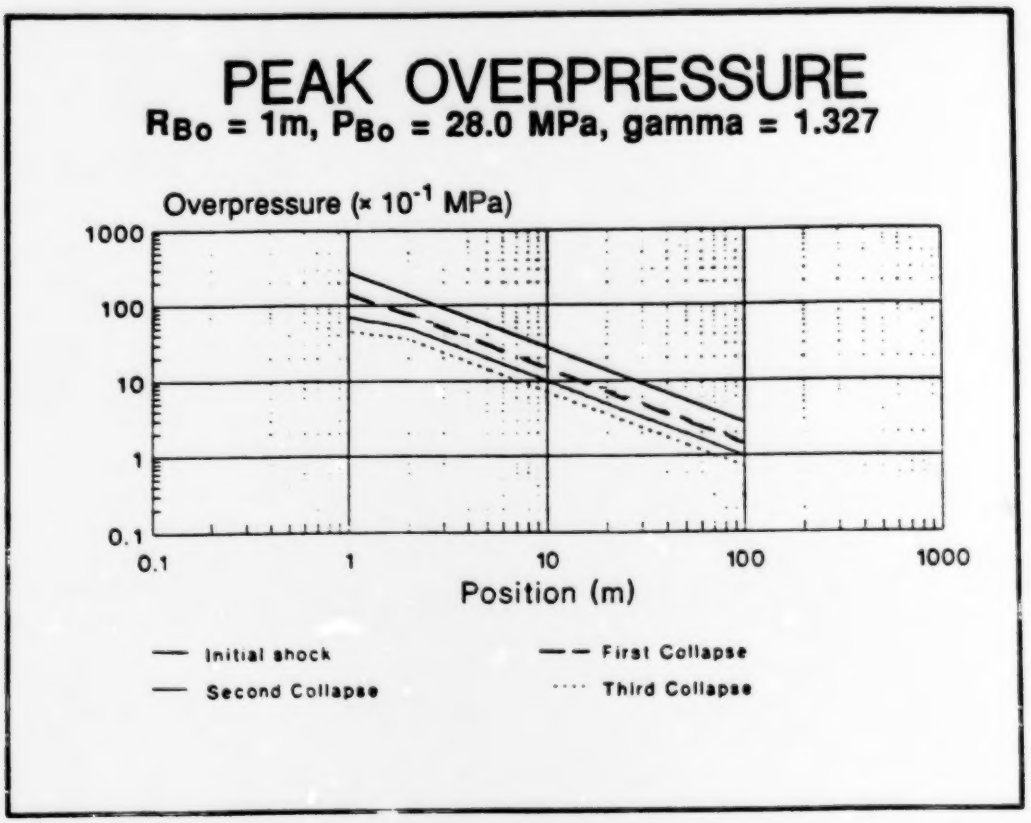

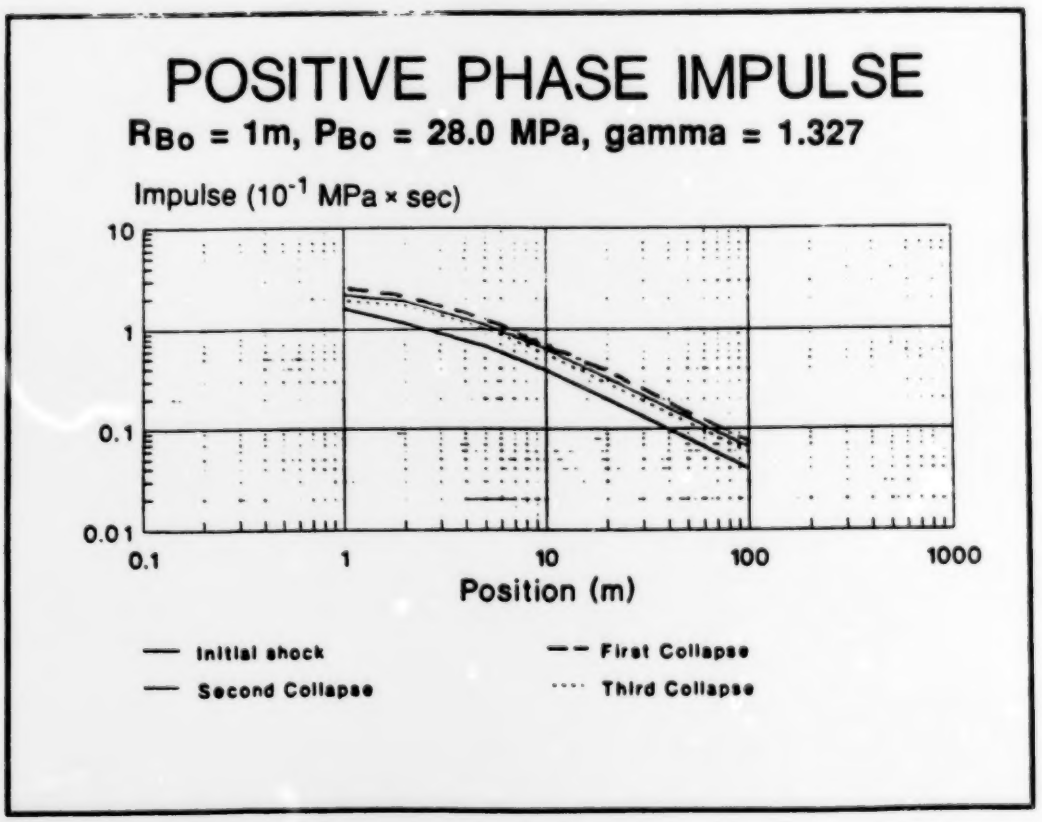

Fig. C-16 Peak overpressure and impulse for initial shock and subsequent bubble collapse pulses

APPENDIX D

DERIVATION OF INITIAL BUBBLE CONDITIONS

(References cited are those listed in the main text)

DERIVATION OF INITIAL BUBBLE CONDITIONS

In Appendix C, numerical simulations of blast waves generated by the sudden bursting of a pressurized gas sphere in water are presented. Calculations were performed using a simple acoustic model and compared with results using a fully nonlinear onedimensional finite-difference code. The determination of the trial initial conditions used for the calculations is described below.

In an earlier contract (Lee and Knystautas, 1987), equilibrium Hicks-Menzies calculations were carried out to find the maximum work potential during a specific steam explosion scenario. It was assumed that, following a fuel channel blockage, the entire contents of one fuel channel melts and interacts with a given amount of coolant. It was further assumed that the fuel and coolant transfer heat at constant volume until an equilibrium temperature is reached. The work done by the subsequent isentropic expansion (back to atmospheric pressure) of the bubble was then calculated. From the earlier contract, it was found that the maximum work is obtained if the mass ratio of the coolant to the fuel is

$$\frac{m_c}{m_f} \approx 0.3 \tag{1}$$

where m_c = mass of the coolant interacting with molten fuel
m_f = mass of the molten fuel

So for a molten fuel mass of 300 kg (corresponding to the total contents of one fuel channel), the corresponding coolant mass of interest is 90 kg. For constant volume heat transfer from the fuel to coolant, the final equilibrium temperature is

$$T_e = \frac{\frac{m_f c_{v_f}}{m_c c_{v_c}} T_f + T_c}{1 + \frac{m_f c_{v_f}}{m_c c_{v_c}}} \tag{2}$$

where T_f = initial temperature of molten fuel
T_c = initial temperature of coolant
c_{v_f} = heat capacity of molten fuel
c_{v_c} = heat capacity of coolant

Initial fuel and water temperatures are taken to be T_f = 3073 K and T_c = 330 K. For m_c/m_f = 0.3, the water will be heated far into the supercritical region. In this region, the specific heat varies considerably, from 4.2 kJ/kgK at low temperature, to large values near the critical region, and decreases to lower values at higher temperatures. However, the final equilibrium temperature is not too sensitive to c_v, e.g., for c_v ranging from 4.2 to 5.0 kJ/kgK, the final equilibrium temperature varies from about 900°C to 800°C, respectively. For a constant volume process, the entropy change is given by

$$s_e = s_1 + c_v \ln T_e/T_1 \tag{3}$$

If we take, as an estimate, c_v = 5 kJ/kgK, then from equations (2) and (3) above, by solving for the equilibrium temperature and entropy and then using steam tables, the initial bubble pressure is found to be 28.0 MPa. From the initial water temperature, the corresponding water density (from tables) is 984 kg/m^3. So the initial 90 kg of coolant occupies a volume of 0.0915 m^3 or assuming the coolant mass is spherical, the effective initial bubble radius is about 0.28 m. So in summary, the initial conditions used for the trial calculations for bubble growth in Appendix C are:

$$p_i = 28.0 \text{ MPa}$$
$$R_i = 0.28 \text{ m}$$
$$\rho_i = 984 \text{ kg/m}^3$$

where the subscript *i* denotes initial condition.